DAC-59301

DEVELOPMENT OF VIBRATION DESIGN PROCEDURES FOR REPRESENTATIVE STRUCTURAL TYPES

AUGUST 1966

Prepared under Contract No. NAS8-20549
by Douglas Aircraft Company, Inc.
Missile and Space Systems Division
Santa Monica, California
for
NATIONAL AERONAUTICS AND SPACE ADMINISTRATION

DAC-59301

DEVELOPMENT OF VIBRATION DESIGN PROCEDURES FOR REPRESENTATIVE STRUCTURAL TYPES

AUGUST 1966

By

D.E. HINES AND J.H. GUNNING

Prepared under Contract No. NAS8-20549
by Douglas Aircraft Company, Inc.
Missile and Space Systems Division
Santa Monica, California
for
NATIONAL AERONAUTICS AND SPACE ADMINISTRATION

PREFACE

This document is submitted to the National Aeronautics and Space Administration. Huntsville, Alabama in compliance with Contract NAS8-20549 "Optimum Design Procedures for Handling Space Vehicle Vibration Environments." This study is a continuation of the activity conducted under Contract NAS8-11617.

The study, performed by Douglas Aircraft Company. Inc., Santa Monica, California, was directed by G. E. Kahre with D. E. Hines as principal investigator. C. Lifer, of the Propulsion and Vehicle Engineering Division of Marshall Space Flight Center, acted as the contract technical manager.

The period of performance for this study was September 1965 to July 1966. This report presents experimental and analytical results of the study and constitutes the final technical report.

ABSTRACT

This report presents the results of an experimental study conducted to (1) define the effects of multiple modes on random fatigue, (2) establish the effect of light damping, resulting from damping tape, on random fatigue results obtained with cantilevered beam type fatigue specimens, (3) establish the feasibility of the design factor approach of Reference 1 for space vehicle bracketry, and (4) establish the feasibility of design nomograms for space vehicle bracketry. The test specimens consisted of four sets of 12 cantilevered beams for goals 1 and 2 and two sets of 6 brackets for goals 3 and 4.

The effects of multi-mode response on random fatigue for a specific case has been treated and a procedure for handling multi-modes developed. Methods for other specific multi-mode responses are discussed and procedures hypothesized. For the tests conducted, the effects of light damping on test data were negligible in that no significant reduction in data scatter (caused by high Q responses) was noted as compared to non-damped specimens. The design factor approach as applied to bracket structure was determined to be a feasible approach and typical design nomographs were developed for specific bracket types.

CONTENTS

CONTENTS

FIGURES

TABLES

SYMBOLS

σ_{eq} = Equivalent stress
F_{tw} = Working stress
K = Design factor-material-properties
K_{dyn} = Dynamic load factor
σ_o = Static stress
k_f = Fatigue stress concentration factor
f = Frequency
S = Stress
k_t = Static stress concentration factor
α = Material constant
R → Root accelerometer
B → Base accelerometer
θ = Rotation in radians
T_p → See page 38
B_p → See page 38
S_T → See page 38
S_B → See page 38
t = Thickness
W, a, c, t, F_b See Figure 3-7 and 3-10
Q = Amplification factor

Section 1
INTRODUCTION AND SUMMARY

The prediction of, and design for, fatigue resulting from random response is of utmost importance in the design and development of aerospace vehicles. This random fatigue study was conducted to obtain fundamental engineering data for multi-mode response, to explore the possibility of improving experimental results by the use of damping tape (that is, to reduce test data scatter resulting from high and varied Q's), and to establish the feasibility of using the design factor approach of Reference 1 and design nomograms for optimizing design of typical support brackets. In addition, analytical methods were hypothesized for predicting the effects of multi-modes for more general cases since experimental results were applicable only to a specific case.

The multi-mode and damping effects were explored by testing 3 sets of 12 beams. The first set will be referred to as the peg point specimens. The set consisted of simple end weighted cantilevered beams differing from those used in Reference 1 only in that they had one rather than two holes as stress raisers. These specimens were tested to confirm the test results obtained in the previous study (Reference 1) and to obtain a basis for comparison for the evaluation of the results obtained from other specimens of this current study. The second set of 12 specimens will be referred to as the two weight, or multi-bending mode beams; and the set is similar to the first set except that an additional weight was added part way along the length of the beam in order to force two significant bending modes. These specimens were used to establish the effects of multi-mode bending stresses. The third set of 12 beams will be referred to as the cantilevered weight bending-torsional beams and, again, the set is similar to the first set except the end weight was cantilevered off one side to induce a torsional mode in addition to a bending mode. The purpose was to establish the effect of non-parallel multi-mode stresses on fatigue. An additional set of 12 beams with single end weights but with no stress raiser was tested. Tests on these specimens were performed to

determine if such test specimens would yield meaningful data required in a program of stress concentration evaluation. The four types of beams are illustrated in Figure 1-1.

In the original study, difficulty was encountered because of the extremely high Q's of the specimens having stress raisers and nonlinear damping with specimens without stress raisers. Therefore, damping tape was added to three beams of each of the first three sets and six beams of the last set to determine if the added damping had a desirable effect in more closely controlling the response of the specimens.

The bracket tests were performed on two sets of six brackets. The first set of specimens consisted of simple hat brackets, all of which were formed of 6061 aluminum alloy in the T6 condition. Three of these were re-heat treated to the T6 condition to relieve residual stresses allowing the evaluation of this effect. The second set of brackets was of the simple shelf type constructed of 6061-T6 aluminum alloy, and again, three of these brackets were re-heat treated. In each case, a 5-lb block was mounted to the brackets to represent the mass of a mounted equipment item. The two types of brackets are illustrated in Figure 1-2.

Results of the beam test are as follows:

1. The experimental results reported in Reference 1 were confirmed as discussed in Section 2.4.
2. The effect of a second bending mode on fatigue was hypothesized, and the results agreed with the limited range of the tests. Data were not available to evaluate other cases.
3. The effect stresses having nonparallel principal axis could not be determined because sufficient torsional stress levels were not obtained on the cantilevered weight beam to yield conclusive results.
4. Because of the high quality (minimum scatter) of the data obtained from all beam specimens, the effect of damping tape was not obvious.

The results of the bracket study were as follows:

1. The design factor approach was determined to be feasible for flight bracketry.
2. Nomographs were shown to be feasible and developed for hat and shelf-type brackets.
3. The prestress of the tested brackets had no detectable effect on the fatigue levels.

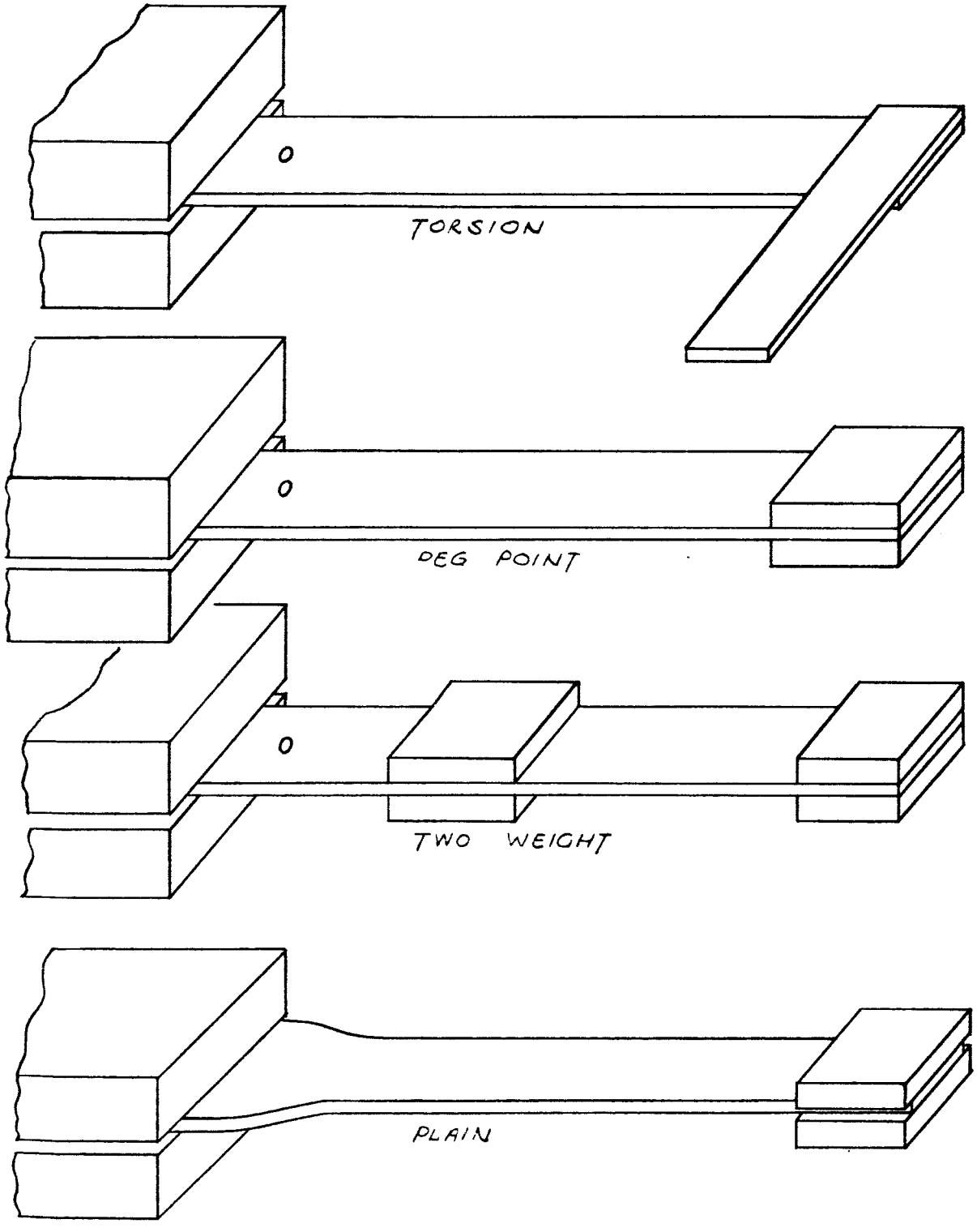

Figure 1-1. Beam Test Specimens

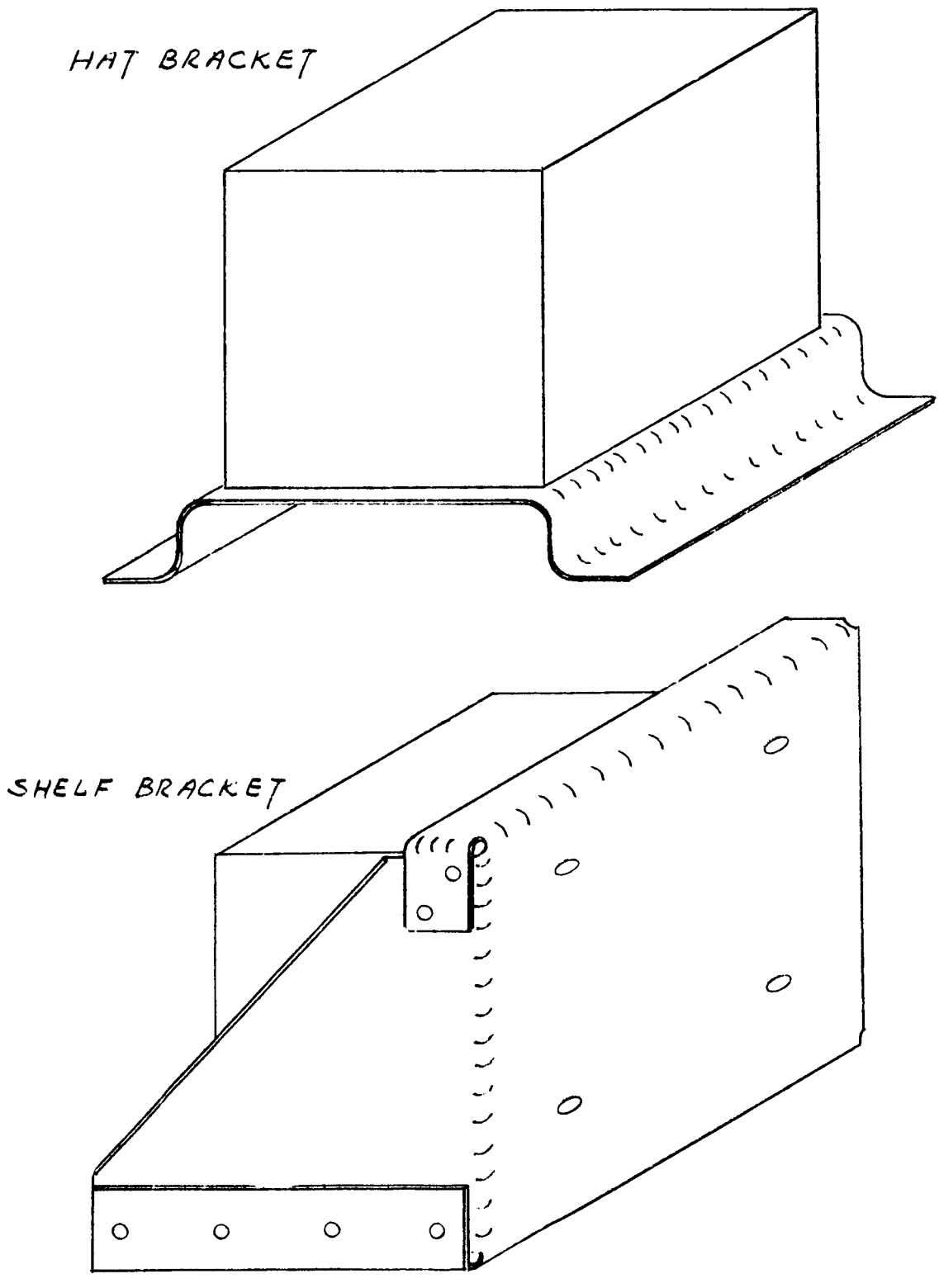

Figure 1-2. Test Brackets

Section 2
BEAM STUDY

2.1 TEST SPECIMENS

This portion of the study was conducted to obtain basic information on random fatigue. Cantilevered beam test specimens were chosen because of their inherent simplicity in design, construction, testing, analysis, and data reduction. The four beam configurations used, and the specific data and analysis for each of these beams, are discussed in the following paragraphs.

2.1.1 Peg-Point Beams

The peg point beams were tested primarily for the purpose of furnishing a standard for comparison in evaluating the multi-mode beam tests. The secondary objective of these tests was to verify and refine the information obtained in the original study (Reference 1). The initial study evaluated a K factor for use in the expression

$$\sigma_{eq} = (K)\,(K_{dyn})\,\sigma_o\,(\text{load})$$

where

σ_{eq} = stress compared to F_{tw}

F_{tw} = working stress which is ultimate over 1.4 or yield over 1.1, whichever is less

K = design factor including the fatigue properties of the material (F_{tw} over fatigue strength at the desired life)

K_{dyn} = dynamic load factor $(\pi/2\ Qf)^{1/2}$ from random; Q for sinusoidal excitation

σ_o = static stress for loads, such as those applied in vibration

load = the excitation force

The beams utilized for this portion of the study were of 2024-T4 Aluminum 1-1/4 in. wide, 1/8 in. thick, 5.44 in. long from the clamped, and had a 1/8 in. diam hole stress raiser located 0.44 in. from the clamped end (Figure 2-1). Three beams had a simple end weight of 0.253 lb, three had an end weight of 0.189 lb, and the remaining six beams had weights of 0.222 lb. Three of the last set were damped with commercial damping tape in order to investigate its effect on the obtained fatigue data.

2.1.2 Multi-Mode Beams

The multi-mode beams were of two types, both utilizing the same basic beam of Figure 2-1.

The two weight beams were designed to study the effect of two significant bending modes on random fatigue. All of these beams had end weights of 0.189 lb with an additional weight located 2.72 in. from the clamped end. The center weight was 0.293 lb for three beams, 0.243 lb for three beams, and 0.253 lb for six beams. Damping tape was again added to three of the last six beams.

The torsion beams were designed to study the effect of a bending and torsion mode on random fatigue. Each beam had end weights of 0.236 lb while the c.g. of the blocks were displaced 1.00, 1.31 and 1.16 in. from the centerline for sets of three, three, and six, respectively. Damping was added to three of the set of six beams.

2.1.3 Plain Beams

The plain beams had no stress raisers and were tested primarily to demonstrate the feasibility of obtaining good random fatigue data from this type of specimen. This is of importance in any work to be done in the evaluation of stress concentration factors for random fatigue, a topic which is of the utmost importance. Figure 2-2 shows the basic beam configuration; end weights of 0.210 and 0.162 lb were added to two sets of six beams. Three beams of each set had added damping in the form of damping tape.

The nomenclature and weight configurations for the beams are shown in Table 2-1.

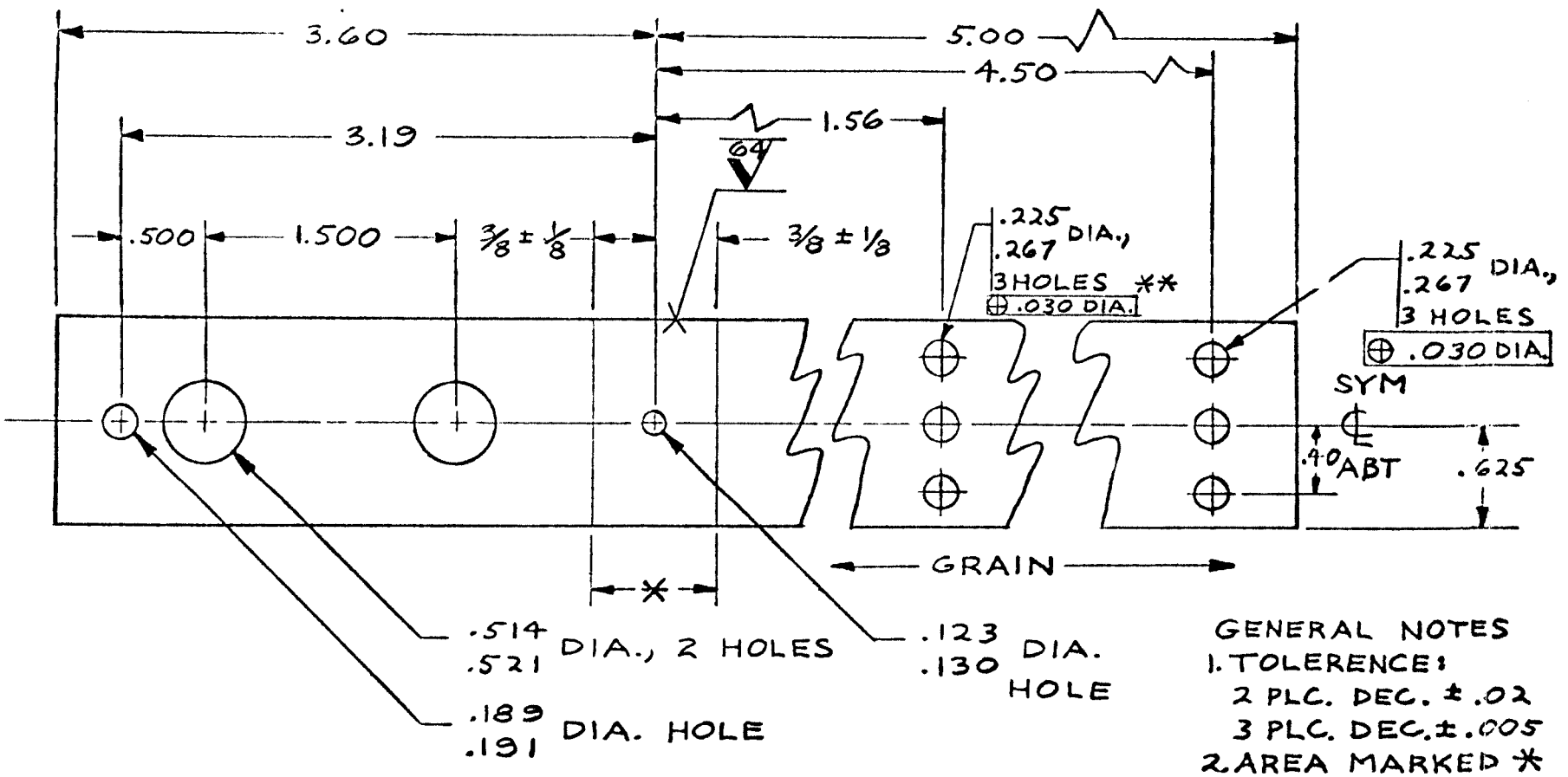

GENERAL NOTES

1. TOLERENCE:
   2 PLC. DEC. ± .02
   3 PLC. DEC. ± .005
2. AREA MARKED * TO BE FREE OF SURFACE DEFECTS (VISIBLE).
3. HOLES MARKED * * APPLY TO PART A2 ONLY

PART NO.	MATERIAL	THICKNESS (STK)	QTY.
A1	2024-T3 AL SHT.	.125	24
A2	2024-T3 AL SHT.	.125	12

Figure 2-1. Fatigue Beam

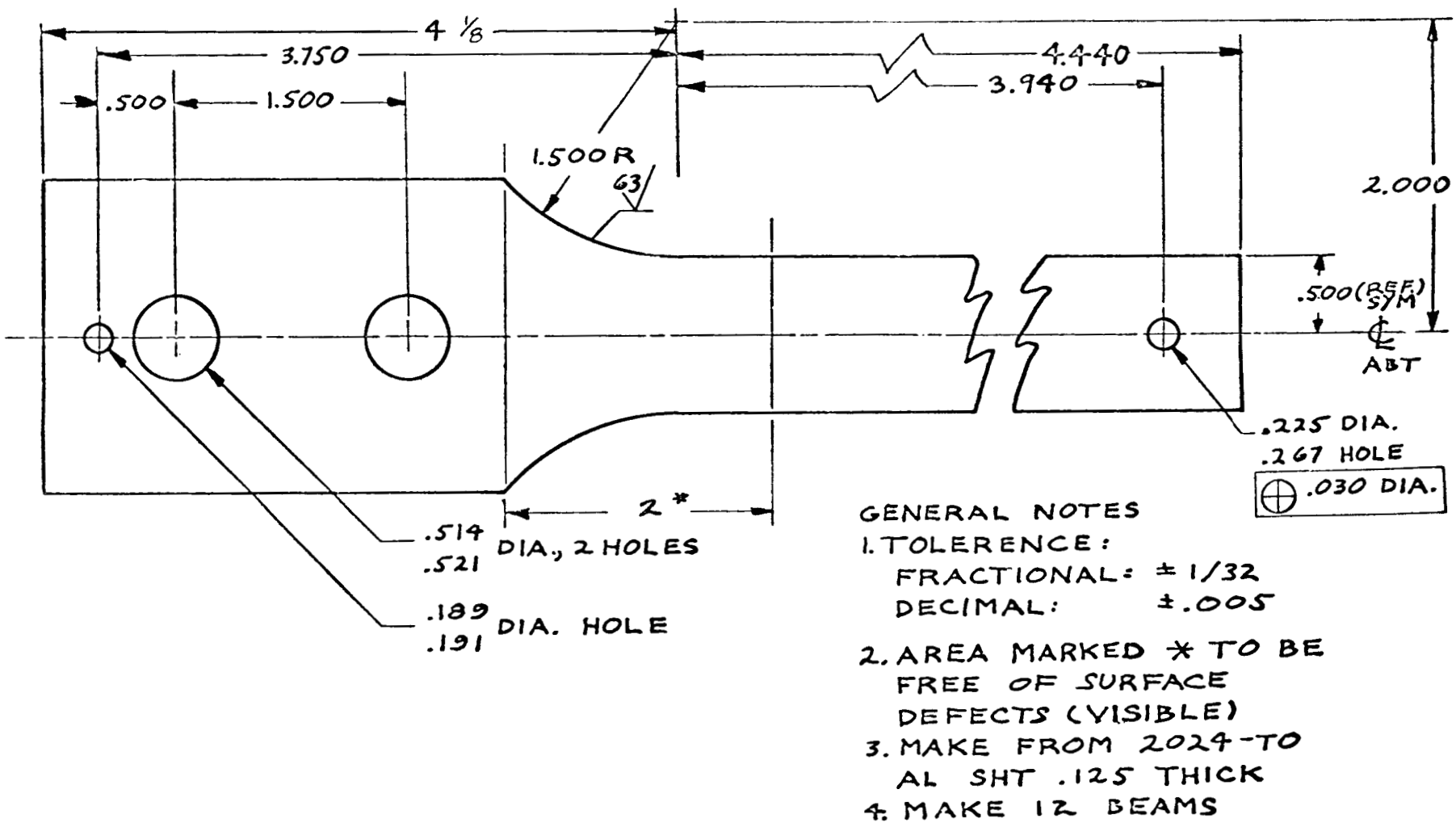

Figure 2-2. Fatigue Beam

Table 2-1

BEAM NOMENCLATURE

Beam No.	End Wt.	Beam No.	Center Wt.	C. G. to Beam Center
Peg Point				
1 - 1	0.222			
2	0.222			
3	0.222			
4	0.222			
5	0.222			
6	0.222			
2 - 1	0.253			
2	0.253			
3	0.253			
3 - 1	0.189			
2	0.189			
3	0.189			
Two Weight		**Two Weight**		
4 - 1	0.189	4 - 1	0.262	
2	0.189	2	0.262	
3	0.189	3	0.262	
4	0.189	4	0.262	
5	0.189	5	0.262	
6	0.189	6	0.262	
5 - 1	0.189	5 - 1	0.293	
2	0.189	2	0.293	
3	0.189	3	0.293	
6 - 1	0.189	6 - 1	0.243	
2	0.189	2	0.243	
3	0.189	3	0.243	
Plain Specimen				
7 - 1	0.210			
2	0.210			
3	0.210			
4	0.210			
5	0.210			
6	0.210			
8 - 1	0.162			
2	0.162			
3	0.162			
4	0.162			
5	0.162			
6	0.162			
Cantilevered Weight				
9 - 1	0.236			1.00
2	0.236			1.00
3	0.236			1.00
10 - 1	0.236			1.31
2	0.236			1.31
3	0.236			1.31
11 - 1	0.236			1.16
2	0.236			1.16
3	0.236			1.16
4	0.236			1.16
5	0.236			1.16
6	0.236			1.16

2.2 TEST SETUP

The specimens were tested to failure in the Douglas test facility where the test equipment consisted of (1) the electrodynamic shaker and its support systems; (2) instrumentation, including strain gages, and accelerometers; (3) recorders, both magnetic tape and oscillograph; and (4) analog data analysis equipment. All test equipment is listed in Table 2-2.

The specimens were mounted 3 or 6 at a time on the C-100 shaker which has a rating of 12,400 force pounds. The shaker was driven by a 90 kVA amplifier, and the system was equalized by an automatic equalizer.

The beams were instrumented with one accelerometer for the peg-point and plain specimens and with two accelerometers for the multi-mode specimens. The accelerometer locations are shown in a typical test arrangement in Figure 2-3.

Table 2-2
INSTRUMENTATION

Quantity	Description	Model
1	Vibration--MB	C-100
1	Oscillator--Ling	Co-10
1	Oscillator--Hewlett-Packard	202B
1	Servo Control Amplifier--Ling	S-10-B
1	True rms Voltmeter--Ballantine	320
1	Servo D&G Amplifier--Ling	S-12-D
1	Frequency Counter--Hewlett-Packard	5512A
1	Oscillograph--CEC	5-124-P4
2	Dynamonitor--Endevco	2702, 2705
6	Accelerometers--Endevco	22126
1	Bruel and Kjaer Spectrometer	2112
1	Bruel and Kjaer Level Recorder	2305
2	Strain Gages	A7-FBE-2
2	Strain Gages	A2217
1	Tape Recorder--Precision Instrument	12114

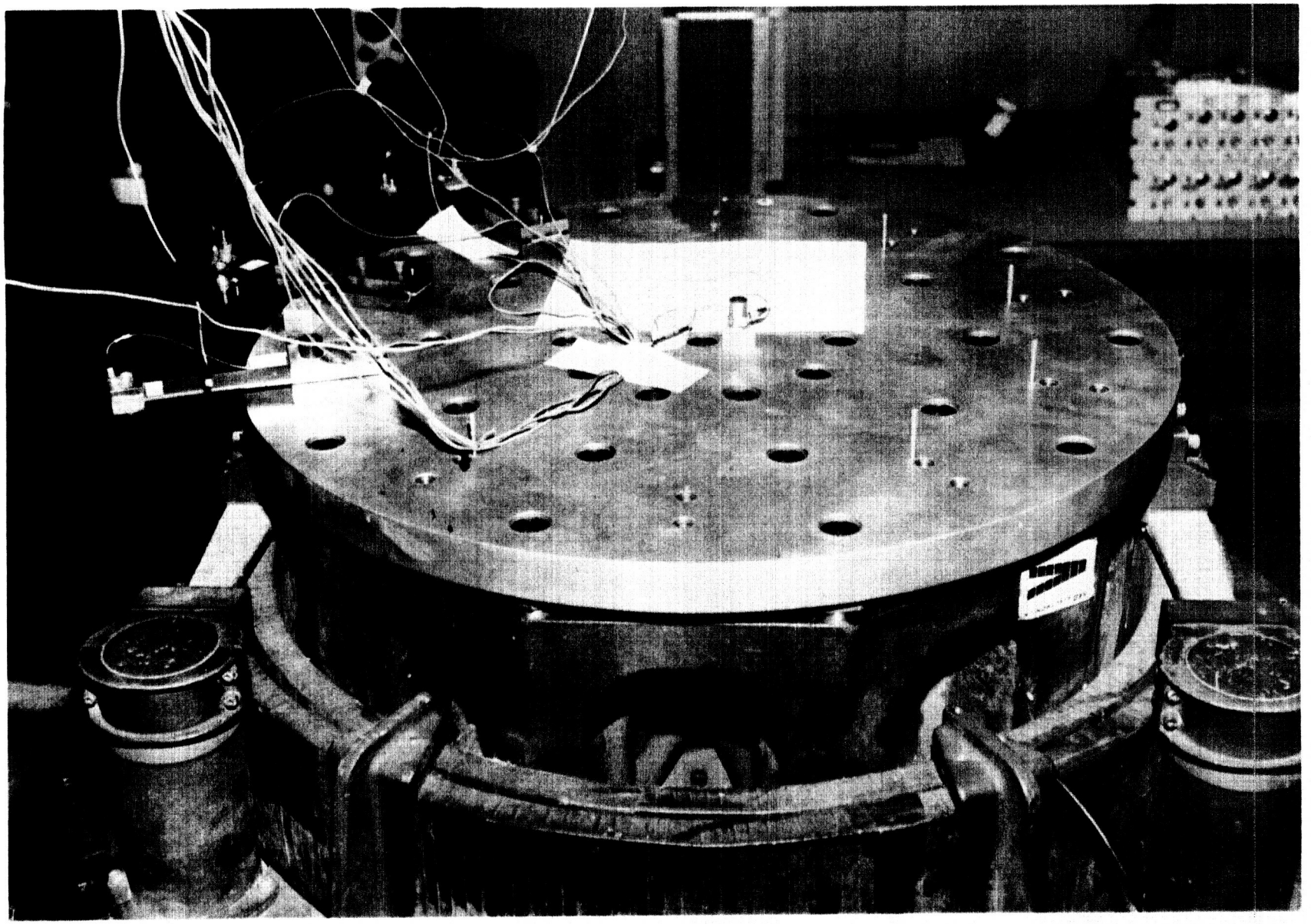

Figure 2-3. Test Specimens

Power spectral density plots for the control accelerometer were obtained with a Technical Products Wave Analyzer. The response data was obtained by filtering the recorded data with a Bruel and Kjaer spectrometer and recording the obtained Grms levels on a level recorder. The overall Grms levels were obtained from the oscillograph record by visually averaging the data over a 30- to 60-sec range. This large sample eliminated the data reduction problem of the previous study, where only 5 to 10 sec of data were reduced. Typical PSD's and oscillographs are shown in Figures 2-4 and 2-5.

2.3 TEST PROCEDURES

The tests on each set of beams were divided into two parts: natural frequency determination and random testing.

2.3.1 Frequency Determination

The first frequency of resonance for each beam was obtained by mounting the beam on the shaker, plucking the beam, and counting the frequency of the signal produced by the beam accelerometer on a Hewlett-Packard electronic counter. This procedure was repeated a sufficient number of times to result in frequency determination to the nearest 1/2 cycle (from 4 to 10 times). Since all of the fundamental frequencies were on the order of 50 cps, the resulting accuracy was 1% for the obtained frequencies. The frequencies for the second modes of the multi-mode beams were obtained by plucking the beam in such a manner that both modes were excited (which, in some cases, took considerable experimentation). The output of the beam accelerometer was recorded on an oscillograph record and the second mode frequency was counted with the use of the first mode as a time scale. At least five first-mode cycles were used, and the second mode cycle count was within a 1/2 cycle. This results in an accuracy of 4% for the torsion modes (f = 150 cps) and 2-1/2 for the second bending modes (f = 300 cps). These include the 1% possible error in the first mode.

2.3.2 Random Testing

After the beam frequencies had been obtained, the beams were tested to failure under an approximately flat random loading from 20 to 500 cps. The

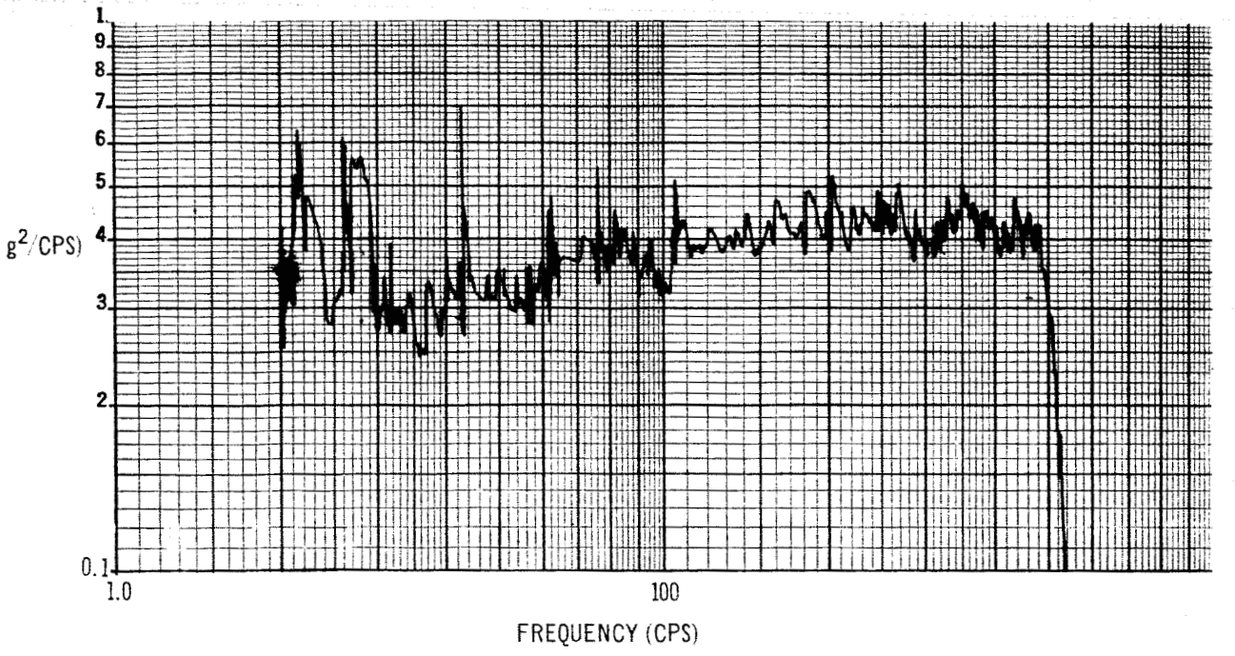

Figure 2-4. Typical Input P.S.D.

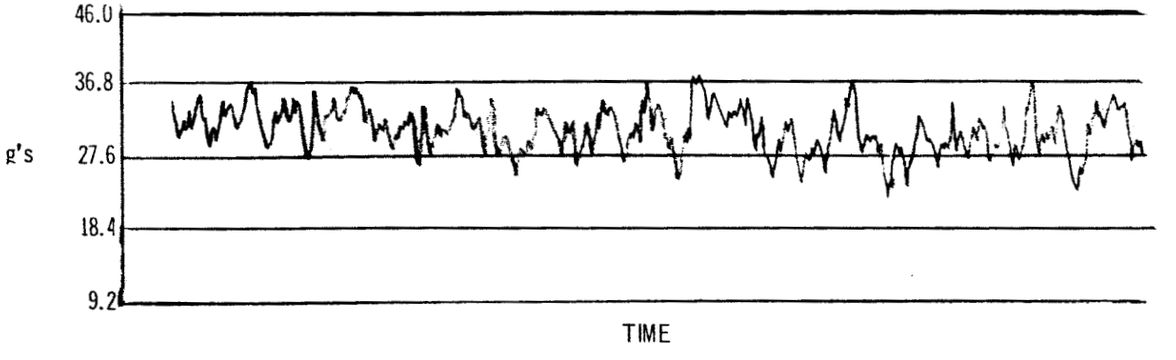

Figure 2-5. Typical Time Dependent GRNS for Beam Response

power spectral density level for the majority of the beams was on the order of 0.5 g^2/cps. However, the actual value to be used was determined prior to each test, based on preceding beam tests to result in optimum failure time.

During the tests the control and all of the beams accelerometer outputs were recorded on magnetic tape for later data reduction and analysis. The test PSD was obtained with a Technical Products Wave Analyzer and the rms response levels were obtained by filtering of the output of the beam accelerometer and reading of the rms levels.

2.4 TEST RESULTS AND ANALYSIS

To obtain the fatigue stress, the data were reduced in the following manner. The rms level from the appropriate beam accelerometer was multiplied by the value of the maximum stress per measured g. This value is a function of frequency for each type of beam and is given in Figure 2-6. In deriving these curves, a stress concentration factor of 1.5 was assumed (Reference 1) for those beams that have a stress raiser. The derivation of Figure 2-6 is given in Appendix A. The number of cycles were obtained by multiplying the observed beam life by the beams natural frequency.

2.4.1 Peg Point Beams

The data obtained from the peg-point beams are presented in Table 2-3 and the fatigue information is plotted on Figure 2-7. The test data presented have been corrected for stress raiser nonlinearity (Figure 2-8); a discussion of this figure is given in Appendix C. In addition, the 95% confidence levels from the comparable specimens reported in Reference 1, and the expected random fatigue curve (Miles k = 1, Reference 2) have been added to this figure.

As can be seen, the corrected data show an appreciable reduction in data scatter and a slight shift of the mean value from the data of Reference 1. This is primarily because of the reduction of a longer time span of data for tip response rms levels.

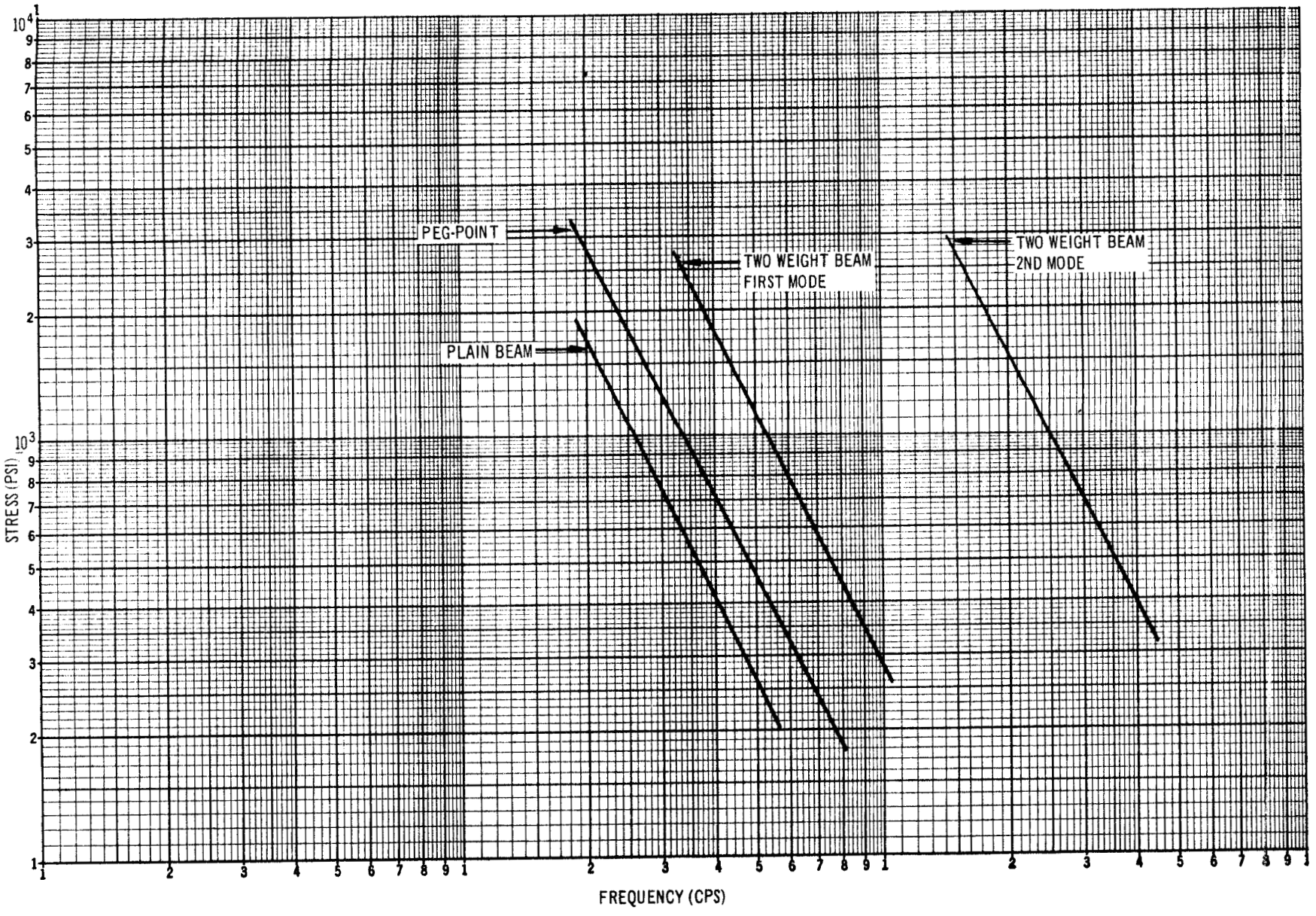

Figure 2-6. Stress Per G for Beam Specimen

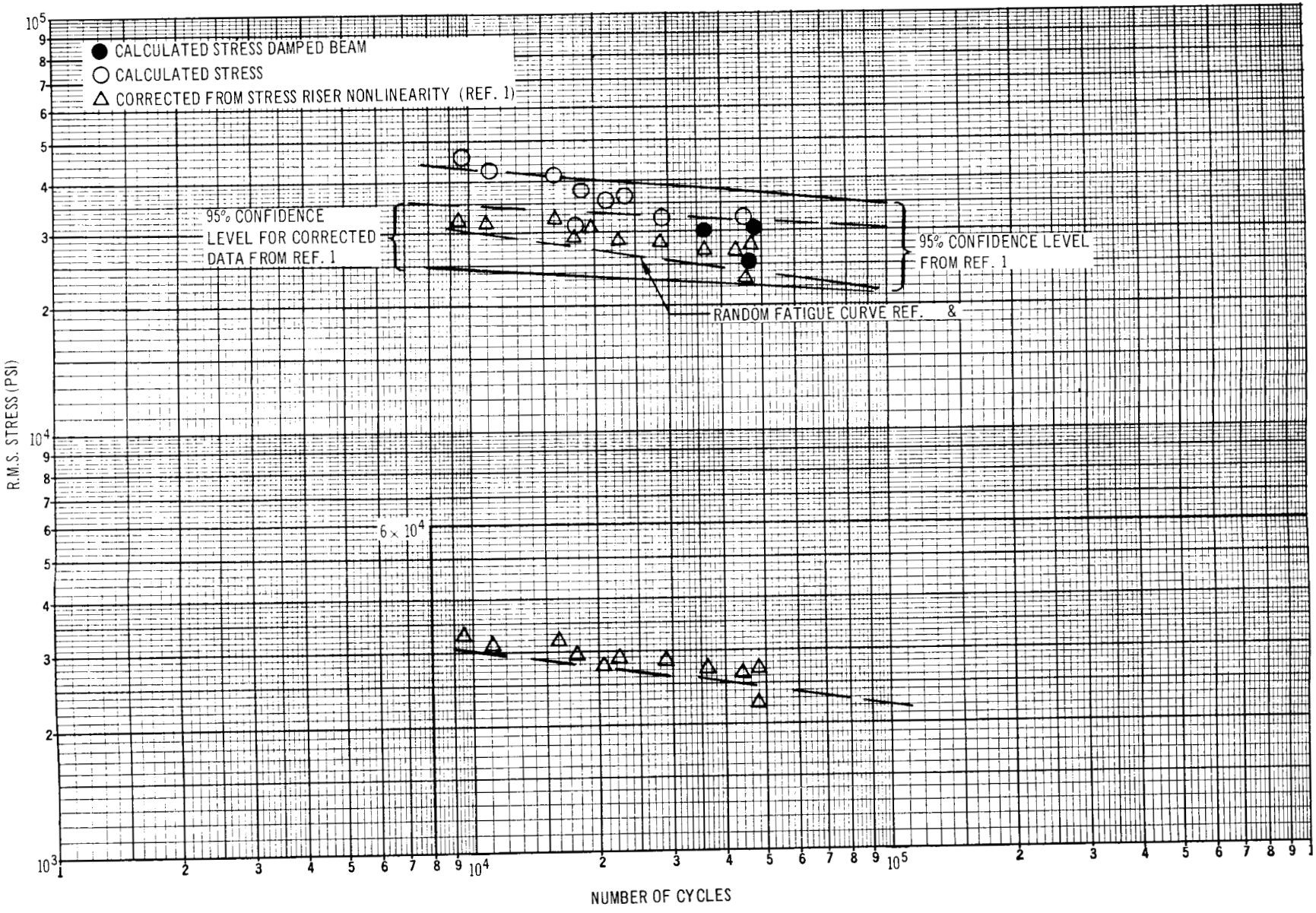

Figure 2-7. Random Fatigue Data – Peg-Point Specimen

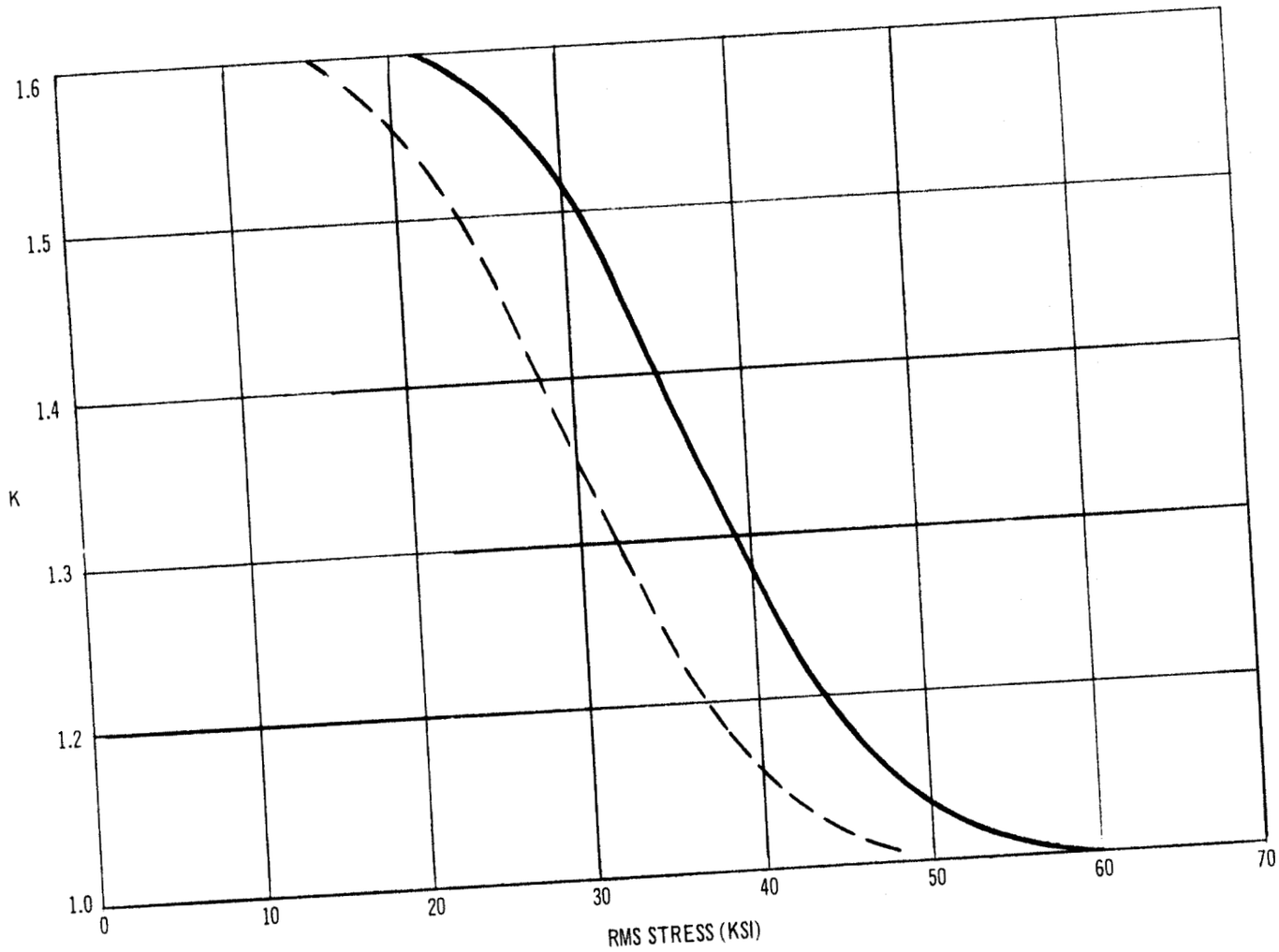

Figure 2-8. Non-Linear Stress Concentration Factor for 2024-T4 Aluminum

Table 2-3

PEG POINT BEAM DATA

Beam No.	f	grms	S (psi/g)	Srms (Kpsi)	Life (min.)	Cycles x 10^{-4}
1-1*	42.5	40	620	25	18.5	4.72
2*	43	50	620	31	18.0	4.64
3*	43.5	50	605	30	14.0	3.68
4	42.0					
5	42.0	50	630	32	7.0	1.77
6	44.0	65	580	38	7.5	1.98
2-1	42.0	50	640	32	18.0	4.50
2	41.0	65	700	44.5	4.5	1.10
3	41.0	60	700	42	6.5	1.60
4	41.0	65	700	45.5	4.0	0.99
3-1	46.5	75	485	36.5	7.5	2.10
2	46.5	75	485	36.5	7.5	2.10
3	46.5	70	485	34	10.0	2.79

*Damping tape was added.

Note the close agreement between the data corrected for the stress raiser nonlinearity and the random fatigue curve obtained using Miles' method and the assumption of the k in Miles' expression $[F(k\alpha/2 + 1)]^{1/k\alpha}$ is unity. This indicates that the stress correction used is reasonable and that the value for the hole fatigue stress concentration (k_f), as obtained by (Reference 3),

$$k_f = (k_t + \alpha/r)/(1 + \alpha/r)$$

where

K_t = static stress concentration factor

α = material content = 0.05 for AL

r = radius

results in fatigue stresses which agrees with the presented Miles' random fatigue curve. This indicates that the above fatigue stress concentration factor yields meaningful results when compared to random fatigue curves computed by the method of Reference 2 if the k in the $k\alpha$ term is assumed to be unity.

As discussed in the introduction to this section, the purpose of the previous study was to evaluate an experimentally determined K value for use in the expression

$$\sigma_{eq} = K K_{dyn} \sigma_o \text{ Load}$$

The data obtained in this study have been replotted in Figure 2-9 and compared to the 95% confidence levels previously obtained for K. The data do fall well within the values previously obtained. Although they indicate a slight change in mean value and a reduction in scatter, as previously indicated, there are not sufficient data to warrant making the indicated minor corrections.

2.4.2 Multi-Bending Mode Beams

The data obtained from the two weight beams are listed in Table 2-4 and presented in Figure 2-10. In this case, the center accelerometer (B) rather than the tip accelerometer was used to define the stress levels, as discussed in Appendix A. This accelerometer was used because the center accelerometer response more closely reflects the effect of both masses and is closer to the high stress point.

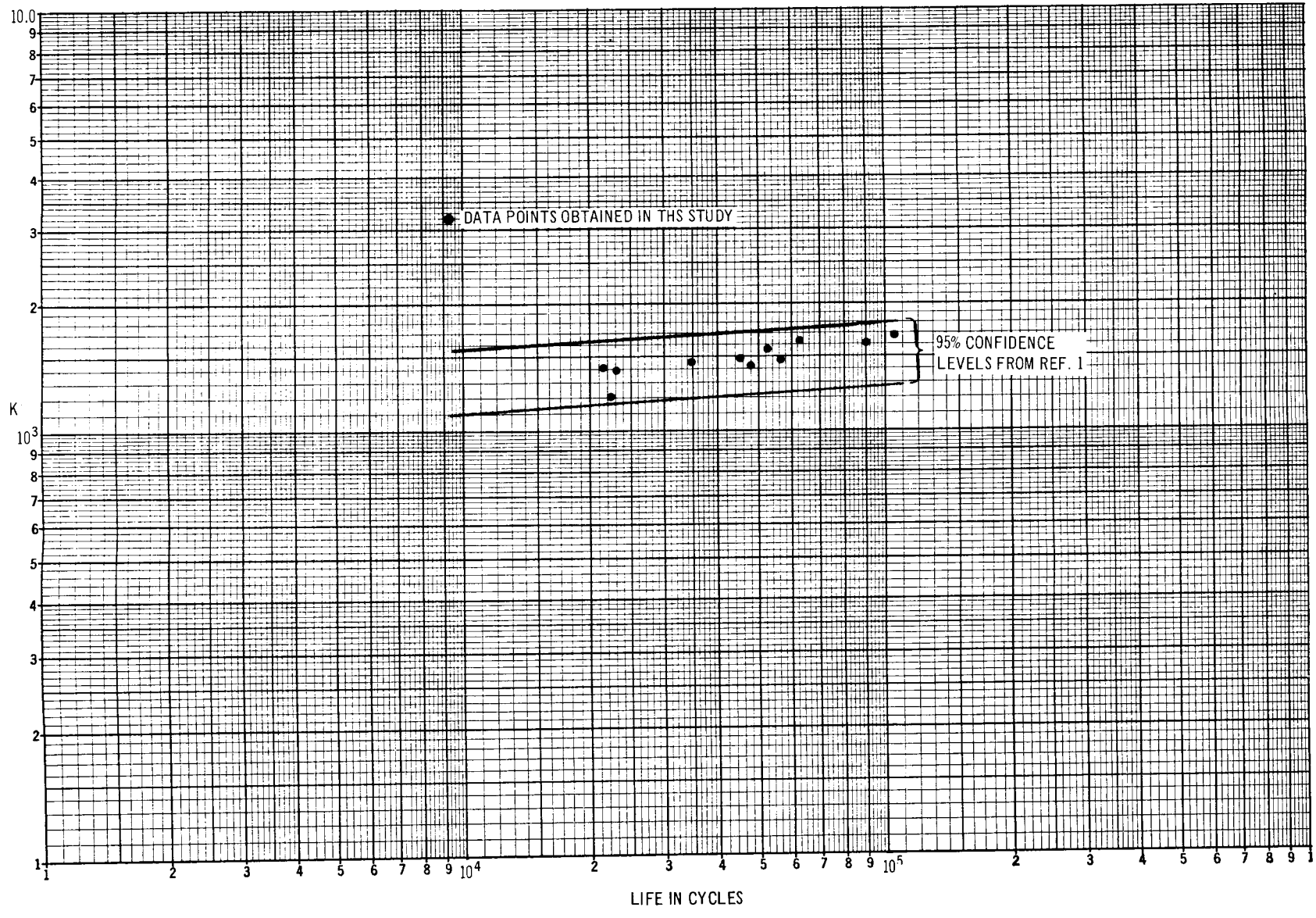

Figure 2-9. 2024-T4 Aluminum Design Factor K

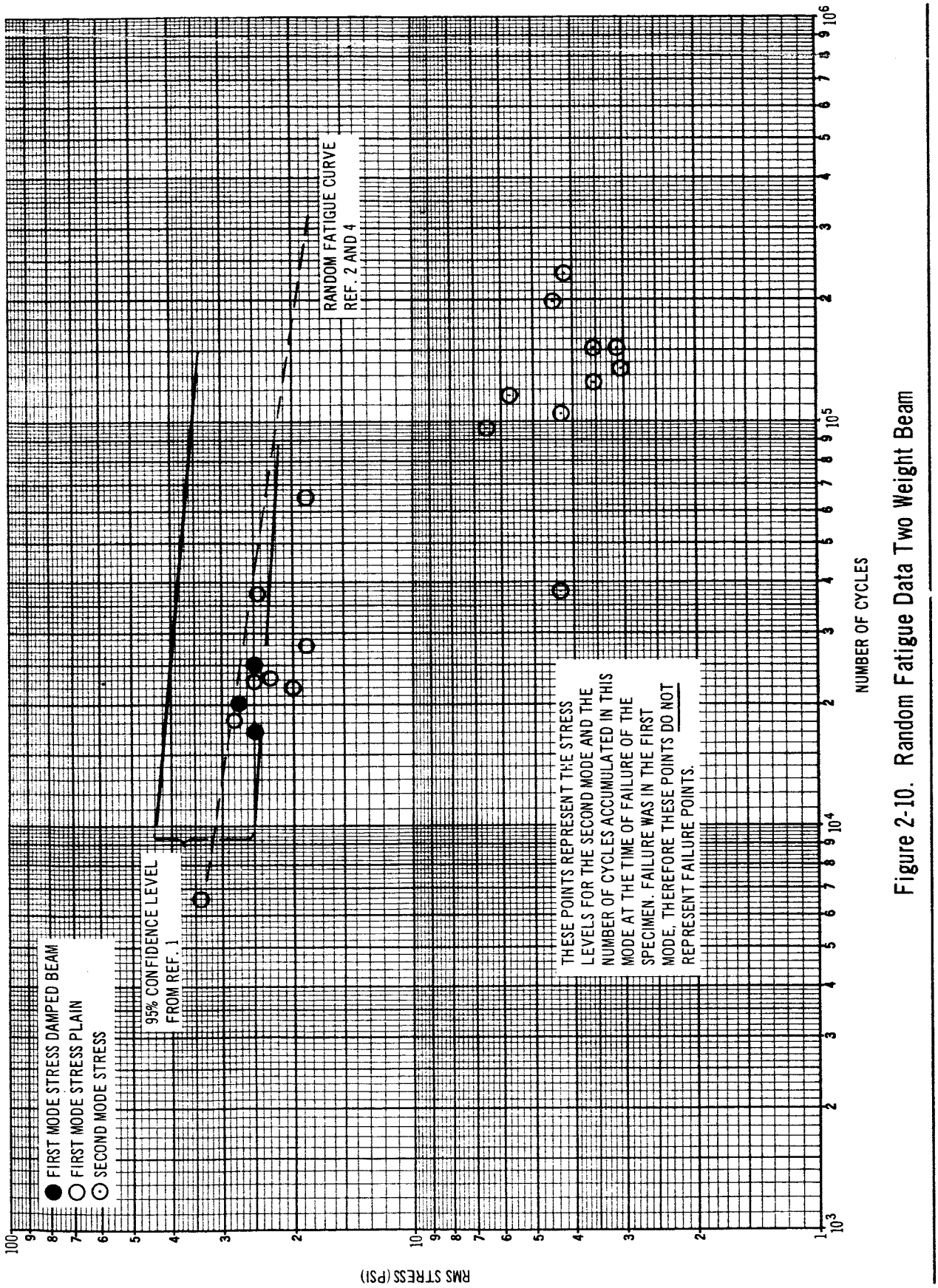

Figure 2-10. Random Fatigue Data Two Weight Beam

Table 2-4

TWO WEIGHT BEAM DATA

Beam No.	f	grms R	S (KSI)/R_g	Srms (KSI)	Life (min.)	Cycles x 10^{-4}
FIRST MODE						
4-1	51.0	24	1.15	28.0	6.5	2.0
2	48.5	19	1.30	25.0	6.0	1.7
3	52.0	22	1.15	25.0	8.0	2.5
4	52.0	22	1.15	25.0	12.0	3.7
5	52.0	30	1.15	34.0	2.0	0.65
6	52.0	16	1.15	18.5	20.0	0.65
5-1	48.0					
2	47.5	16	1.40	25.0	8.0	2.3
3	49.0	22	1.25	28.0	6.0	1.8
6-1	53.0	19	1.10	20.0	7.0	2.2
2	52.0	17	1.15	18.5	9.0	2.8
3	52.0	20	1.15	23.0	8.0	2.4
SECOND MODE						
4-1	306	55	0.063	3.5	6.5	12.5
2	291	60	0.071	4.3	6.0	10.5
3	312	55	0.063	3.5	8.0	15.0
4	312	65	0.063	4.1	12.0	22.5
5	312	75	0.063	4.3	2.0	3.7
6	312	55	0.063	3.5	20.0	37.0
5-1	240					
2	238	55	0.105	5.8	8.0	11.5
3	245	65	0.100	6.5	6.0	9.5
6-1	318	50	0.060	3.0	7.0	13.5
2	312	70	0.063	4.4	9.0	19.5
3	312	50	0.063	3.1	8.0	15.0

Comparison of these data to those for the peg-point configuration (Figure 2-7) indicates that there is an effect of the second mode on the fatigue data.

The actual time history of the stress is approximately that shown in Figure 2-11.

Fatigue data and theory indicate that the approximate fatigue accumulated as the result of an oscillatory stress (stress reversal) is dependent on the amplitude of the stress and prestress, but independent of the wave form. Therefore, if the fatigue resulting from the second-mode stress oscillating about the first-mode stress is neglected, then an equivalent amount of fatigue should be accumulated by a time history or wave motion that envelopes the maximum of the combination (the dashed line in Figure 2-11). Neglecting the fatigue resulting from the second mode should be a good assumption, providing its stress amplitude is much less than that of the first mode. This satisfies the limit where the second mode stress goes to zero. Assuming this is the case and recalling that the second-mode stress is caused by a random response, then the average increase for each cycle of the first mode will be the rms value of the second mode.

The stress caused by the first mode is also random in nature and is assumed to have a Rayleigh peak distribution. Increasing each peak of the first mode by the rms of the second would result in an equivalent time history with a distorted Rayleigh peak distribution which would be difficult to handle analytically. However, converting the first mode-stress to an equivalent sinusoid fatigue level (approximately 2 rms sin ωt), adding the rms level of the second mode and converting back to the random level seems to be a reasonable approach. This is approximately the same as adding $rms_1 + (rms_2/2) = rms_{EQ}$. This correction is only hypothesized for the cases (1) that have large frequency differences, and (2) in which the first-mode stresses are high compared to those of second mode. These two restrictions, as well as hypothesized multi-mode damage theory excluded by those restrictions, are presented and discussed in Appendix B.

This correction, when applied to the two-weight-beam data, results in the points shown in the upper portion of Figure 2-12. The agreement with the

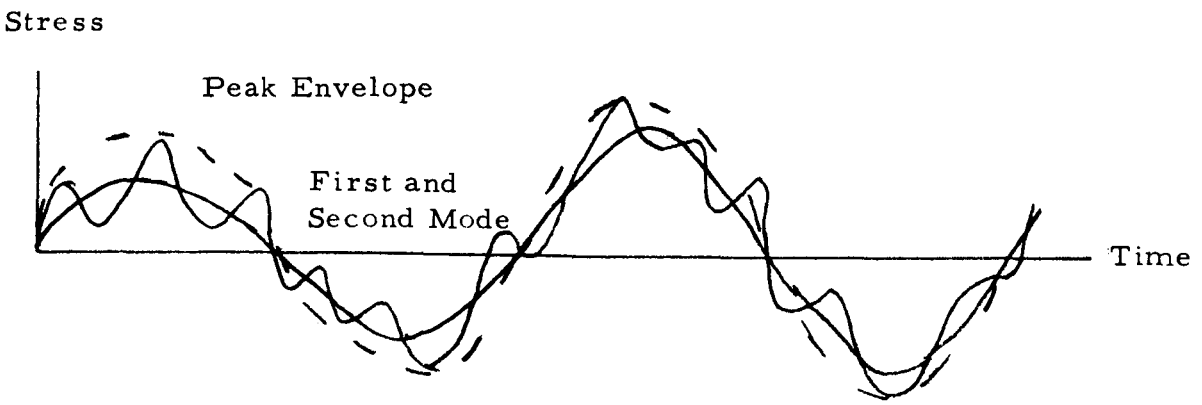

Figure 2-11. Approximate Stress Time History

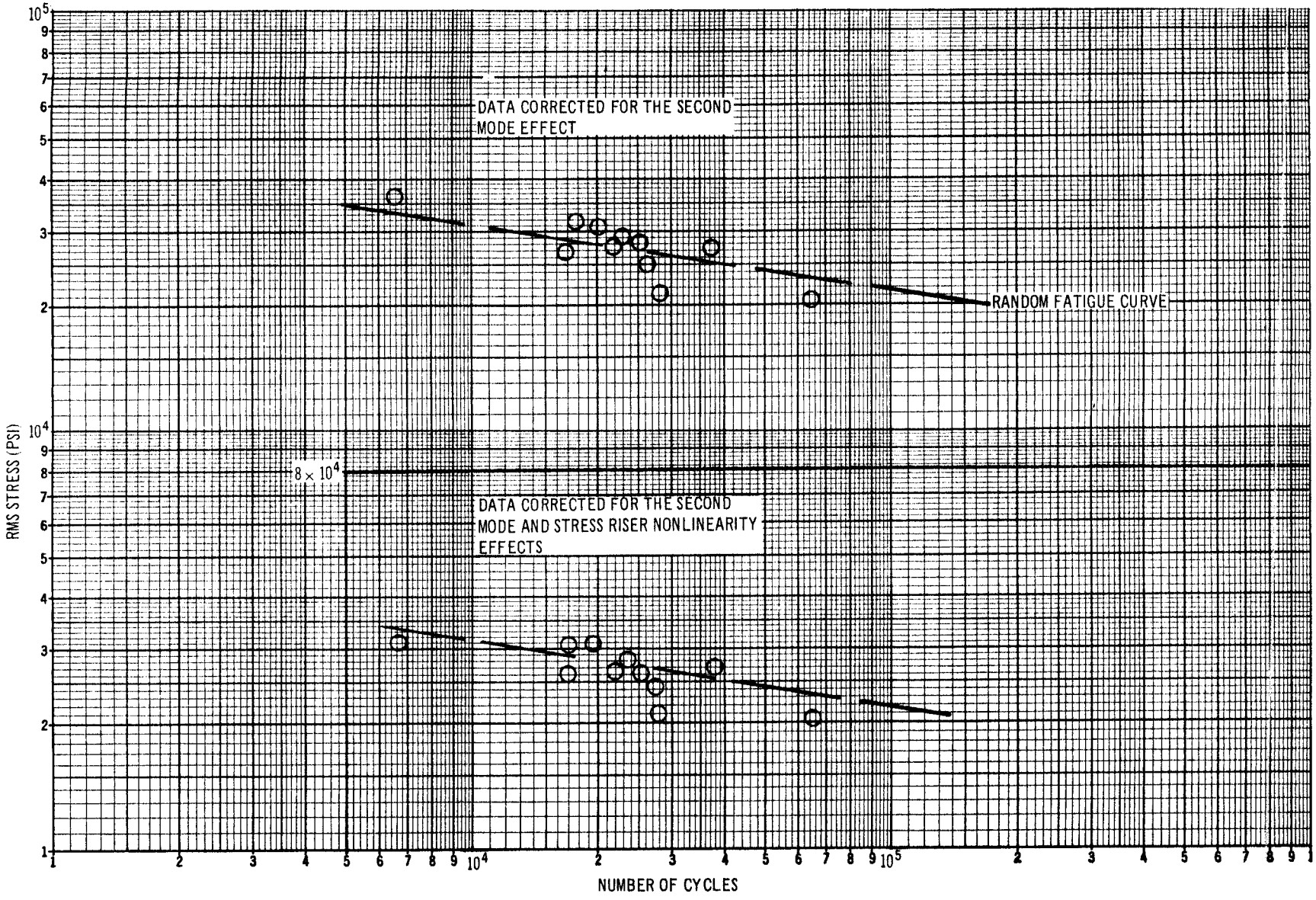

Figure 2-12. Two Weight Beam Data Corrected for Multimode Effect

predicted curve and the peg point data is much improved and indicates that the correction is of the proper magnitude. However, the stress nonlinearity correction should be made prior to comparison to corrected data for the first mode. This correction results in the data shown in the lower portion of Figure 2-11. This improves the slope of the experimental data but it does drop the data slightly below the random fatigue curve. However, the data remain very close to the proper magnitude. The existing discrepancy could easily be caused by the fatigue resulting from the second mode oscillation about the high prestress of the first mode which was neglected.

In general, the correction seems to be good. However, this conclusion is based on a limited amount of specialized data. Additional analytical and experimental work is definitely required to substantiate the basic approach, range of application, and to hypothesize and to check, experimentally, modal combination methods beyond the range of application of the above. As mentioned previously, methods of corrections for the majority of encountered cases have been hypothesized and are presented in Appendix B.

2.4.3 Torsion-Bending Beam

The data obtained from the cantilevered weight beam and the stress per tip g (Tg), for the bending modes and stress per tip radian, S/θ, for the torsion modes are presented in Table 2-5. The accelerometer locations are approximately those shown below.

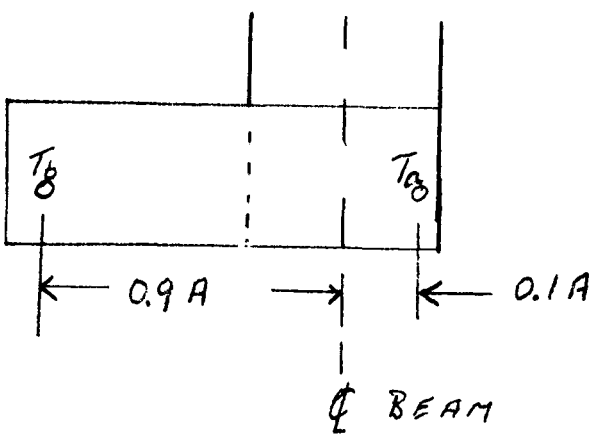

The spacing is sufficiently accurate to obtain the first mode bending stress. Therefore, the acceleration for the center of the beam was assumed to be

$$G = \frac{9\,T_a + B}{10}$$

$$G = T_a + \frac{B - T_a}{0.1}$$

The S/g, the same as that for the peg point specimens, were obtained from Figure 2-6 and the stress per unit rotation (S/θ) is derived as being 1.13×10^5 psi in Appendix C. In addition, it is shown in Appendix C that for radian bending stress much larger than torsional stress, the principal stress is approximately $rms_M = (rms_1^2 + 2rms_2^2)^{1/2}$.

The effect of the second mode (torsional mode) will be the result of the component of the stress which is in the direction of the first mode bending stress. The effects of the bending stresses for the torsion mode have been added to the effects of the stresses of the first mode, entered under column Srms Cor for the first mode in Table 2-5 and are plotted in Figure 2-13. In addition, the data have been corrected for stress riser nonlinear and entered on the graph. Also, these data have been separated from the other data and replotted for clarity.

The corrected data show good agreement with the predicted random curve and the peg point data indicating that all of the fatigue, within the accuracy of the data, was accounted for in the data reduction.

2.4.4 Plain Specimen

The data obtained from the plain specimens, including strains from four strain gages and the stress per tip g is presented in Table 2-6. The data, the available sinusoidal fatigue curve, and the Miles fatigue curve are shown in Figure 2-14. The stresses were actually measured 1 in. forward of the high stress point, but the resulting stresses were corrected prior to being entered in the table and the curve. Not a large but a random discrepancy

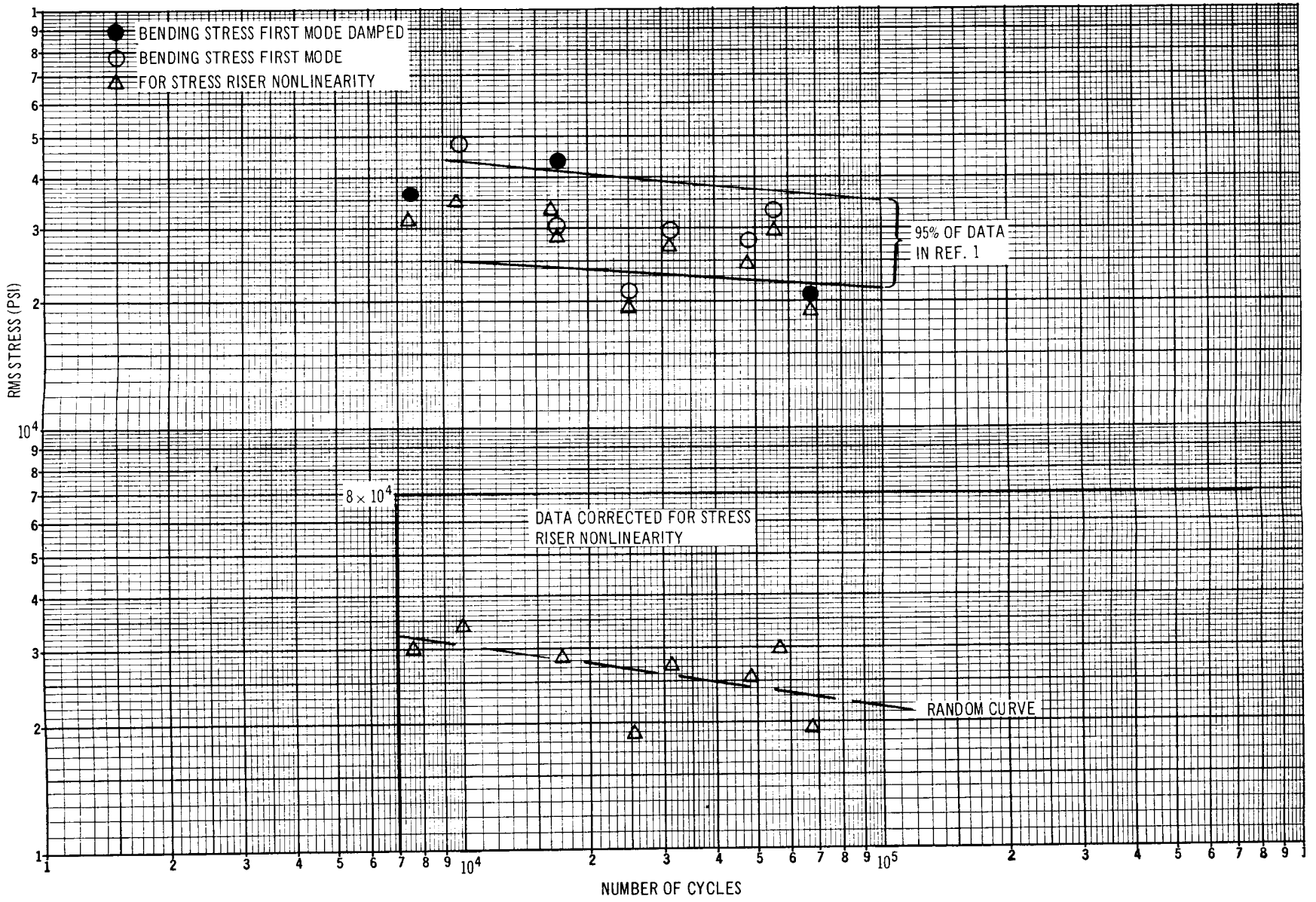

Figure 2-13. Random Fatigue Data – Cantilivered Weight Beam

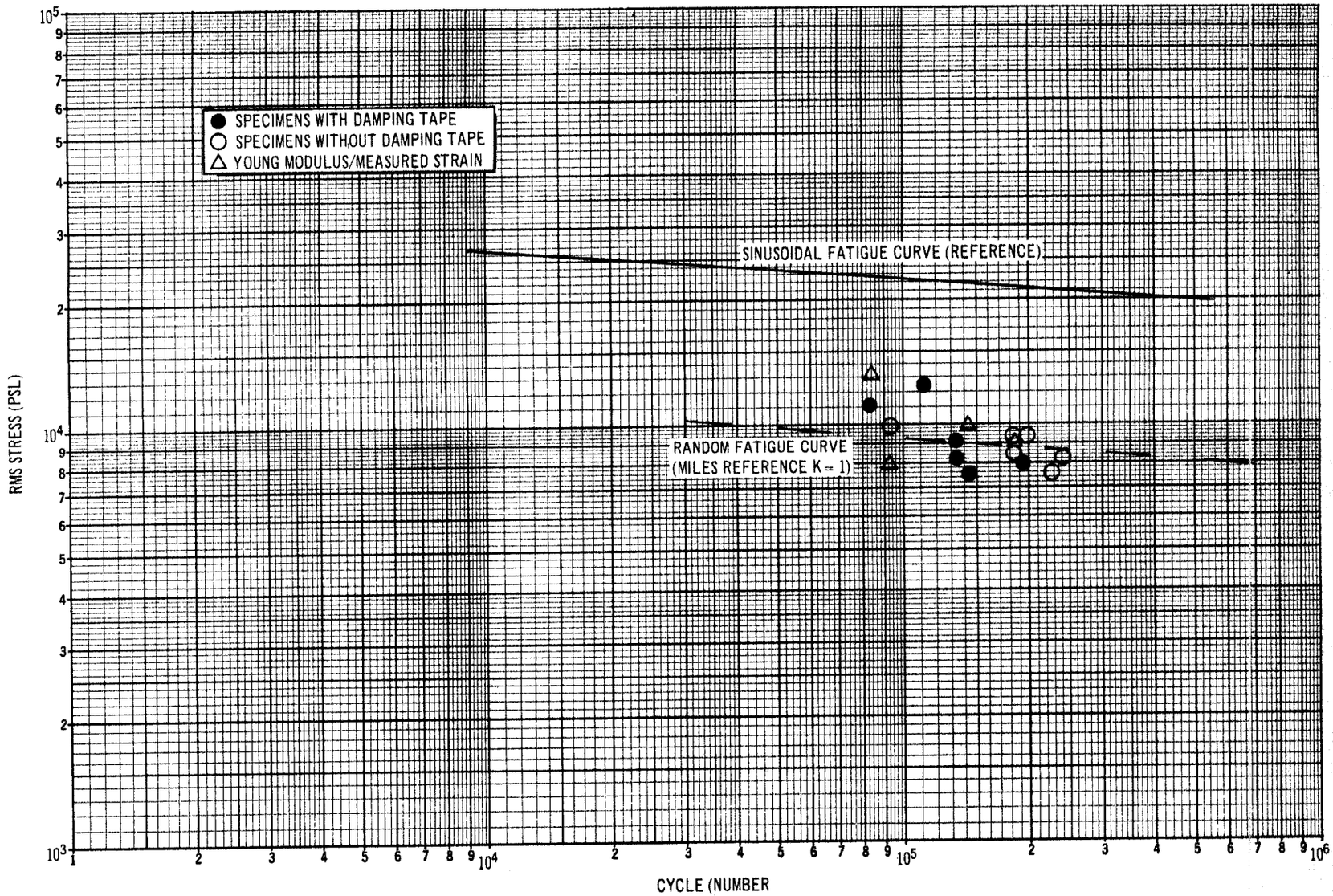

Figure 2-14. Plain Specimen Fatigue Data (Al 2024-TD)

Tab

CANTILEVER

Beam No.	F	TaGs	Bgs	tGs	B-T^{in}/din	θrms
BENDING MODE						
9-1	41	60	65	61	0.08/2.93	2.7×10^{-2}
2	39		Beam Failed at Root Data Omitted			
3	41	50	80	53	0.17/2.85	6.0
10-1	41	26	45	28	0.12/3.53	3.4
2	39	60	75	63	0.1/3.53	2.7
3	41.5					
11-1	40.5	35	50	38	0.08/3.25	2.4
2	39	41	50	43	0.08/3.28	1.8
3	41	27	40	30	0.07/3.32	2.1
4	39					
5	40.5	40	45	41	0.08/3.23	2.5
6	41	45	50	42	0.03/3.25	0.92
TORSION						
9-1	164	14	16	0.011/2.93	3.8×10^{-3}	
2	156					
3	164	16	19	0.0125/2.85	4.4	
10-1	140	19	25	0.022/3.53	6.2	
2	133	25	29	0.03/3.35	8.5	
3	141	22	25	0.025/3.48	7.2	
11-1	162	17	17	0.012/3.25	3.7	
2	156	20	20	0.016/3.28	4.9	
3	164	16	22	0.014/3.32	4.2	
4	156					
5	162		20	0.016/3.23	4.9	
6	164	19		0.016/3.25	4.9	

le 2-5

ED BEAM DATA

S/G	S/θ	Sx (KS)	Sθ (KS1)	Srms	N x 10^4	Srms Cor
680	1.13 x 10^5	41.5	3.0	41.5	1.7	42
	1.13 x 10^5					
680	1.13 x 10^5	36	7.0	37	0.74	37.5
680	1.13 x 10^5	19	4.0	19.5	2.5	20.5
750	1.13 x 10^5	47	3	47	0.98	48
	1.13 x 10^5					
710	1.13 x 10^5	27	3	27	4.8	27.5
750	1.13 x 10^5	32	2	32	5.6	33.
680	1.13 x 10^5	20	2	20	6.9	20.5
	1.13 x 10^5					
710	1.13 x 10^5	29	3	29	3.1	29.5
680	1.13 x 10^5	29	1	29	1.7	30

				Sg
11	1.13 x 10^5	40	S > 1	0.44
	1.13 x 10^5			0.65
13	1.13 x 10^5	50	S > 1	0.90
15	1.13 x 10^5	60	S > 1	1.20
20	1.13 x 10^5	60	S > 1	1.20
17	1.13 x 10^5	60	S > 1	1.00
14	1.13 x 10^5	40	S > 1	0.56
16	1.13 x 10^5	50	S > 1	0.80
12	1.13 x 10^5	40	S > 1	0.48
	1.13 x 10^5			
16	1.13 x 10^5	40	S > 1	0.640
15	1.13 x 10^5	50	S > 1	0.75

2

Table 2-6

PLAIN SPECIMEN DATA

Beam No.	f	G	S/G	St Cal	N	St. Measured
7-1	42	32		11.200	7.5	13.060
2	40.5	24	370	8.900	13.4	
3	42	33	350	11.500	10.6	
4	42	27	350	9.500	9.3	8.000
5	41	24	360	8.650	18.2	
6	42	25	350	8.750	19.5	
8-1	48	27	280	7.850	14.5	10.880
2	44.5	25	320	8.000	19.6	
3	47	28	290	8.100	13.2	
4	46.5	27	290	7.850	18.2	7870
5	45	25	310	7.750	22.8	
6	47	29	290	8.400	24.0	

was observed between the measured and calculated stresses. This condition cannot be completely attributed to the test, and data calculated values are more accurate because of the inherent difficulties in strain gaging a smooth unroughed surface.

The data show a reasonable agreement with the predicted fatigue curve. In comparing the data to the curve, it must be recalled that a minimal amount of fatigue data is available for 2024-TO aluminum. Therefore, the fatigue curve used for comparison is not so accurate as that previously used for 2024-T4. In addition, the specimens with damping tape display more scatter than those without the tape. It is felt that this was caused by bonding difficulties with the tape and not by the added damping itself. Considering just the specimens without the tape, it does appear that the plain specimens do result in sufficiently good data to be of use in the study of stress raisers in random fatigue.

Section 3
BRACKET STUDY

3.1 TEST SPECIMENS

Secondary space vehicle structures and, in particular, support bracketry do not lend themselves to simplified accurate dynamic analyses because of their complexity and varied configurations. Such analyses are not only complex but also time-consuming. Yet the preliminary analysis required to effect optimum design of such structure to ensure minimum weight and maximum reliability is of the utmost importance. It therefore becomes necessary to equip the designer with simple but accurate techniques for establishing optimum designs during early development of a vehicle. This study was conducted to establish the feasibility of two modifications of such a simplified approach. These are (1) the design factor approach reported in Reference 1 as it can be applied in the design of brackets and (2) the construction of nomograms to aid in the design of typical brackets.

To establish these feasibilities, two sets of six brackets each were designed, analyzed, and then tested to failure. Because the analytical work is recorded in its entirety in Appendix D, it will be discussed here only where pertinent. The majority of the text will discuss the experimental work and results.

The two bracket configurations chosen were a simple hat bracket (Figure 3-1) and a shelf-type bracket (Figure 3-2), each having an attached mass (Figure 3-3). The hat section was chosen because of its simplicity and common use. The shelf was chosen because it is a sufficiently complex bracket to prove the general applicability of the design factor and nomograph approaches to a broader spectrum of brackets and because it is a fairly common configuration.

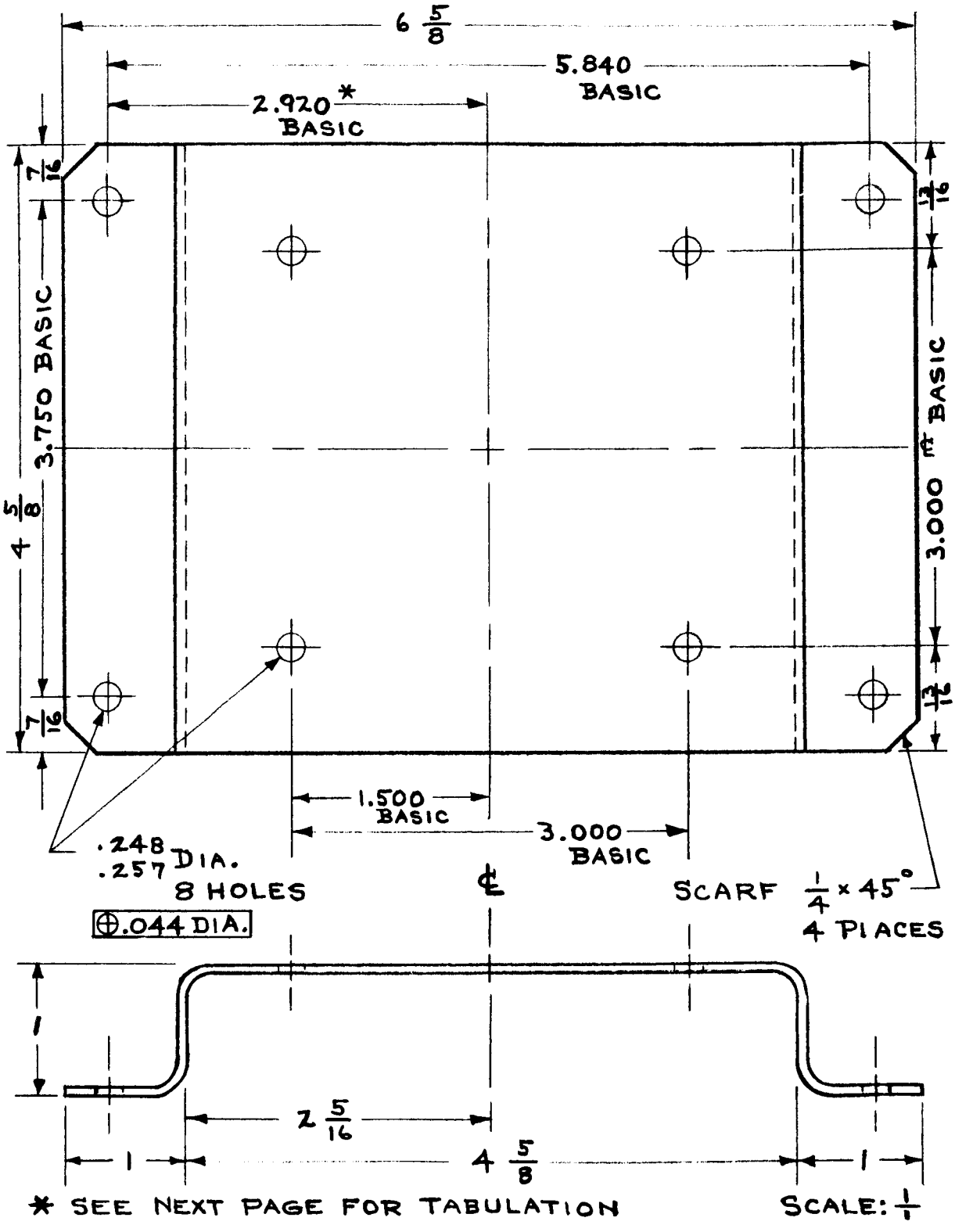

Figure 3-1. Hat Section Support for 5-lb Block

STOCK SIZE	MATERIAL DESCRIPTION	MATERIAL SPECIFICATION
.063×5×9	AL. SHEET 6061-T6	QQ-A-250/11 TEMP. T6

GENERAL NOTES

1. UNLESS OTHERWISE SPECIFIED
   a. DIMENSIONS ARE IN INCHES.
   b. FRACTION TOLERANCES ARE $\pm \frac{1}{32}$
   c. DECIMAL TOLERANCES ARE $\pm$ .010
   d. ANGLE TOLERANCES ARE $\pm \frac{1}{2}^{\circ}$
2. ALL DIMENSIONS ARE ON SURFACE OF PART.
3. ALL BEND RADII ARE 0.19 IN.
4. ATTACHMENTS:
   a. NAS -603 SCREWS PROCUREMENT SPEC. MIL-S-7839
   b. MS 35338-43 LOCK (SPLIT) WASHERS UNDER SCREW HEADS
   c. AN960-10 FLAT WASHERS UNDER LOCK WASHERS
   d. TORQUE SCREWS TO 20-25 IN.LB. FOR MAX. FRICTION

MAXIMUM DIMENSIONS (REF.)

℄ HAT TO INSIDE OF SHEET	$2\frac{5}{16} \pm \frac{1}{32}$	=	2.344 IN.
SHEET GAGE	$.063 \pm .004$	=	.067
BEND RADIUS	$.190 \pm .010$	=	.200
WASHER WIDTH	$\frac{1}{2}\left[\left(.438 \pm \frac{.020}{.005}\right) - \left(.203 \pm .010\right)\right]$	=	.133
HOLE RADIUS	$.257/2$	=	.129
HOLE TRUE POSITION + MISC.	$.044 + .003$	=	.047
MAX. DIMENSION - ℄ HAT SEC. TO ℄ HOLE		=	2.920

Figure 3-1. Hat S ction Support for 5-lb Block (Continued).

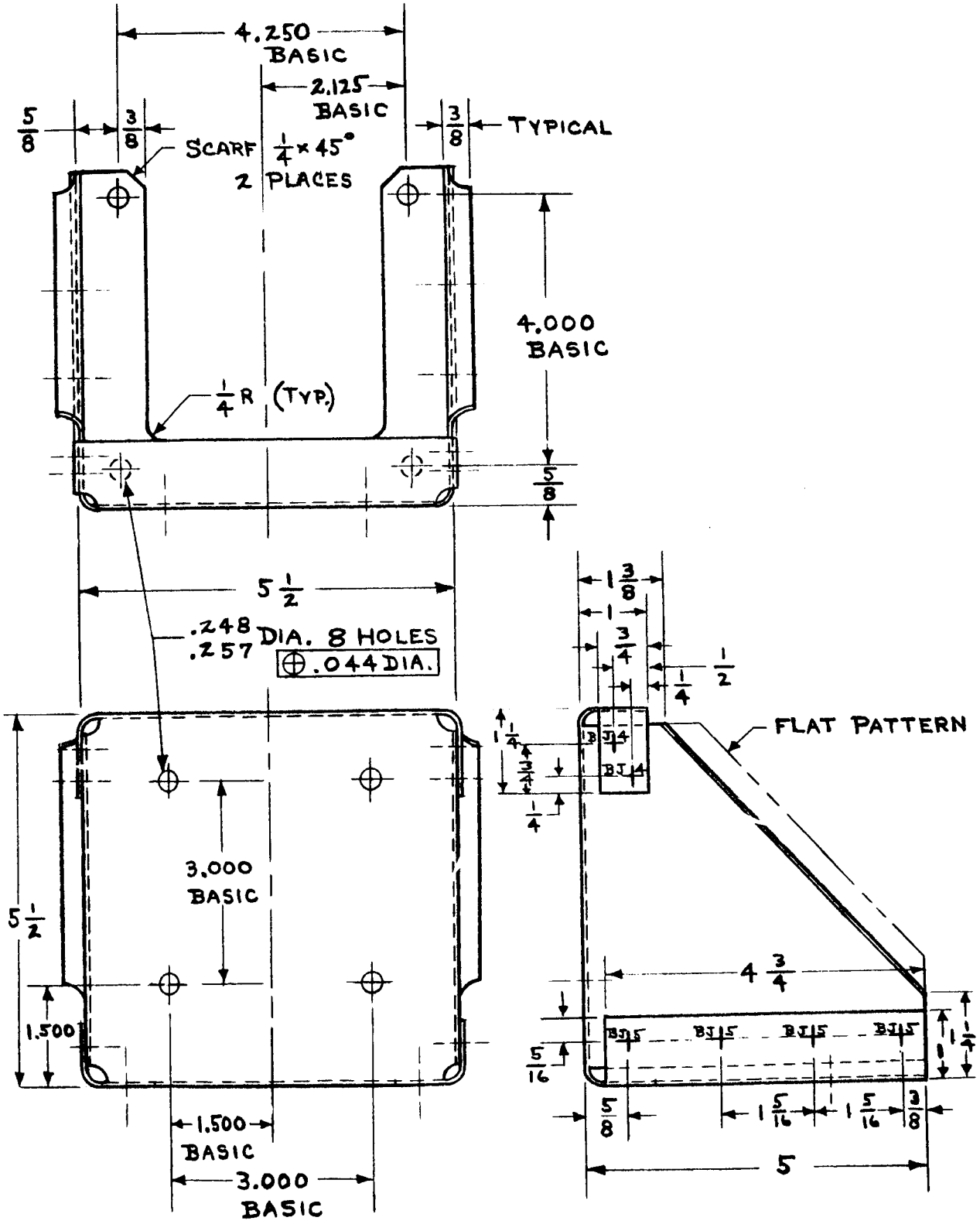

Figure 3-2. Cantilever Mount for 5-lb Block

STOCK SIZE	MATERIAL DESCRIPTION	MATERIAL SPECIFICATION
.063×12×17	AL. SHEET 6061-T6	QQ-A-250/11 TEMP. T6

GENERAL NOTES

1. UNLESS OTHERWISE SPECIFIED:
   a. DIMENSIONS ARE IN INCHES.
   b. FRACTION TOLERANCES ARE $\pm \frac{1}{32}$
   c. DECIMAL TOLERANCES ARE $\pm .010$
   d. ANGLE TOLERANCES ARE $\pm \frac{1^\circ}{2}$
2. ALL DIMENSIONS ARE ON SURFACE OF PART.
3. BEND RELIEFS ARE PER SO-219
4. BEND RADII ARE 0.19 IN.
5. PREPARE HOLES FOR RIVETS PER IP00092
6. INSTALL RIVETS PER SO 217
7. MS 20470 AD4 RIVET INDICATED THUS BJ|4
8. MS 20470 AD5 RIVET INDICATED THUS BJ|5
9. ATTACHMENTS:
   a. NAS-603 SCREWS PROCUREMENT SPEC. MIL-S-7839
   b. MS 35338-43 LOCK (SPLIT) WASHERS UNDER SCREW HEADS
   c. AN 960-10 FLAT WASHERS UNDER LOCK WASHERS
   d. TORQUE SCREWS TO 20-25 IN. LB. FOR MAX. FRICTION

Figure 3-2. Cantilever Mount for 5-lb Block (Continued)

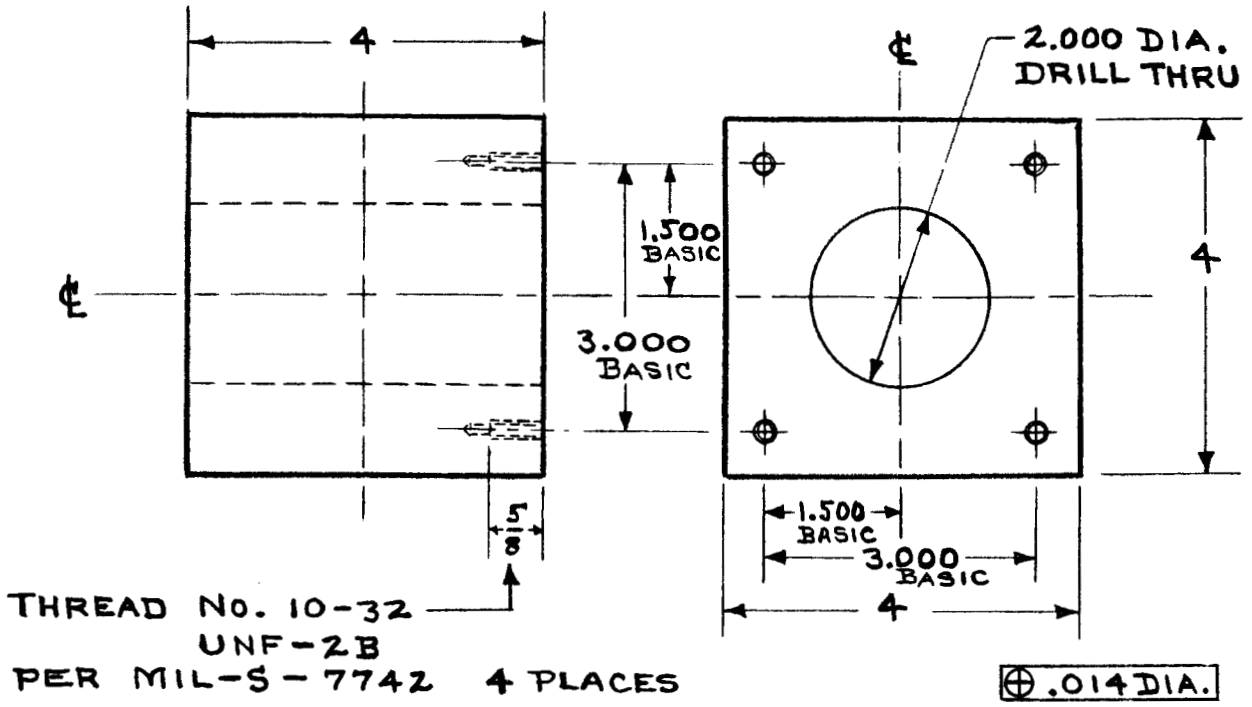

STOCK SIZE	MATERIAL DESCRIPTION	MATERIAL SPECIFICATION
4×4×4+	AL. BAR 2024-T351	QQ-A-225/6 TEMP. T351

GENERAL NOTES

1. UNLESS OTHERWISE SPECIFIED
   a. DIMENSIONS ARE IN INCHES.
   b. FRACTION TOLERANCES ARE $\pm \frac{1}{32}$
   c. DECIMAL TOLERANCES ARE ± .010
2. BREAK ALL SHARP EDGES
3. ATTACHMENTS:
   a. NAS 603-8P SCREWS PROCUREMENT SPEC. MIL-S-7839
   b. MS 35338-43 LOCK (SPLIT) WASHERS UNDER SCREW HEADS
   c. AN 960-10 FLAT WASHERS UNDER LOCK WASHERS
   d. TORQUE SCREWS 20-25 IN. LB. FOR MAX. FRICTION.

Figure 3-3. 5-lb Block

3.2 TEST SETUP

The test setup was basically the same as that discussed in Section 2. The exceptions were that the specimens were tested either one or two at a time, each had three accelerometers, and four of the hat sections were instrumented with two strain gages. Typical accelerometer and strain gage location and the mounting method are shown in Figure 3-4. However, after the brackets were constructed, it appeared that the primary direction of excitation may not be the most severe. Therefore, four brackets were tested in this direction and two were tested in the secondary direction.(see Figure 2-1).

3.3 TEST PROCEDURE

The test procedure was basically the same as that discussed in Section 2. The exceptions were that the frequencies were obtained first by a sinusoidal sweep for approximate definition, then the responses were peaked by slowly varying the input frequency by hand control to obtain better frequency definition.

In addition, model surveys were made on three of the shelf brackets.

3.4 TEST RESULTS AND ANALYSES

The test results and analyses for the two brackets are discussed separately below.

3.4.1 Hat Section Bracket

The data obtained from the hat section bracket are presented in Table 3-1. These data consist of the following: (1) accelerations measured on the block, (2) bracket resonance frequencies (f_1 and f_2), (3) input PSD values at f and f_2, (4) rms g's for each block accelerometer (T_P and B_P top and bottom accelerometers parallel to the shacker plate, T_n top accelerometer normal to the plate) the CG rms acceleration (T_P and $B_P)^{1/2}$, (5) rms strains at the top and bottom bends (S_T and S_B) of the brackets for four specimens, (6) the square root of the input PSD value, and (7) the time and number of cycles to failure. There is a considerable difference between the predicted frequency of 105 cps and the frequencies measured. This probably results from the fact that

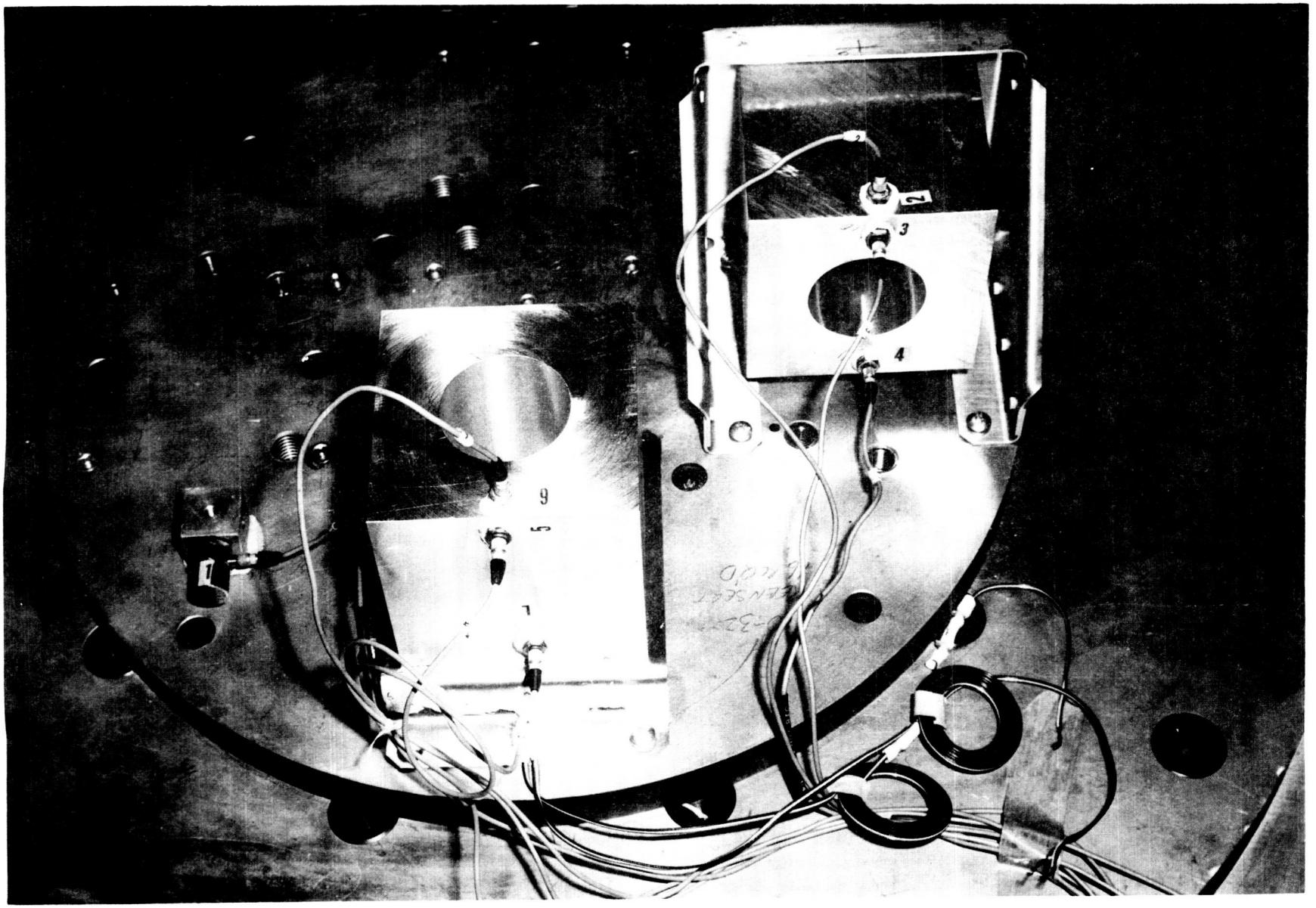

Figure 3-4. Bracket Test Configuration

Table 3-1

HAT BRACKET DATA

Bracket	Location	f_1	PSD (in.)	f_2	PSD (in.)	G_{rms}	$\frac{T_p + B_p}{2}$	S_T	S_B	$PSD^{1/2} \times 10^2$	Time (min)	Cycles
H-1	TP	170	0.20	178	0.19	17	29.0	16,500	17,000	4.35	2:08	2.23×10^2
	TN					17						
	BP					41						
H-2	TP	175	0.21	179	0.20	22	40.0	12,550	9,810	4.45	4:00	4.25×10^4
	TN					34						
	BP					57						
H-3	TP	175	0.14	181	0.13	25	35.5	70,800*	11,400	36.0	5:31	5.88×10^4
	TN					28						
	BP					46						
H-4	TP	175	0.15	195	0.14	13	14.0	9,360	5,270	3.75	19:10	2.13×10^5
	TN					17						
	BP					15						
H-5	TP	175	0.16	197	0.14	28	39.0			3.75	3:21	3.74×10^4
	TN					28						
	BP					50						
H-6	TP	172	0.16	182	0.15	21	34.5			38.5	3:21	3.56×10^4
	TN					30						
	BP					48						

*This stress is obviously too high and could be the result of a small fatigue crack under the gage for the portion of the tape reduced.

δR (C. G. static displacement caused by rotation) is actually much less than predicted (Appendix D). The extreme stiffening effect of the block restricted the motion of the bracket resulting in this deflection component. If this static deflection does go to zero results in frequencies higher than the measured value by approximately 4%. This will be assumed.

Considering the data measured, either the strain (or attendant stress levels) acceleration, or input PSD values, or any combination could be used in conjunction with the cycles to failure for further analysis to establish random fatigue characteristics. Determination of which of these data to use was based on which appeared most meaningful and showed the least scatter when compared to predicted random fatigue curve for the material used, 6061-T6 (References 2 and 4). Therefore, as shown in Figure 3-5, the highest measured stress levels (excluding the obviously bad point), the average of the G_{rms} values from the two accelerometers measuring in the direction of excitation, and the square root of the input PSD (S_{rms} proportional to PSD $^{1/2}$) were plotted as a function of life. In addition, the sinusoidal and random fatigue curves for 6061-T6 were plotted to furnish a reference slope for the data.

The strain gage data show good agreement with the predicted random fatigue curve, if the point at 2.23×10^4 cycles is assumed to be a little high and a stress concentration factor of about 1.4 is assumed. All of the hats failed at one of the two strain gage locations.

The average rms acceleration data show considerable scatter. It is believed that this condition results from the two modes being close in frequency.

The PSD$^{1/2}$ points show surprisingly good agreement with the predicted slope, indicating a consistent amplification factor for the stress producing motion. Therefore, the input PSD values and the stress levels were used to obtain the required information.

The design factor approach to be tested is expressible in the form of

$$\sigma_{eq} = K K_{dyn} \sigma_o \text{ Load}$$

where the parameters are as defined in Section 2.1.1.

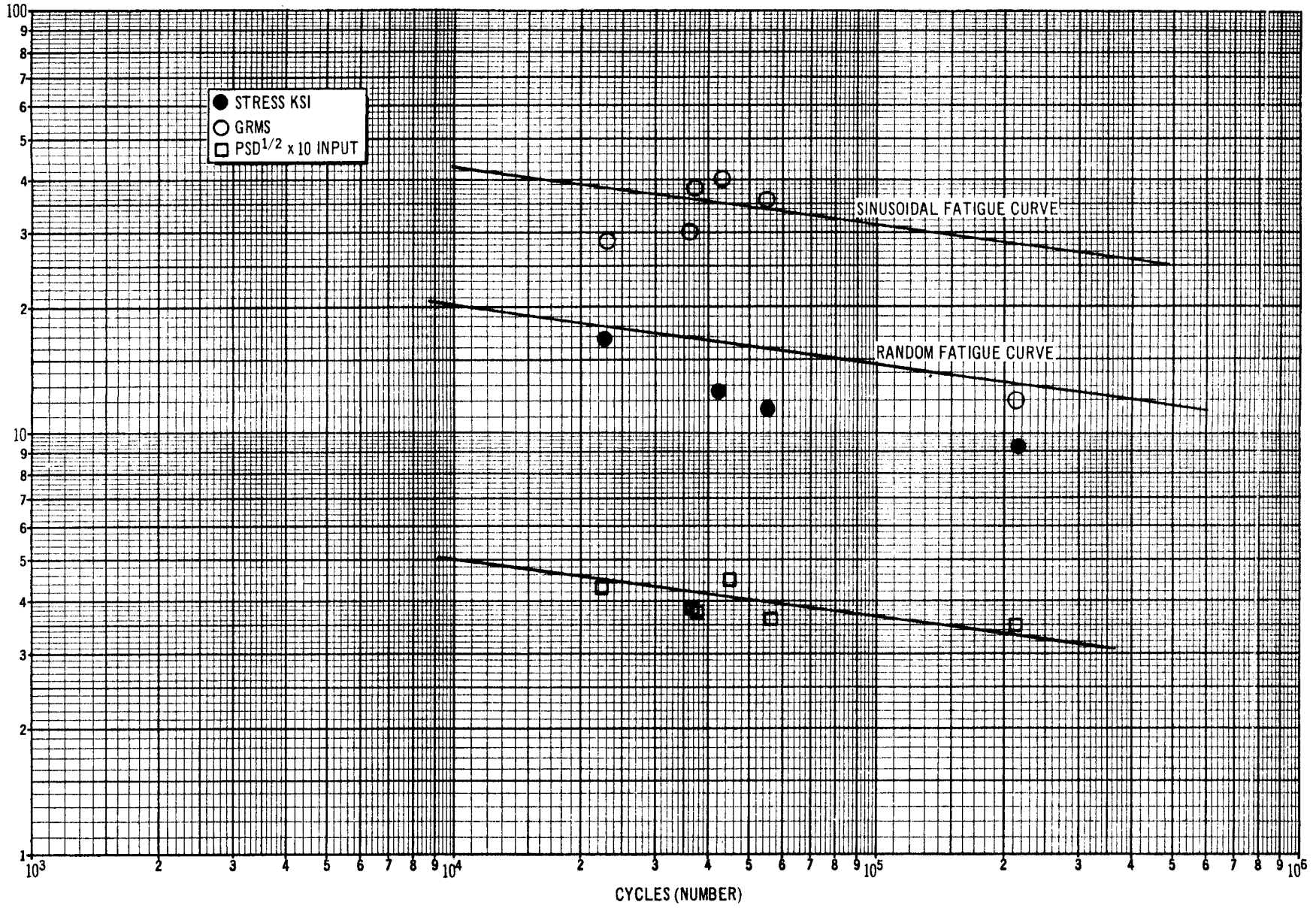

Figure 3-5. Hat Section Data

In this case, the static stress σ_o would be caused primarily by parallelograming (equal moment at each bend), as assumed in Appendix D and as indicated by the stress measurements. This value is

$$\sigma_o = (350\ k/h^2)\ psi$$

where

h = thickness = 0.063

k = stress concentration = 1.4

In addition,

$$\sigma_{eqn/K} = \text{random fatigue stress at n cycles}$$

And, of course,

$$K_{dyn}\ \text{Load} = (\tfrac{\pi}{2} Q \text{ for } PSD)^{1/2}$$

Therefore, at 10^4 cycles, from Figure 3-5 one obtains

$$2 \times 10^4\ psi = \frac{88.2\ psi}{g}(\tfrac{\pi}{2} f_o Q\ PSD)^{1/2}$$

Because of the two frequencies, it is difficult to define f_o; however, Table 3-1 indicates that 180 cps should give good results (within 5%) for any of the brackets tested. With this value, and a value of

$$PSD^{1/2} = 0.5\ (g^2/cps)^{1/2}$$

from Figure 3-5 at 10^4 cycles yields

$$Q^{1/2} = 2.72$$

and

$$Q = 7.5$$

This Q is the amplification of the motion in the direction of excitation only and may not represent the actual Q of the mode. However, this is the Q to be used in the design factor approach for this bracket carrying a rigidly attached mass. This Q may be reduced for less rigid loads to account for other damping effects, but care must be taken in any such reduction.

The above results in the following:

1. K as shown in Figure 3-6
2. $K_{dyn} = (\frac{\pi}{2} Qf)^{1/2}$ where Q is as discussed.
3. A stress concentration factor of 1.4 for the bend radius of the bracket.

Items 2 and 3 must be used in conjunction. If they are, then these design factors will have the accuracy reflected by the $PSD^{1/2}$ versus N curve of Figure 3-4, which is more than sufficient to prove the feasibility of the design factor approach for the hat bracket configuration.

The test information and the information presented in Appendix D can be incorporated into a nomograph, such as that shown in Figure 3-7, which provides the obvious advantage of allowing simple and expedient sizing and evaluations of bracket structure.

The alignment chart method was chosen over the Cartesian chart method because of its simplicity, and its resolution is greater than the accuracy of the input values (this accuracy is the advantage of the Cartesian method). The chart was constructed by first making a nomograph for the expression

$$t = 203.81 \left(\frac{w}{cl}\right)^{0.6} \left(\frac{a}{F_b}\right)^{0.8} PSD^{0.4}$$

(see Figure 3-7 for nomenclature) which includes, implicitly, the effect of frequency on stress level (Appendix E presents the equation derivation). Then the parameters for the specimens tested and PSD were entered and the value of F_b adjusted to give the proper values. One disadvantage of this chart is that some knowledge of frequency is required to obtain the fatigue strength

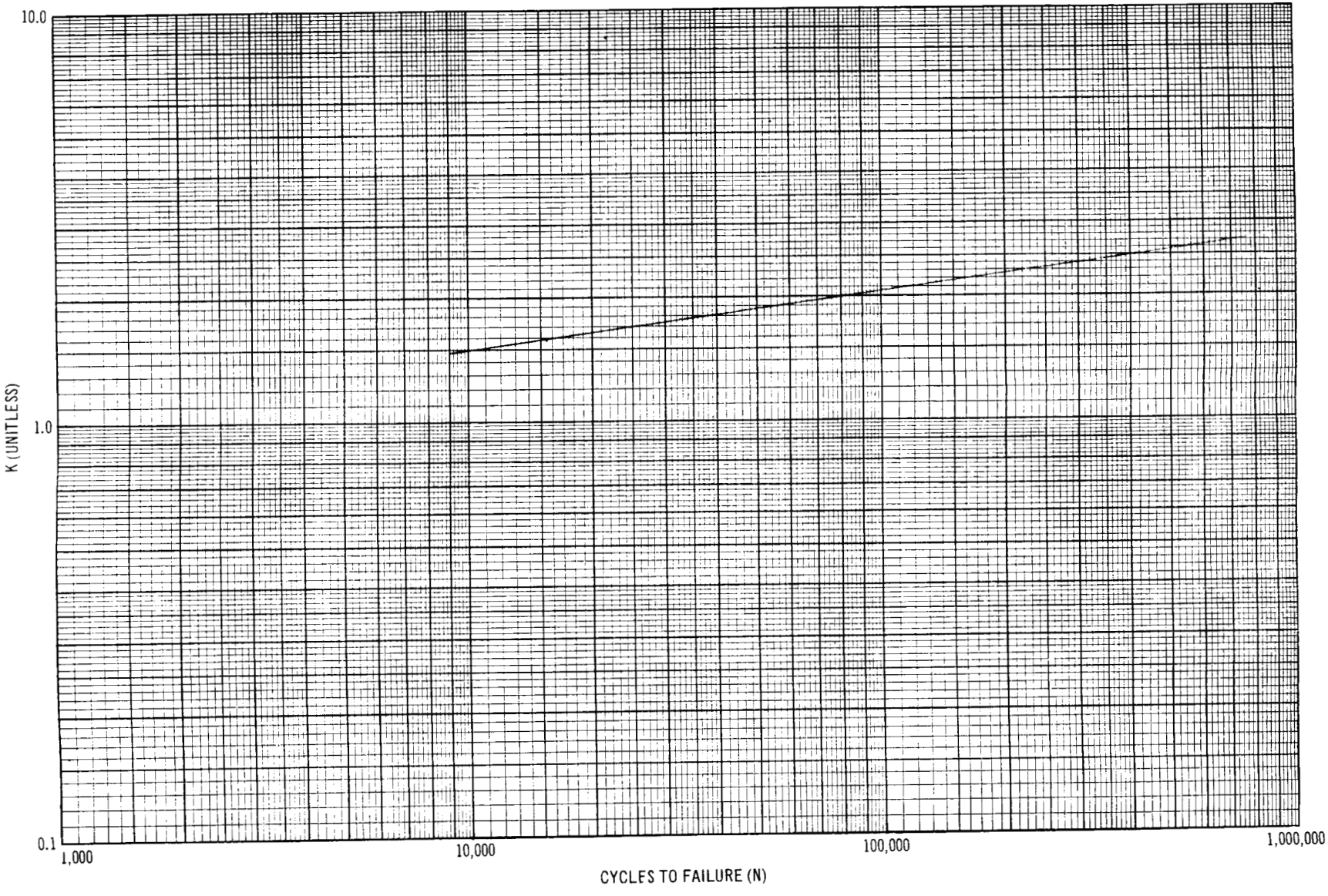

Figure 3-6. K Values for 6061-T6 Aluminum (Random)

$$t = \text{BRACKET SHEET GAGE} = 203.81 (W)^{0.6} \times \left(\frac{a}{F_b}\right)^{0.8} \times \frac{1}{(c)^{0.6}} \times \frac{1}{(l)^{0.6}} \times (PSD)^{0.4}$$

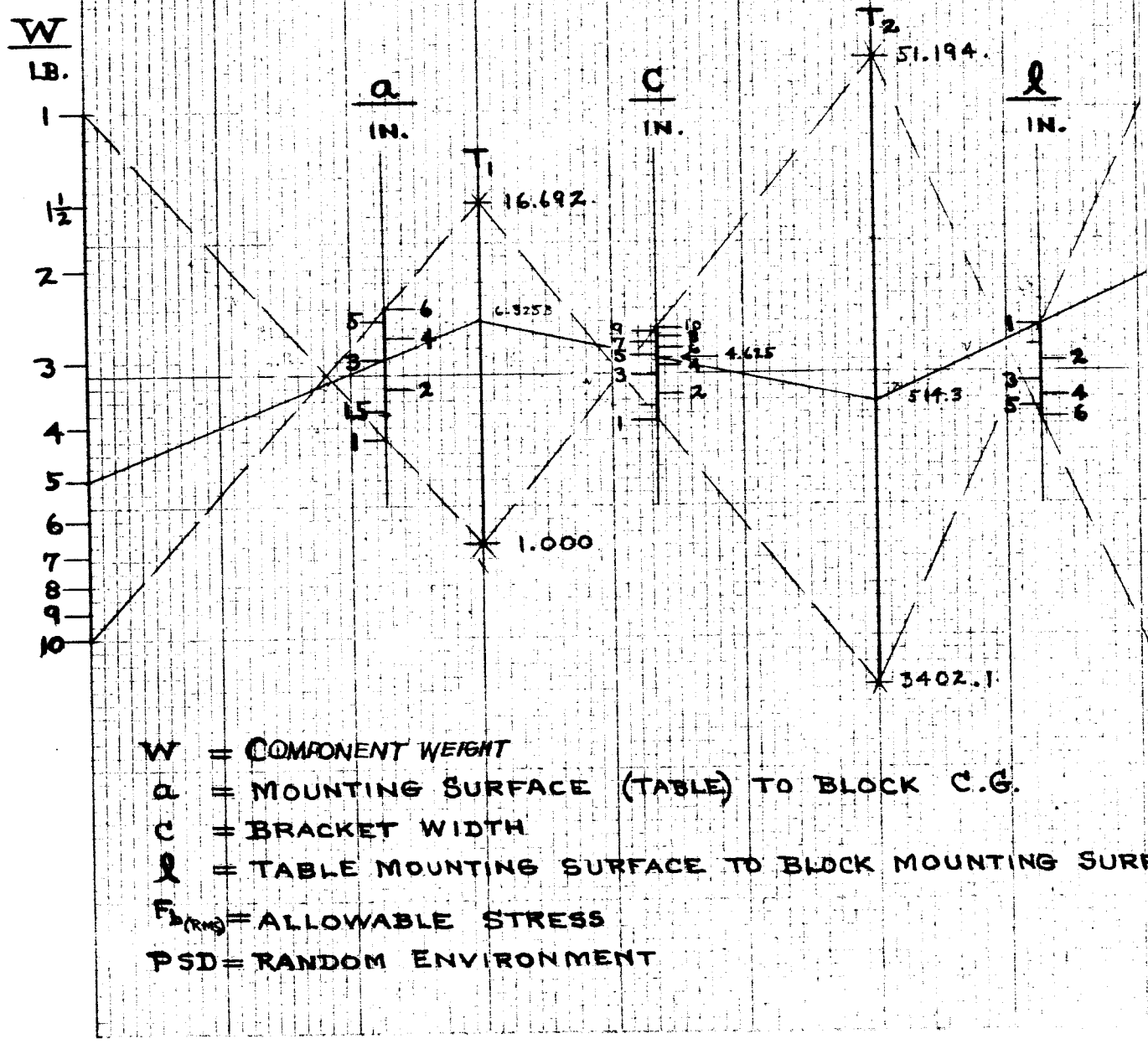

W = COMPONENT WEIGHT
a = MOUNTING SURFACE (TABLE) TO BLOCK C.G.
c = BRACKET WIDTH
l = TABLE MOUNTING SURFACE TO BLOCK MOUNTING SURF
$F_{b(RMS)}$ = ALLOWABLE STRESS
PSD = RANDOM ENVIRONMENT

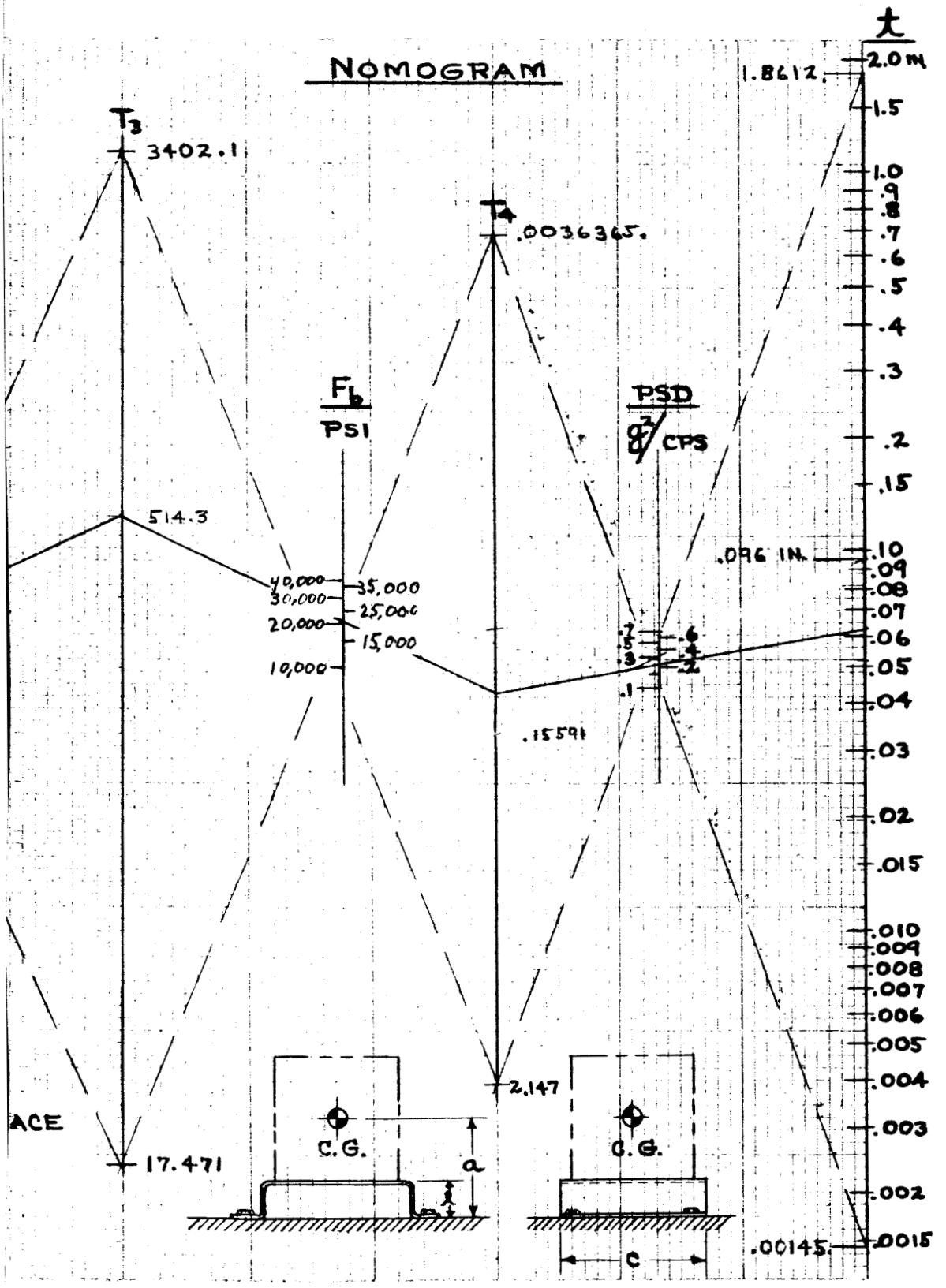

Figure 3-7. Box Mounted on Hat Section

(2)

and PSD levels. However, it can be shown that t is proportional to N(f x Time) to approximately the 1/8 power and the PSD of the forcing function is usually fairly flat in the region of the bracket's fundamental frequencies. Therefore, this required frequency information should cause little difficulty.

This nomogram could be constructed in a variety of ways. For example, if a given life were assumed, then one value representing an allowable stress for various materials could be put on a scale F_b eliminating the necessity of estimating f for the number of cycles calculation or sinusoidal rather than random fatigue curves could be used to define F_b (the ratio of random fatigue stress over sinusoidal fatigue stress would be a constant) if the nomograph were only for materials with the same slope on a log stress log cycles curve. In addition, Q could have been included in the nomogram in an explicit form. It was felt that there would not be sufficient variation in this value to warrant this.

The approach chosen was used because it was felt the added flexibility would be well worth the minor inconveniences eliminated by the above approaches. This flexibility is increased by the sinusoidal-random conversion factor of Figure 3-8. To use this, first read the value of A for the given value of α (the negative reciprocal of the slope of the fatigue curve on log-log paper), and divide this value into the sinusoidal curve. This gives a random fatigue curve which is compatible with the presented nomogram.

The above establishes the feasibility of the nomogram approach to the hat bracket design. However, the developed nomogram is based on one bracket size, test duration, and load configuration and should be checked through additional experimentation before being used in general hat bracket design.

3.4.2 Shelf Bracket

The data obtained from the shelf bracket test is presented in Table 3-2. Brackets 1 through 4 were excited in a direction normal to the mounting surface of the block, the primary test direction (see Figure 1-2), while 5 and 6 were excited in the secondary test direction to determine the comparative severity of the bracket response in two directions.

The modal survey data were not felt to be accurate because of the effect of the hand-held accelerometer on the response. Therefore, the data are not listed in the table.

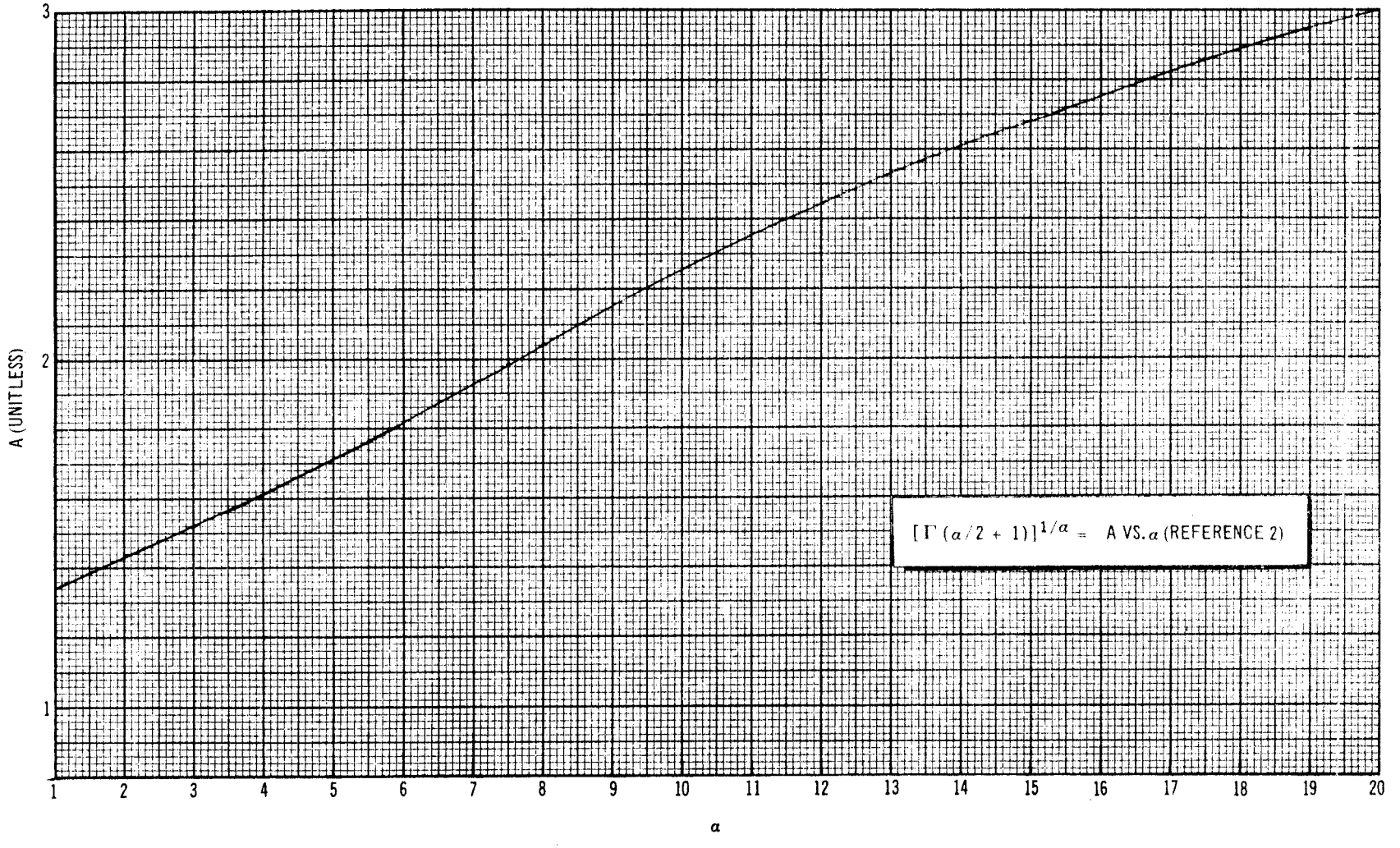

Figure 3-8. Sinusoidal Random Conversion

Table 3-2

SHELF BRACKET DATA

Bracket Description	Run No.	Channel No.	Location	f_1	PSD (in.)	f_2	PSD (in.)	g_{out}	$\frac{T_p + B_p}{2}$	Time (min)	Cycles	$PSD^{1/2} \times 10^2$
L-1	15		TN	107	0.30	125	0.32	21.0	18	0:48	5.56×10^2	5.5
			TP					16.5				
			BP					19.0				
L-2	15		TN	112	0.30	133	0.33	20.0	13	0:48	5.87×10^3	5.5
			TP					15.0				
			BP					11.0				
L-3	17	2	TN	112	0.20	133	0.21	20.0	22	4:14	3.10×10^4	4.7
		3	TP					21.0				
		4	BP					23.0				
L-4	18	2	TN	113	0.14	134	0.15	20.0	23	5:31	4.09×10^4	3.75
		3	TP					21.0				
		4	BP					24.0				
L-5	19	2	TN	92	0.15		0.15	8.0	13	8:01	4.42×10^4	3.85
		3	TP					22.0				
		4	BP					4.0				
L-6	20	2	TN	90	0.14	123	0.15	10.0	10	5:26	3.47×10^4	3.85
		3	TP					16.0				
		4	BP					4.0				

Both the average of the G_{rms} values obtained from accelerometers measuring in the direction of the excitation and the $(PSD)^{1/2}$ of the input accelerometer plotted as a function of cycles to failure of Figure 3-9. In addition, the G_{rms} levels for 5 and 6 have been multiplied by the square of the frequencies in the two directions so that a factor proportional to displacement could be compared.

The G_{rms} values again show considerable scatter while the $PSD^{1/2}$ values for the primary axis are quite close to the expected slope. In addition, the $PSD^{1/2}$ values for the secondary direction fall on the same line and the CG displacement was approximately the same as for brackets tested in the primary direction with similar lives in cycles. Since the moment of inertia-to-weight ratio for the square weight used is probably an upper bound for any actual load, it can be concluded that the proper axis for the primary testing (of the two axes tested) was chosen for the majority of applications.

The failure for Brackets 1 through 4 occurred at the attach points of the bracket to the shaker head as predicted (Appendix D) and the failures for both 5 and 6 started at the attach points and at a lower corner. This indicates that simple fixes will improve the strength for the primary direction, resulting in conservative values from the chart. In the other direction, the corner strength had been reached.

The values for the $PSD^{1/2}$ for this bracket are sufficiently close to that for the hat section so that the value of Q (in K_{dyn}) can be obtained ratioing the static stresses, i.e.,

$$Q_S = Q_H \left(\frac{\text{static stress}_S}{\text{static stress}_H}\right)^2$$

Assuming that the stress risers are the same,

$$Q_S = 7.5 \times \left|\left(\frac{4.73}{(0.172 + 15h)h^2}\right) \Big/ \left(\frac{3.50}{h^2}\right)\right|^2$$

$$= 11$$

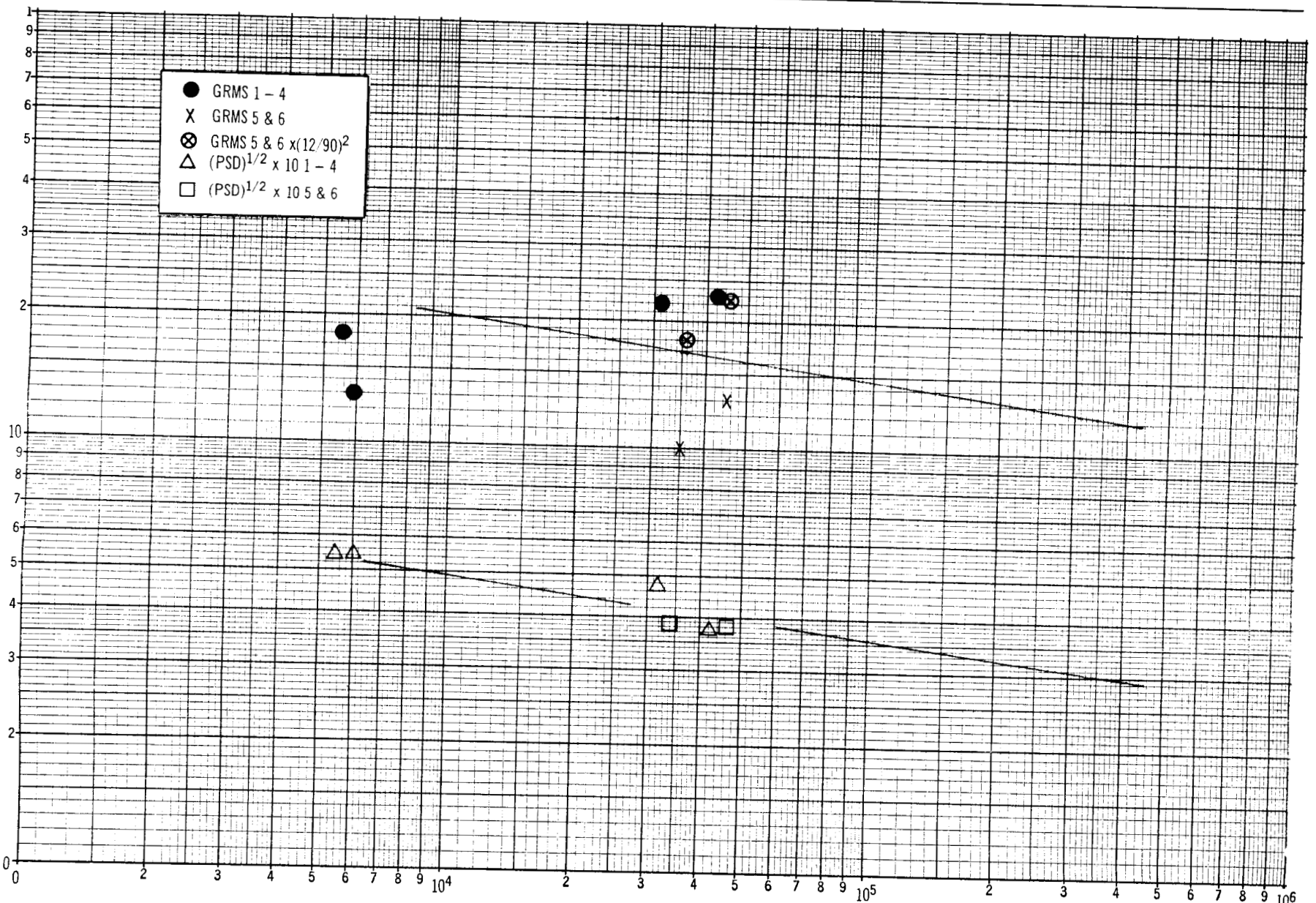

Figure 3-9. Shelf Bracket Data

The K is a material constant and will not change from that previously given.

The test information and the information of Appendix D have been combined in the nomograph shown in Figure 3-10, which was developed in much the same way as that previously discussed for the hat bracket. However, in this case, frequency had to be included explicitly because of the form of the frequency equation. Q has also been included as an explicit function since a wider range of Q could be expected for this configuration because of complexity, added mass, attachment of wire bundles, and so forth.

The nomograph developed for the cantilevered bracket could also take variations similar to those discussed for the hat bracket. Again, the feasibility of the design factor and nomograph approach has been demonstrated for the hat bracket.

t = SHEET GAGE – CANTILEVER MOUNT

W = BLOCK WEIGHT

a = MOUNTING SURFACE TO BLOCK C.G.

C = BEND RESISTANCE LINE TO ℄ WEB

ℓ = CRITICAL BOLT TO PIVOT

$F_{b(rms)}$ = ALLOWABLE STRESS

PSD = RANDOM ENVIRONMENT

Q = AMPLIFICATION FACTOR

f_o = NATU… FREQ…

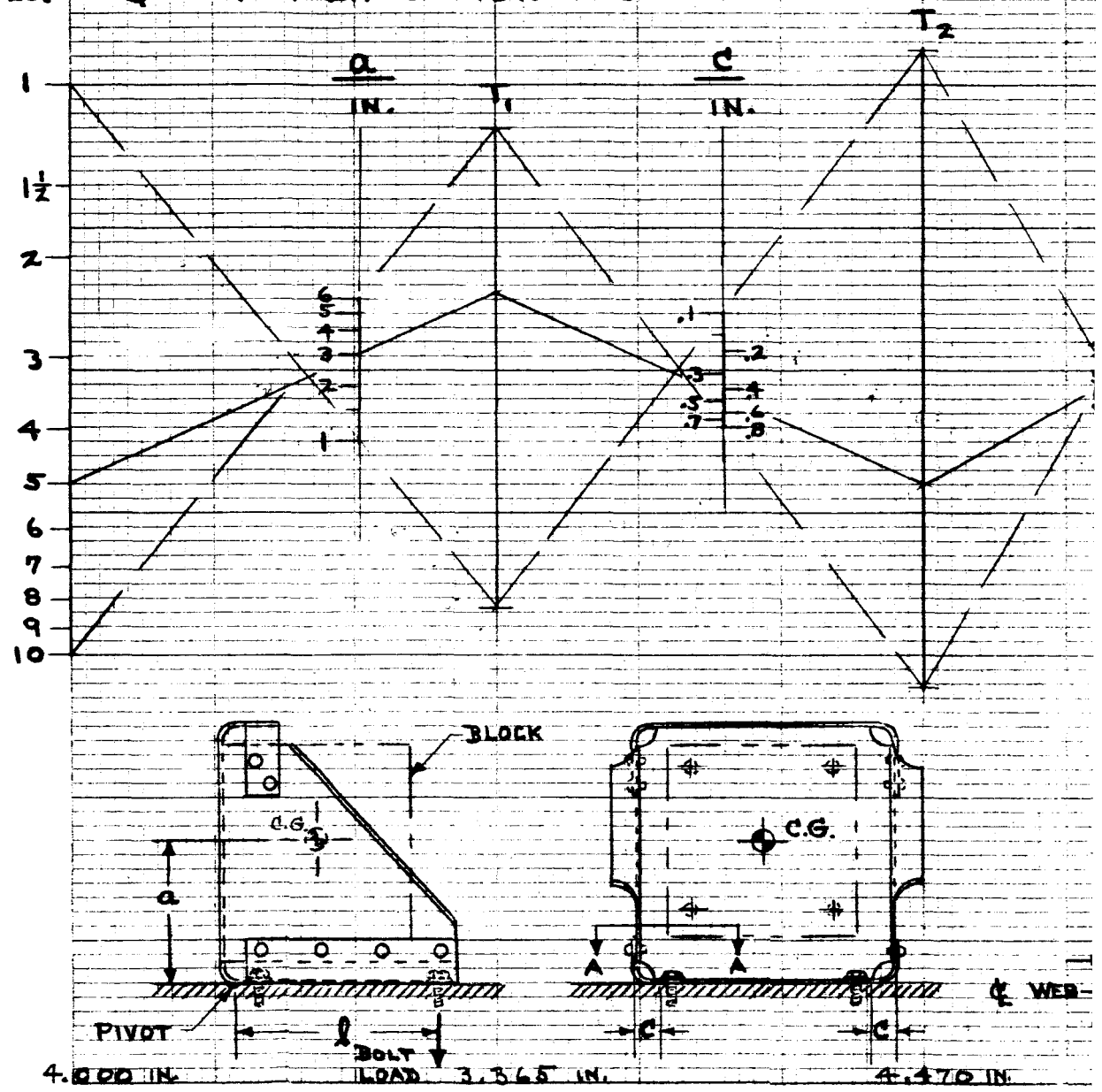

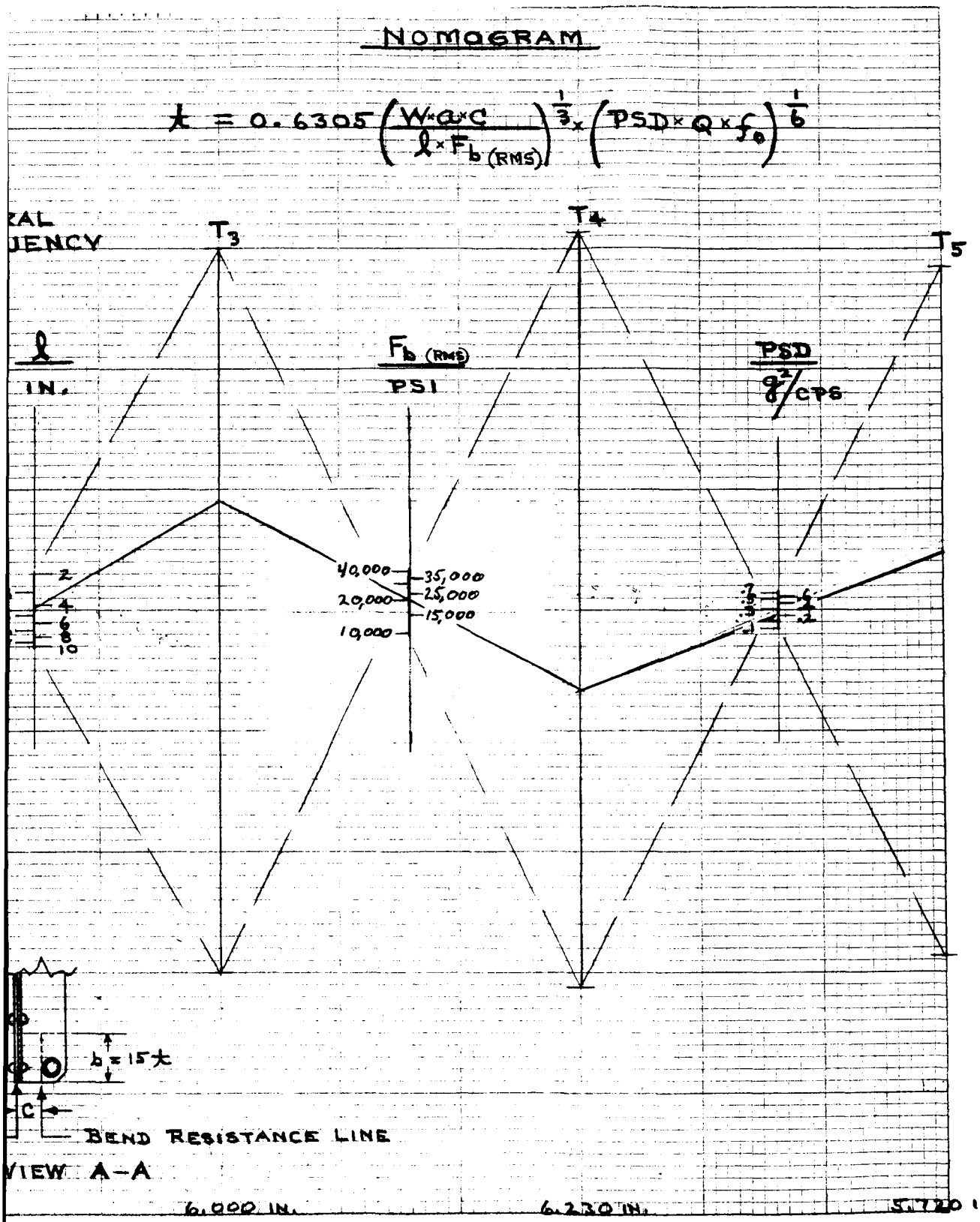

Figure 3-10. Cantilever Mount

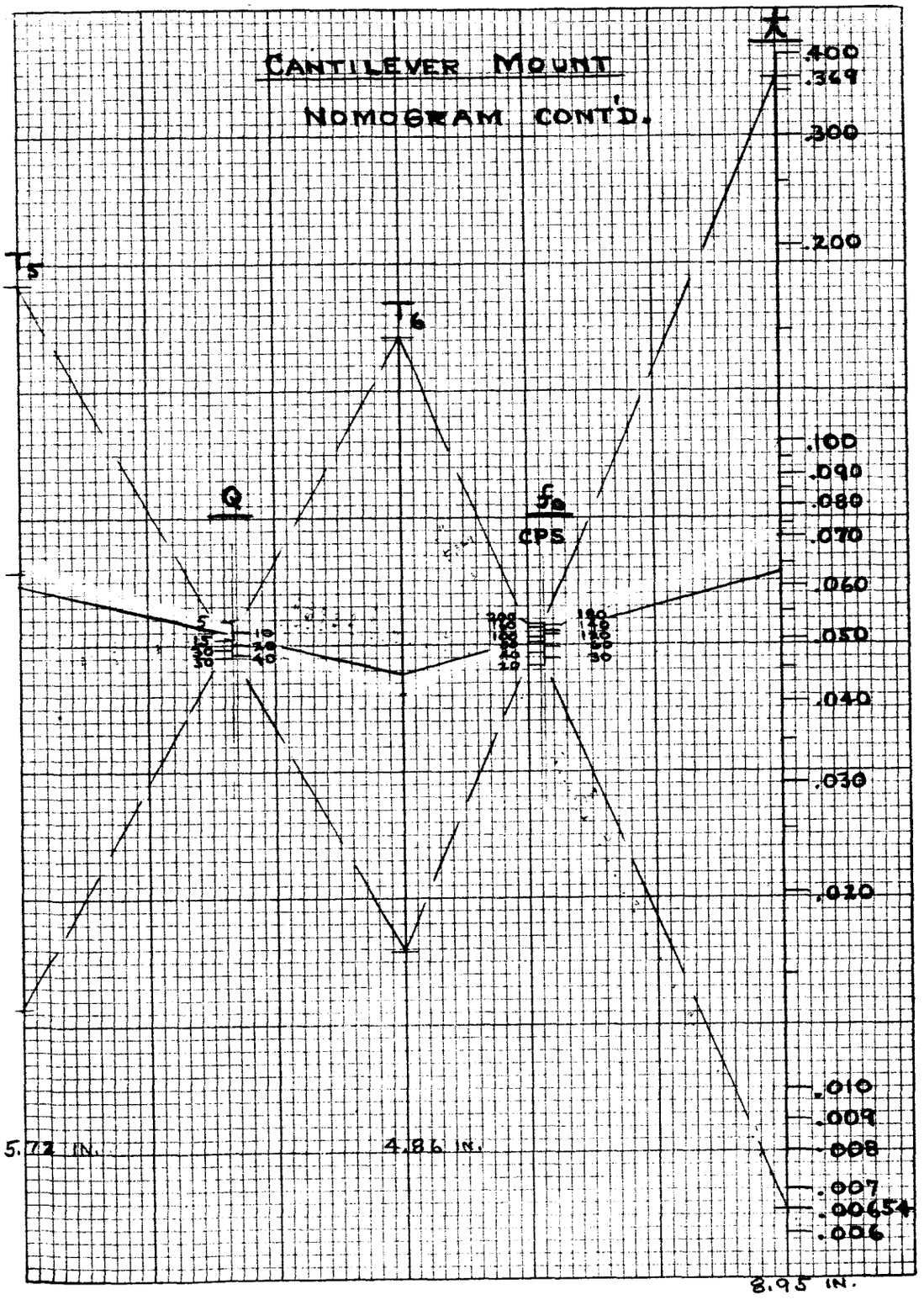

Figure 3-10. Cantilever Mount (Continued)

Section 4

CONCLUSIONS AND RECOMMENDATIONS

The conclusions to be drawn from the beam portion of the study are as follows:

1. The design factor approach and data reported in Reference 1 were verified.
2. The effect on random fatigue for two modes resulting from parallel principal stresses can be established.
3. Extreme care must be taken in beam specimen design to obtain data on the effect of a torsion and bending mode on random fatigue.
4. Useful information can be obtained from simple cantilevered beams without stress raisers, opening the door to basic work on the effective value of stress raisers on random fatigue.

For the second conclusion, Item 2, an analytical approach for the prediction of the effect of multiple bending modes was hypothesized for a limited case and substantiated by the test data obtained. Additional combination approaches were hypothesized, expanding the range of application, but data were not available for verification.

The high quality of the data is indicated by Figure 4-1. In this figure, the peg-point data, the two weight, and the cantilevered weight data corrected for multi-mode effects show good agreement with one another and with the predicted curve. In fact, the scatter resulting from the three types of beams is less than that obtained in the previous study. In addition, acceptable agreement was obtained from the plain specimen, but the figure indicates the lack of apparent effect of the damping tape except for this specimen. The plain specimen shows an increase of scatter for the specimens which have damping tape.

The conclusions of the bracket portion of the study are as follows:

1. The design factor approach for design of brackets is feasible.
2. The development and the use of design nomographs are shown to be feasible.

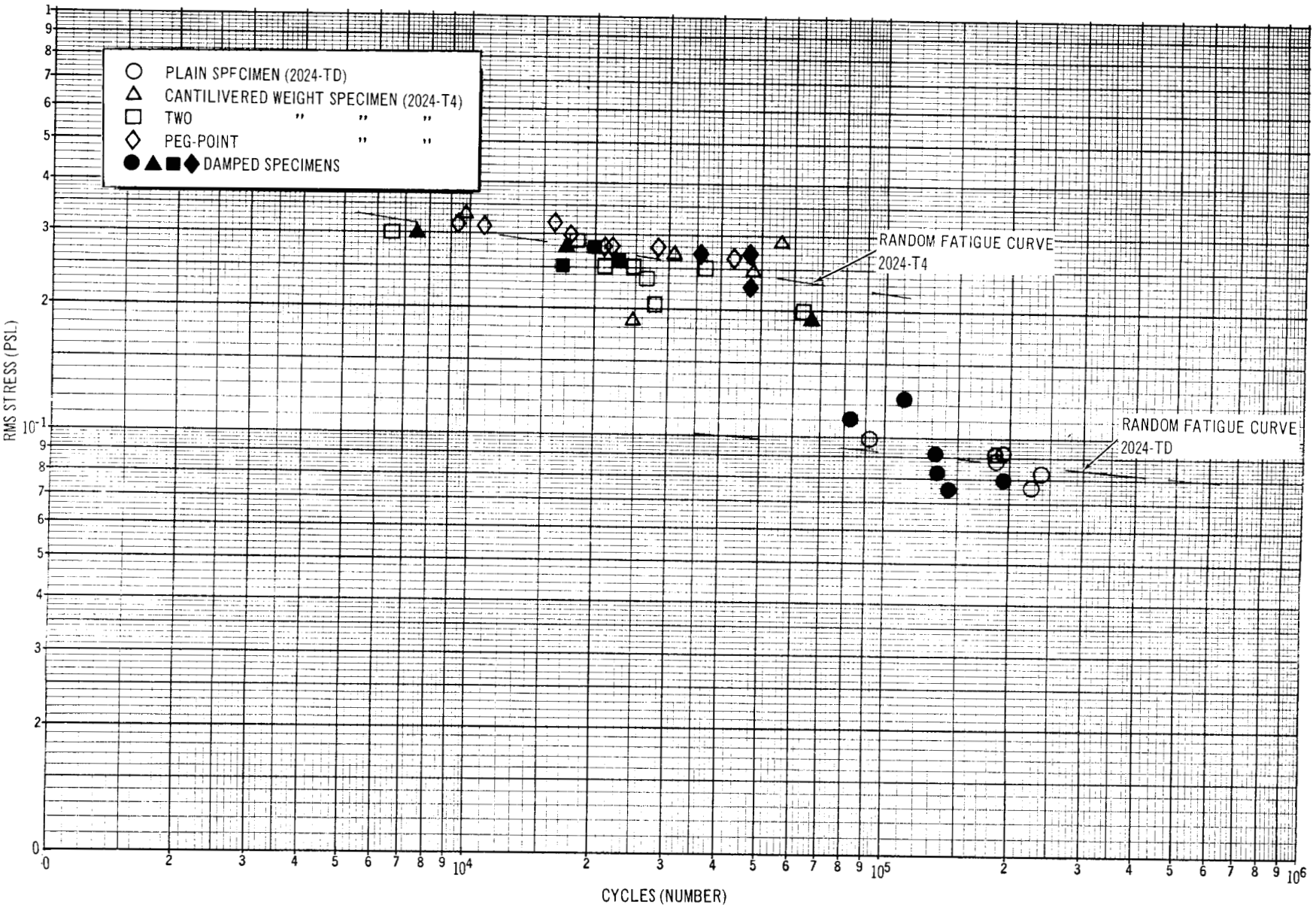

Figure 4-1. Combined Fatigue Test Results

Design nomographs were developed for two specific brackets and were verified with experimental data: These brackets were a hat and a shelf bracket. Before their use for actual design, they are subject to further refinement and verification either through the use of existing data gathered on development programs or of new experimental data.

Difficulty was encountered in the analysis and use of the test data of the brackets because of the closeness of the first two modes or frequencies of resonance. In future work, care should be taken to ensure that the frequencies of the first two modes are well separated.

The results of this study indicate several important areas of random fatigue research for which future work is required and would be fruitful. These areas include the following:

1. Additional analytical and experimental work in multi-mode effects on random fatigue for a variety of stress and frequency relationships.
2. Experimental work on the effective values of stress raisers for random fatigue and their dependence on stress levels.
3. Additional work to verify and refine the nomographs for bracket design. Included in this work should be a larger variety of bracket configurations, attachment methods, and loading conditions.

Appendix A
BEAM ANALYSIS

The stresses for the beam test specimens were obtained by measuring the response at a given point and multiplying this value by the computed stress per unit response. These computed values are derived below.

A. 1 PEG-POINT BEAM

The first mode shape of an end weighted beam is nearly independent of variations in the end weight. This results in approximately constant stress at the stress raiser per unit deflection.

The mode shape and the corresponding moment for one of the beams were obtained by the Douglas programmed version of the Mykelstad Method (DB 11). From this, the moment at the stress raiser for a deflection at the accelerometer of

$$\frac{Ms}{Xa} = \left(\frac{2.414 \times 10^2}{1.075}\right) \text{in. lb/in} = 2.245 \times 10^2 \text{ lb}$$

was obtained since

$$S = kMC/I = 6M/bh^2$$

where

b = width = 1.125 in.
h = thickness = 1/8
k = stress concentration = 1.5

The value of stress per tip displacement is

$$\frac{Ss}{Xa} = \frac{2.245 \times 10^2 \times 1.5 \times 6 \times 64}{1.125} \text{ psi/in.} = 1.15 \times 10^5 \text{ psi/in.}$$

The acceleration in gs per unit displacement is

$$G = \frac{\omega^2 \times \text{in g}}{386.4 \text{ in./sec}^2}$$

Therefore, the stress per measured G as a function of frequency is

$$\frac{Ss}{GA} = \frac{1.15 \times 10^5}{(2\pi)^2 f^2} \times 386.4 = \frac{1.125 \times 10^6}{f^2} \text{ psi/sec}^2$$

This is the value plotted in Figure 2-6.

A.2 TWO-WEIGHT BEAM

The stress per unit displacement was obtained in much the same way for the two-weight beam. The one exception is that the acceleration levels measured at the center accelerometer must be used. The calculated moment at the stress raiser to center accelerometer displacement were computed to be

$$\frac{M}{X} = \frac{2.564 \times 10^2}{0.4503} \text{ in.-lb/in. for the first mode}$$

and

$$\frac{M}{X} = \frac{1.8555}{1.3895} \times 10^3 \text{ in.-lb/in. for the second mode.}$$

The computer frequencies for these modes are 48.6 and 275.8 cps.

The procedure used previous gives

$$\frac{S}{g} = \left(\frac{2.86 \times 10^6}{f^2}\right) \text{ psi sec}^2/\text{g for the first mode}$$

$$\frac{S}{g} = \left(\frac{6.7 \times 10^6}{f^2}\right) \text{ psi sec}^2/\text{g}$$

for the second mode. These values are also plotted in Figure 2-6.

A.3 TORSION-BENDING BEAM

The two modes of this beam result from the coupling of the modes that would be obtained if torsion and bending were considered independently. The first coupled mode is predominately bending, and the second is predominately torsion. The stresses caused by the bending portion of either mode can be obtained from the peg-point curve of Figure 2-6.

The stress at the concentration point per tip rotation was also obtained from the Douglas DB11 computer program. The resulting torsional moment at the stress raiser per tip radian was

$$\frac{M_T}{\theta} = 6.89 \times 10^3 \text{ in.-lb}$$

From Timoshenkos, "Theory of Elasticity," the outer fiber stress at the center of a beam is

$$S = \frac{M_T}{K_2(2a)^2(2b)}$$

where

a = half thickness of the beam = 0.125/2 in.
b = half width of the beam = 1.25/2 in.
K_2 = constant which = 0.312 for b/a = 10

This gives

$$\frac{S}{\theta} = 1.13 \times 10^5 \text{ psi/tip radian}$$

A concentration factor of 1.5 gives

$$\frac{S}{\theta} = 1.17 \times 10^5 \text{ psi/tip radian}$$

The bending and torsion stresses must be combined. To do this let

σ_x = bending stress

σ_y = 0 = normal to the maximum bending stress

T_{xy} = torsion stress

The stress in any direction can be obtained from

$$\sigma_x = \frac{\sigma_x + \sigma_y}{2} + \frac{\sigma_x - \sigma_x}{2} \cos 2\theta + T_{xy} \sin 2\theta$$

where

θ = angle or rotation*

and can be maximized by

$$\frac{\sigma_x}{2} \sin 2\theta = T_{xy} \cos 2\theta$$

---

*An Introduction To The Mechanics Of Solids, edited by Crandell F. Dahl

The maximizing angle for this case is described by:

$$\frac{2T_{xy}}{\sigma_x} = \text{Tan } 2\theta = 2\theta$$

If

$$\sigma_x \gg 2T_{xy}$$

Then

$$\sigma'_x = \sigma_x + \frac{2T_{xy}^2}{\sigma_x}$$

which can be rewritten as

$$\sigma'_x \sigma_x = \sigma_x^2 + 2T_{xy}^2 \simeq \sigma_x'^2$$

For the above inequality ($\sigma_x \gg 2T_{xy}$). This is the case for the bending and torsion parts of the first mode.

The component of the stress of the second mode, which is the same direction as σ'_x of the first mode, must be nearly equal to the value of the bending portion of that mode. This is so because of the small value of θ for the first mode.

Appendix B
STRESS CONCENTRATION NONLINEARITY

The stress concentration nonlinearity for a hole was developed in Reference 1 and is included here for completeness.

The computed stress at a stress raiser for a constant concentration factor has approximately a Rayleigh distribution if the stress results from a modal response to random excitation. This obviously cannot be the case for high sigma stress levels. This is corrected for in the following way for a Rayleigh distribution of peaks.

The probability of a peak stress occurring in each $(1/2)\sigma$ increment was obtained with the assumption of a Rayleigh distribution, and the mean stress in each band was assumed to be at the center of the band. Miner's accumulation was assumed, and it was also assumed that $\alpha = 6$.

The sum of the probabilities of occurrence in each band, times the mean stress value for that band, raised to the sixth power, yields an approximate damage factor. If the calculated value of a given σ peak exceeds the yield strength of the material, then the actual stress for that value must be on the order of, or less than, the yield strength. The relationship between yield and calculated rms stress values of 1, 1-1/2, 2, and 2-1/2 were chosen, and the probability of occurrence for stresses greater than yield were added to the band just below yield. The damage factor was calculated as discussed above, and the ratio of this factor to the factor obtained for low stress was obtained. This factor, times the stress concentration factor of 1.5, is shown as a dashed line in Figure 2-8.

Since the stress probably exceeds the yield and the method of including the effect has been conservative, the curves resulting from the above calculations have been shifted 20% to the right. This new curve has been used to correct the data obtained and is shown as a solid line in Figure 2-8.

Appendix C
MULTI-MODE EFFECTS ON RADOM FATIGUE

The existence of more than one mode contributing appreciably to the stress at a critical fatigue point will obviously have an effect on the fatigue life of that structure. This appendix discusses methods of accounting for these effects when two modes exist and are responding to a random excitation.

This problem will be approached by first considering the two modes, close in frequency and amplitude, and then expanding the differences in these parameters. The hypothesized combination methods will be altered as required by either the physics of the situation or engineering limitations of the application.

First, consider two uncoupled modes of a structure sufficiently close in frequency to produce a beat effect, i.e., if each mode is responding sinusoidally at its natural frequency, then the combination would have only one extreme amplitude $\left(\frac{df}{dt} = 0\right)$ between zero crossings.

If these modes are excited with a random field and the response of each mode has a Rayleigh peak distribution and a normal amplitude distribution, then the only requirement for the combination to have a Rayleigh peak distribution is the one extreme amplitude between the zero crossings. The frequency of the zero crossings, and therefore of the peaks, will be the same as that for a third response having a frequency equal to the weighted average of the two actual frequencies. These conclusions are obtainable by expanding the discussion in Section 1.8 of Random Vibration in Mechanical Systems by S. H. Crandall and W. D. Mark, Academic Press 1963.

In addition, if this third response has an rms level equal to the rms value of the combined modes, then the amplitude and peak distribution, as well as the frequency of the combination, is duplicated by this third response. Therefore,

this third response should result in an equivalent amount of fatigue, within engineering accuracy, and can be used in fatigue prediction.

Using the above, the random fatigue equivalent system for two modes having rms stress levels of σ_1 and σ_2 and corresponding frequencies of f_1 and f_2 is a system having rms response of

$$\sigma_E = (\sigma_1 + \sigma_2)^{1/2}$$

and a frequency of

$$f_E = \frac{\sigma_1 f_1 + \sigma_2 f_2}{\sigma_1 + \sigma_2}$$

This approach should be sufficiently accurate, for engineering applications, for frequency separations up to an octave.

In the range in which the two frequencies are separated by more than an octave, the apparent procedure is quite different. Consider the two sinusoidal wave forms shown in Figure C-1a and b, which add to yield the waveform shown in C and can be described as

$$S = A \sin \alpha t + B \sin \beta t$$

A fatigue combination process which covers this situation must satisfy both the cases in which A = 0 and in which B = 0. One such combination is

$$F = F(A) + F(B)$$

where

F = the fatigue accumulated
F(A) = the fatigue which would be accumulated by A $\sin \alpha t$
F(B) = fatigue accumulated by B $\sin \beta t$ with prestress A $\sin \alpha t$

F(A) should follow the Miles-Miner type random fatigue theory and satisfies the limit where F(B) = 0. However, F(B) requires some discussion. F(B) must describe the fatigue accumulated by the high-frequency oscillation shown in Figure C-1. Assume that this fatigue can be obtained by summing the damage accumulated in each cycle: include the level of the lower frequency as a prestress, then the contribution of this component for sinusoidal response can be obtained from a constant life chart as shown in Figure C-2. However, for random fatigue the prestress will have a statistical value described by the normal distribution.

Therefore, F(B) can be described as

$$F(B) = \sum_{i=1}^{J} n_i/N_i$$

Here, the normal distribution of the prestress has been separated into j equal prestress values, and

N_i = random fatigue life for the higher frequency with prestress of S_i obtainable from constant life charts similar to that in Figure C-2.

n_i = number of cycles accumulated at S_i.

If the lower frequency stress goes to zero, this reduces to standard Miles-Miner random fatigue theory, satisfying F(A) = 0, and results in a method satisfying both extremes.

This method would be difficult to use and physically inaccurate due to non-linearity in the engineering sense for the cases where the stress levels of the mode having the higher frequency are much smaller than those for the lower frequency mode. Therefore, the following approach has been hypothesized.

Fatigue data and theory indicate that the approximate fatigue accumulated as the result of an oscillatory stress is dependent on the amplitude of the stress and of any prestress, but is independent of the wave form. Therefore, if the fatigue resulting from the second mode stress about the first mode stress is

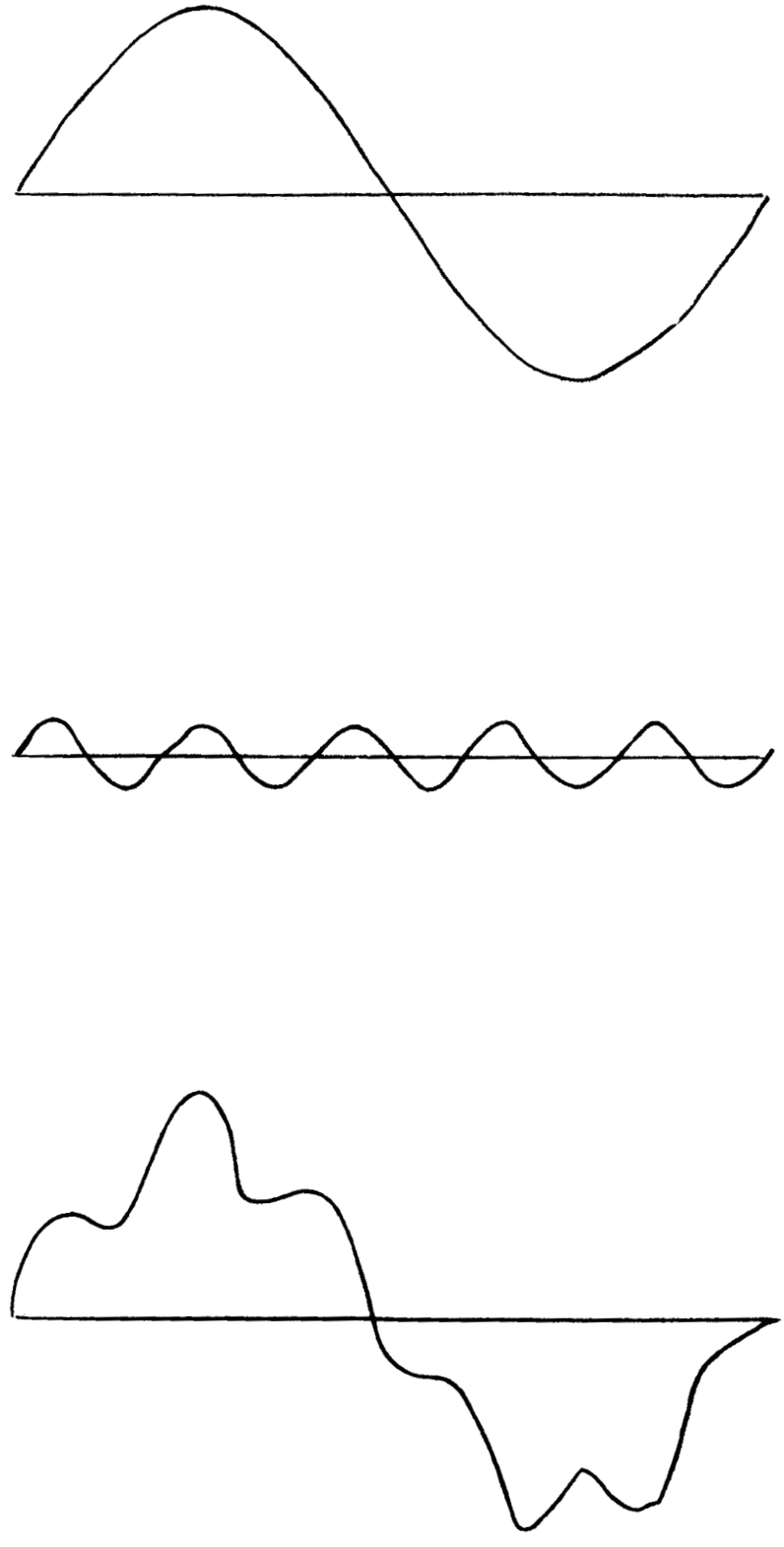

Figure C-1. Addition of Sinusoids Constant Life Chart 2024-T4 Aluminum (Extrapolated from Reference)

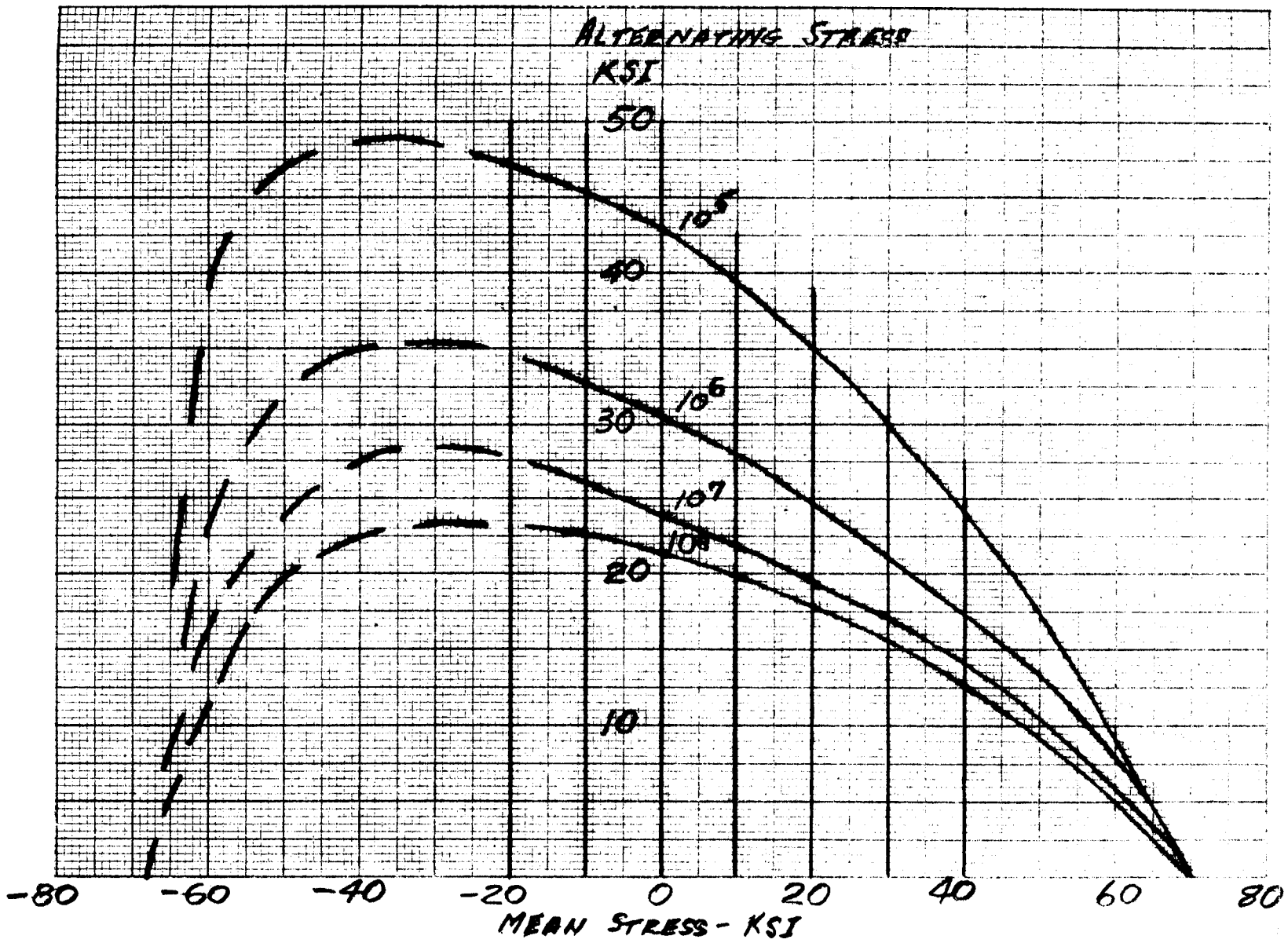

Figure C-2. Constant Life Chart 2024-T4 Aluminum (Extrapolated From Reference)

neglected, an equivalent amount of fatigue should be accumulated by a time history that envelopes the maximum of the combination. Assuming that this is the case, and recalling that the second mode stress is caused by a random response then the average increase for each cycle of the first mode will be the rms value of the second mode. The stress caused by the first mode is also random in nature and is assumed to have a Rayleigh peak distribution. Increasing each peak of the first mode by the rms of the second would result in an equivalent time history with a distorted Rayleigh peak distribution that would be difficult to handle analytically. However, converting the first mode stress to an equivalent sinusoid, adding the rms level of the second mode, and converting back to the random level seems to be a reasonable approach.

This is approximately the same as adding $rms_1 + (rms_2/2) = rms_{EQ}$ and assuming it is applied at f_1.

The data obtained in this study indicate that this approach results in a correction of the proper magnitude.

Appendix D
BRACKET ANALYSIS

REF: FIG. 2-5
P. 11 SM48789P

RMS ACCELERATION
$= \left(\frac{\pi}{2} Q f_o PSD\right)^{\frac{1}{2}}$

WHEN:
Q = 20
EST. f_o = 60 CPS
PSD = .3 g^2/CPS

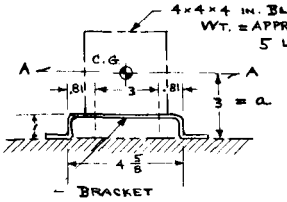

$= \left(\frac{\pi}{2} \times \frac{10}{20} \times 60 \times .3\right)^{\frac{1}{2}}$
$= 24$

W = BLOCK WT. × RMS ACCELERATION
$= 5 \times 24 = 120$

PARALLELOGRAMING VIBRATION DIRECTION A-A
$M = W \times a/4 = 120 \times 3/4 = 90$ IN. LB.

EST. CYCLES DURING DESIGN LIFE OF 10 MIN.
$= 10_{\text{MIN.}} \times 60_{\text{SEC.}} \times 100_{\text{AVG. CPS}} = 60000$

ALLOW. STRESS (SMOOTH & R=-1) OF 2024-T4 FOR 60,000 CYCLES TO FAILURE
= 25,000 PSI = F_b (RMS)

REQUIRED BRACKET THICKNESS AT BENDS
$= t = \sqrt{\frac{6M}{F_b C}} = \sqrt{\frac{6 \times 90}{25{,}000 \times 4.625}} = \sqrt{.00467} = .069$
= .071 IN. (NEAREST SHEET GAGE)

PARALLELOGRAMING VIBRATION DIRECTION A-A
MAX. MOMENT AT EACH (4) BEND OF HAT SECTION
$= W \times a/4$ IN. LB.

REF: SM-48789P
P. 20

MAX. MOMENT DERIVED BY MORE DETAILED METHOD

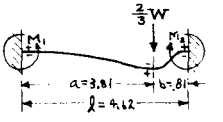

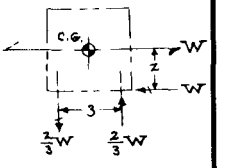

$M_1 = \frac{2}{3} W \frac{ab^2}{l^2} = \frac{2}{3} W \times \frac{3.81 \times .81^2}{(4.62)^2}$
$= \frac{2}{3} W \times .117$

$M_2 = \frac{2}{3} W \frac{a^2 b}{l^2} = \frac{2}{3} W \times \frac{3.81^2 \times .81}{(4.62)^2} = \frac{2}{3} W \times .551$

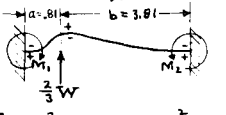

M IS POSITIVE (+) WHEN CLOCKWISE

$M_1 = \frac{2}{3} W \times \frac{.81 \times 3.81^2}{(4.62)^2} = \frac{2}{3} W \times .551$

$M_2 = \frac{2}{3} W \times \frac{.81^2 \times 3.81}{(4.62)^2} = \frac{2}{3} W \times .117$

$\Sigma M_1 = \frac{2}{3} W (-.117 + .551) = \frac{2}{3} W \times .434 = .289 W$ (COMP. (-) ON TOP)

$\Sigma M_2 = \frac{2}{3} W (.551 - .117) = .289 W$ (TENSION (+) ON TOP)

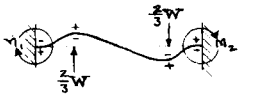

REF: ROARK III, P. 108
CASE 32

IN SKETCH, FORCES HAVE BEEN TRANSFERRED FROM BOX C.G. TO HAT SECTION.

IF HAT SECTION (OR SUPPORT) IS CONSIDERED PIN JOINTED AT "B" & "C", FORCES ARE:

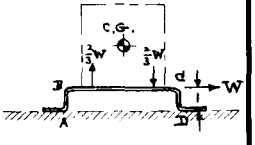

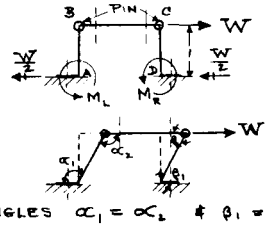

SINCE EI FOR ALL MEMBERS IS SAME, $M_L = M_R$

FORCE "W" CAUSES SUPPORT TO DEFLECT IN SUCH A MANNER THAT A PARALLELOGRAM IS FORMED.

ANGLES $\alpha_1 = \alpha_2$ & $\beta_1 = \beta_2$

IF PIN JOINTS BECOME BENT SHEET, BENDS A, B, C, & D HAVE SAME RESISTANCE TO PARALLELOGRAMING.

M_R IS EQUALLY DIVIDED BETWEEN C & D

M_L IS EQUALLY DIVIDED BETWEEN A & B

SINCE $M_L = M_R$ ∴ M @ A, B, C, & D ARE ALL EQUAL
OR: $M_L = M_R = M_{@B} = M_{@C} = 1W/4 = .25W$

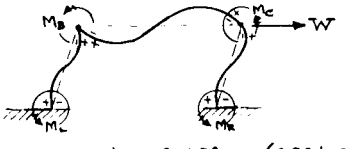

$\Sigma M_{@B} = \Sigma M_{@C} = M_1 + M_3 = (.289 + .25)W = .539W$
MAX. $M = W \times a/4 = 3/4 W = .750 W$
∴ IN DESIGN, LATTER FORMULA IS CONSERVATIVE

MAXIMUM STATIC STRESSES

CONFIGURATION SHOWN ON PAGE 1 (1-11-66)

MAX. M VIA DERIVATION = $\Sigma M_{@B} = \Sigma M_{@C}$
$= .539 W$ REF: PAGE 3 (1-11-66)

MAX. STATIC STRESS (S_{st}) AT B & C

$S_{st} = \frac{6M}{C t^2} = \frac{6 \times .539 W}{C t^2}$

$= \frac{6 \times .539 \times 5}{4.625 \times t^2}$ WHEN W @ 1g = 5 LB.

$= \frac{3.50}{t^2}$

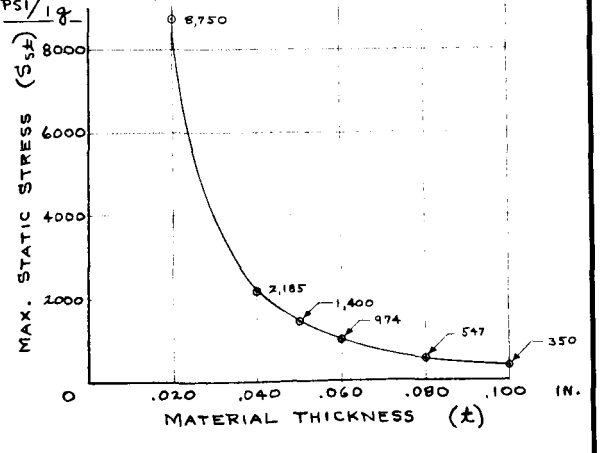

PARALLELOGRAMING — HAT SECTION

FROM PREVIOUS PAGE3, MOMENTS AT JOINTS

$= M_A = M_B = M_C = M_D = .25\ W$

REACTIONS FROM W ACTING HORIZONTALLY ALONG B—C ARE DETERMINED AS FOLLOWS:

$\Sigma M_C = 0$

$R_B = \frac{2 \times .25W}{4.625}$

$= .108\ W$

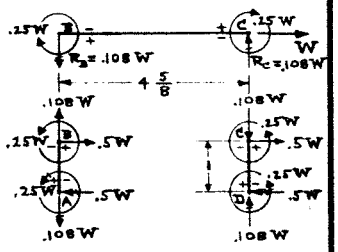

$\Sigma M_A = \Sigma M_B = 0$

$= .5W \times 1 - 2 \times .25W$

BLOCK ROTATION

REACTIONS FROM BOX LOADS $\frac{2}{3}W$

$R_3 = \frac{2W}{3(4.125)^2}\left[-3.81^2(3\times3.81+3.81) + 3.81^2(3\times3.81+8)\right] = -R_4$

$= .556\ W$

REF: ROARK III P. 108, CASE 32

REF: P. 2

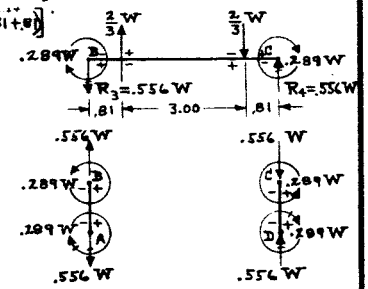

FLANGES — HAT SECTION

PARALLELOGRAMING

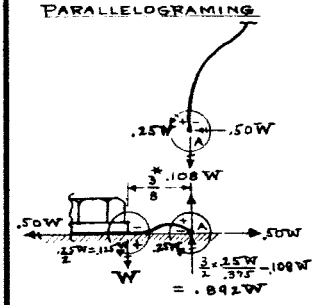

REF: ROARK III P. 107 CASE 29

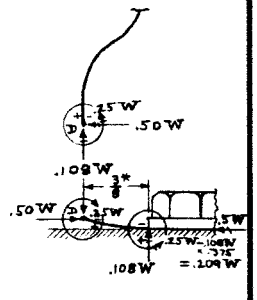

REF: P. 5 1-14-66
ROARK III P102 CASE 9

BLOCK ROTATION

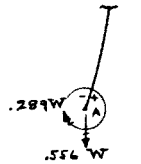

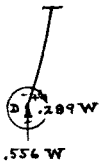

BLOCK ROTATION COMBINED WITH PARALLELOGRAMING

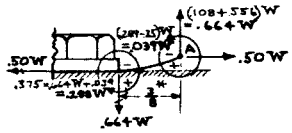

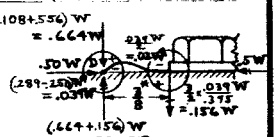

* MEAN DISTANCE OF FLANGE IN BENDING

DEFLECTIONS — HORIZONTAL (A↔A) — C.G. OF BLOCK

PARALLELOGRAMING — HAT SECTION

$\delta_P = \frac{M\ell^2}{6EI}$

REF: PEERY I P. 545

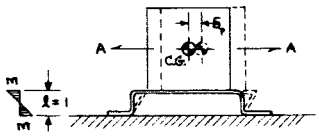

$M = .25W \times 1$

W @ 1g = 5 LB.

$M = .25 \times 5 \times 1 = 1.25$ IN. LB.

$I = \frac{1}{12} \times 4.625 t^3$

$\delta_P = \frac{1.25 \times 1^2 \times 12}{6 \times 10.5 \times 10^6 \times 4.625\ t^3}$

$= \frac{0.515 \times 10^{-7}}{t^3}$

E = 10.5 × 10⁶ PSI

MATERIAL: 2024-T4 ALUM. ALLOY

REF: PAGE 3

GAGE (t)	DEFLECTION (δ_P)
.020 IN.	.0064400 IN.
.040	.0008050
.050	.0004120
.060	.0002390
.080	.0001006
.100	.0000515

FLANGE DEFLECTIONS — HAT SECTION

$\delta_1 = \frac{.664W\ell^3}{3EI}$

REF: P. 6 (1-21-66)

$= \frac{.664 \times 5 \times .375^3}{3 \times 10.5 \times 10^6 \times I}$

$= \frac{.555 \times 10^{-8}}{I}$

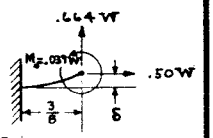

$\delta_2 = \frac{M_0 \ell^2}{2EI}$

REF: ROARK III PP.100 & 102 CASES 1 & 9

$= \frac{.039 \times 5 \times .375^2}{2 \times 10.5 \times 10^6 \times I}$

$= \frac{.1306 \times 10^{-8}}{I}$

$\delta = \delta_1 + \delta_2$

$= \frac{.555 \times 10^{-8}}{I} + \frac{.1306 \times 10^{-8}}{I}$

$= \frac{.6856 \times 10^{-8}}{I}$

$= \frac{.6856 \times 10^{-8} \times 12}{2.0 \times t^3}$

$= \frac{.412 \times 10^{-7}}{t^3}$

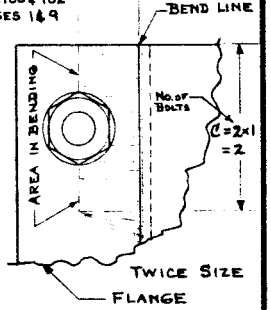

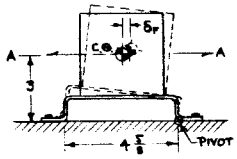

$\delta_F = .412 \times 10^{-7} \times \frac{3}{4.625}$

$= \frac{.267 \times 10^{-7}}{t^3}$

GAGE (t)	DEFLECTION (δ_F)
.020 IN.	.0033400 IN.
.040	.0004180
.050	.0002140
.060	.0001235
.080	.0000522
.100	.0000267

FLANGE DEFLECTIONS CONT'D.

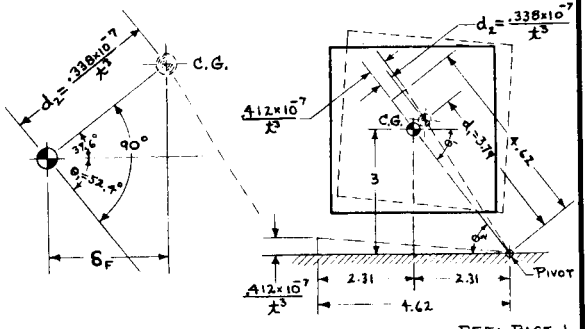

REF: PAGE 1

$d_1 = (2.31^2 + 3.00^2)^{\frac{1}{2}} = 3.79$ IN.

$d_2 = \frac{.412\times10^{-7}}{t^3} \times \frac{d_1}{4.62} = \frac{.412\times10^{-7}}{t^3} \times \frac{3.79}{4.62}$

$= \frac{.338\times10^{-7}}{t^3}$

$\theta_1 = \theta_2 = \tan^{-1}\frac{3.00}{2.31} = 52.4°$

$\delta_F = d_2 \times \cos 37.6° = \frac{.338\times10^{-7}}{t^3} \times \cos 37.6°$

$= \frac{.267\times10^{-7}}{t^3}$

BLOCK ROTATION

REF: TECH. PROGRESS REPORT NAS 8-20849 DEC. 65-JAN. 66, FIG. 5

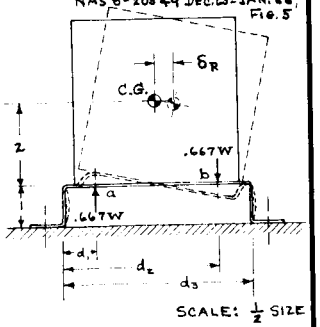

SCALE: $\frac{1}{2}$ SIZE

$d_1 = .810$ IN.
$d_2 = 3.810$
$d_3 = 4.625$
$d_2 - d_1 = 3.000$

WHEN .667 W↑ @ b

$I_{@b} = I_{@a}$

$= \frac{1}{12} c\, t^3$

$= \frac{1}{12} \times 4.625\, t^3$

$= .385\, t^3$

WHEN .667 W↑ @ a

$I_{@a} = \frac{1}{12} \times 2.0 \times t^3$

$= .1667\, t^3$

$I_{@b} = \frac{1}{12} \times 4.625\, t^3$

$= .385\, t^3$

c = EFFECTIVE WIDTH IN BENDING

DEFLECTION WHEN .667 W↑ @ b

$\delta_{1\uparrow @b} = \frac{.667W\times(d_3-d_2)^2\times d_2^2}{6EI\,d_3^3}\left[3d_2^2 + (d_3-d_1)\times d_2 - 3\times d_2\times d_3\right]$

$= \frac{.667\times5\times3.81^2\times3.81^2}{6\times10.5\times10^6\times(4.625)^3\times.385\,t^3}\left[3\times3.81^2+.81\times3.81-3\times3.81\times4.625\right]$

$= \frac{.1320\times10^{-7}}{t^3}\times(-6.32) = -\frac{.835\times10^{-7}}{t^3}$

$\delta_{2\uparrow @a} = \frac{.667W(d_3-d_2)^2\times d_1^3}{6\times EI\,d_3^3}\left[3\times d_1^2 + (d_3-d_2)\times d_1 - 3\times d_2\times d_3\right]$

$= \frac{.667\times5\times.81^2\times.81^2}{6\times10.5\times10^6\times(4.625)^3\times.385\,t^3}\left[3\times3.81\times.81+3^2-3\times3.81\times4.625\right]$

$= \frac{.598\times10^{-9}}{t^3}\times(-43.0) = -\frac{.257\times10^{-7}}{t^3}$

REF: ROARK III, P. 108, CASE 32

BLOCK ROTATION CONT'D.

DEFLECTION WHEN .667 W↑ @ a

$\delta_{3\uparrow @a} = \frac{.667W(d_3-d)^2\times d_1^2}{6EI\,d_3^3}\left[3\times d_1^2 + (d_3-d_1)\times d_1 - 3\times d_1\times d_3\right]$

$= \frac{.667\times5\times3.81^2\times.81^2}{6\times10.5\times10^6\times4.625^3\times.1667\,t^3}\left[3\times.81^2+3.81\times.81-3\times3.81\times4.625\right]$

$= .306\times10^{-7}\times(-6.2)\times(-1)\uparrow = \frac{.190\times10^{-6}}{t^3}$

$\delta_{4\uparrow @b} = .667W\,d_1^2\,(d_3-d_2)^2\left\{\left[3(d_3-d_1)+d_1\right]\left[d_3-d_2\right]-3(d_2-d_1)d_3\right\}$

$= \frac{.667\times5\times.81^2(4.625-3.810)^2}{6\times10.5\times10^6\times4.625^3\times.385\,t^3}\left\{\left[3\times3.815+.81\right]\times.815-3\times3.815\times4.625\right\}$

$= \frac{.605\times10^{-9}}{t^3}\times(-43.0)\times(-1)\uparrow = \frac{.260\times10^{-7}}{t^3}$

DEFLECTION - .667 W↑ @ a + .667 W↑ @ b

$\delta\uparrow @a = \delta_{3\uparrow} - \delta_{2\uparrow} = +\frac{1.90\times10^{-7}}{t^3} - \frac{.257\times10^{-7}}{t^3}$

$= +\frac{1.643\times10^{-7}}{t^3}$

$\delta\uparrow @b = -\delta_{1\uparrow} + \delta_{4\uparrow} = -\frac{.835\times10^{-7}}{t^3} + \frac{.260\times10^{-7}}{t^3}$

$= -\frac{.575\times10^{-7}}{t^3}$

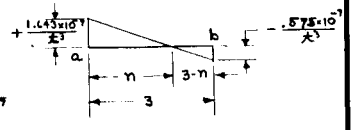

$\frac{n}{1.643\times10^{-7}} = \frac{3-n}{.575\times10^{-7}}$

$\frac{.575\times10^{-7}}{t^3}\,n = \frac{1.643\times10^{-7}}{t^3}(3-n)$

$n = \frac{4.929}{2.218} = 2.23$ IN.

BLOCK ROTATION CONT'D.

$d_1 = (.73^2 + 2.00^2)^{\frac{1}{2}}$

$= 2.13$ IN.

$d_2 = \frac{1.643\times10^{-7}}{t^3} \times \frac{2.13}{2.23}$

$= \frac{1.570\times10^{-7}}{t^3}$

$\theta_2 = \tan^{-1}\frac{2.00}{.73} = 70°$

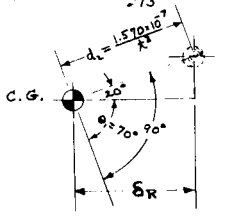

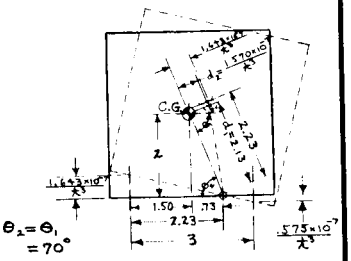

$\delta_R = d_2 \times \cos 20°$

$= \frac{1.570\times10^{-7}}{t^3} \times .9397$

$= \frac{1.475\times10^{-7}}{t^3}$

GAGE (t)	DEFLECTION (δ_R)
.020 IN.	.0184600 IN.
.040	.0023100
.050	.0011800
.060	.0006830
.080	.0002880
.100	.0001475

SUMMATION — DEFLECTIONS

GAGE (t)	δ_P	δ_F	δ_R	$\Sigma\delta$
.020 IN.	.0064400	+.0033400	+.0184600	=.0282400 IN.
.040	.0008050	+.0004180	+.0023100	=.0035330
.050	.0004120	+.0002140	+.0011800	=.0018060
.060	.0002390	+.0001235	+.0006830	=.0010455
.080	.0001006	+.0000522	+.0002880	=.0004408
.100	.0000515	+.0000267	+.0001475	=.0002257
REF:	P. 7	P. 8	P. 12	

NATURAL FREQUENCIES

f_o .020 GAGE $= \frac{1}{2\pi}\left(\frac{386}{.02824}\right)^{\frac{1}{2}} =$ 18.7 CPS

f_o .040 GAGE $= \frac{1}{2\pi}\left(\frac{386}{.0035330}\right)^{\frac{1}{2}} =$ 52.8

f_o .050 GAGE $= \frac{1}{2\pi}\left(\frac{386}{.001806}\right)^{\frac{1}{2}} =$ 73.6

f_o .060 GAGE $= \frac{1}{2\pi}\left(\frac{386}{.0010455}\right)^{\frac{1}{2}} =$ 96.6

f_o .080 GAGE $= \frac{1}{2\pi}\left(\frac{386}{.0004408}\right)^{\frac{1}{2}} =$ 149.3

f_o .100 GAGE $= \frac{1}{2\pi}\left(\frac{386}{.0022257}\right)^{\frac{1}{2}} =$ 209.0

MAX. STATIC STRESS × SQUARE ROOT OF NATURAL FREQ.

GAGE (t)	S_{st}	f_o	$f_o^{\frac{1}{2}}$	$S_{st} \times f_o^{\frac{1}{2}}$
.020 IN.	8,750 PSI	18.7 CPS	4.33	37,900 $(CPS)^{\frac{1}{2}}$ PSI
.040	2,185	52.8	7.27	15,900
.050	1,400	73.6	8.59	12,020
.060	974	96.6	9.83	9,550
.080	547	149.3	12.21	6,680
.100	350	209.0	14.46	5,060
REF:	P. 4	P. 13		

σ_{RMS} = ROOT-MEAN-SQUARE STRESS

$= \left(\frac{\pi}{2} \cdot Q \cdot f_o \cdot PSD\right)^{\frac{1}{2}} \frac{S_{st}}{g}$

$\frac{S_{st}}{g} \cdot f_o^{\frac{1}{2}} = \frac{\sigma_{RMS}}{\left(\frac{\pi}{2} \cdot Q \cdot PSD\right)^{\frac{1}{2}}}$

WHEN:

σ_{RMS} = 25,000 PSI

Q = 20

PSD = 0.3 g^2/CPS

$\frac{S_{st}}{g} \cdot f_o^{\frac{1}{2}} = \frac{25{,}000 \text{ PSI}}{\left(\frac{\pi}{2} \times 20 \times 0.3 \frac{g^2}{CPS}\right)^{\frac{1}{2}}}$

$\frac{S_{st}}{g} \times f_o^{\frac{1}{2}} = \frac{25{,}000 \text{ PSI}}{(\pi \times 3.0)^{\frac{1}{2}}} \times \frac{(CPS)^{\frac{1}{2}}}{g}$

$S_{st} \times f_o^{\frac{1}{2}} =$ 8,150 $(CPS)^{\frac{1}{2}}$ PSI

REF: FIG. 2-6, P. 12
SM-48789P

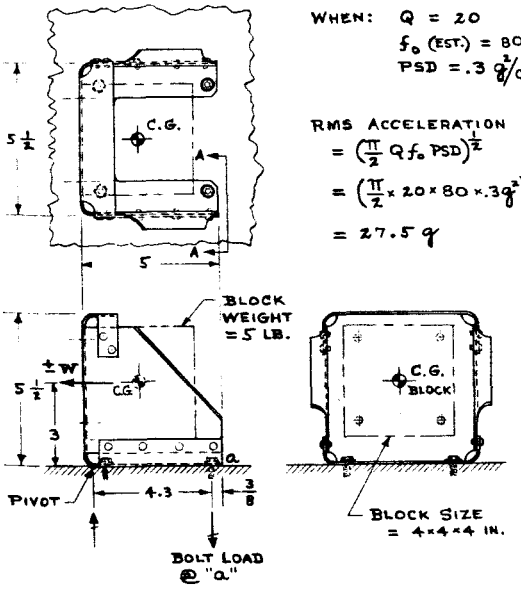

WHEN: Q = 20

f_o (EST.) = 80 CPS

PSD = .3 g^2/CPS

RMS ACCELERATION

$= \left(\frac{\pi}{2} Q f_o PSD\right)^{\frac{1}{2}}$

$= \left(\frac{\pi}{2} \times 20 \times 80 \times .3 g^2\right)^{\frac{1}{2}}$

$= 27.5\, g$

W = BLOCK WEIGHT × RMS ACCELERATION

= 5.0 × 27.5 = 138 LB.

		TOL.	
EDGE TO BOLT	= 3/8 + 1/32		= .406 IN.
SHEET GAGE	= .063	+.004	= .067
BEND RADIUS	= .190	+.010	= .200
	TOTAL		= .67

DISTANCE ℄ BOLT TO PIVOT = 5.00 − .03 (TOL.) − .67 = 4.3 IN.

LOAD PER BOLT @ "a" $= \frac{3 \times 138}{4.3 \times 2} =$ 48 LB. TENSION

IMAGINARY BEND LINE IS ESTIMATED TO EFFECTIVELY EXTEND FOR (b) 1 INCH FROM END.

EST. CYCLES DURING DESIGN LIFE OF 10 MIN.

$= 10 \times 60 \times 100$ (MIN. × SEC. × AVG. CPS) $= 60{,}000$

ALLOW. STRESS, F_b (RMS), FOR 60,000 CYCLES TO FAILURE

= 25,000 PSI

REQUIRED SHEET STOCK THICKNESS

$= t = \sqrt{\frac{6M}{b \times F_{b(rms)}}}$

$= \sqrt{\frac{6 \times 48 \times .45}{1 \times 25{,}000}}$

= .071 IN.

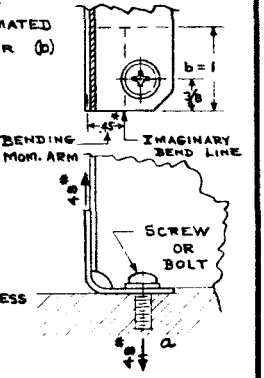

* BENDING MOMENT ARM

SHEET GAGE/2	=	.032
ALLOW. BEND RAD	=	.190
WASHER DIA. (0.D.)/2	=	.219
MISC.	=	.009
TOTAL	=	.450 IN.

REF: SM-48789P P. 21

* SKETCH MOM. ARM ALSO SCALES .450 IN.

EFFECTS OF BLOCK LOAD DISTRIBUTIONS ON C.G. DEFLECTIONS

BLOCK LOAD W CONCENTRATED AT C.G. LOCATION

$$\delta_{@\,c.g.} = \frac{W}{3EI}\left(\frac{3}{5}\ell\right)^3$$

$$= \frac{W\ell^3}{EI} \times \frac{1}{3} \times \frac{9}{125}$$

$$= .072\,\frac{W\ell^3}{EI}$$

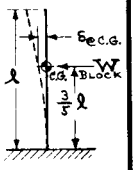

FROM FOLLOWING CALCULATIONS OF δ (ALSO SEE NEXT PAGE), MAX. VARIATION IS FROM .072 TO .074 $W\ell^3/EI$ OR 2.8%.

BECAUSE OF SMALL VARIATION AND SOME BLOCK STIFFENING EFFECT, BLOCK LOAD WILL BE CONSIDERED CONCENTRATED AT C.G. LOCATION.

BLOCK DISTRIBUTED AS PARTIAL UNIFORM LOAD WITH ABOVE C.G. LOCATION

$$\delta_{@\,C.G.} = \frac{W}{24EI}\left[6\left(\tfrac{1}{5}\ell+\ell\right)\left(\ell-\tfrac{2}{5}\ell\right)^2 - 4\left(\ell-\tfrac{2}{5}\ell\right)^3 + \frac{\left(\ell-\frac{2}{5}\ell-\frac{1}{5}\ell\right)^4}{\ell-\frac{1}{5}\ell}\right]$$

$$= \frac{W}{24EI}\left[6\left(\tfrac{6}{5}\ell\right)\left(\tfrac{3}{5}\ell\right)^2 - 4\left(\tfrac{3}{5}\ell\right)^3 + \frac{\left(\frac{2}{5}\ell\right)^4}{\frac{4}{5}\ell}\right]$$

$$= \frac{W}{24EI}\left[6\left(\frac{54\ell^3}{125}\right) - 4\left(\frac{27\ell^3}{125}\right) + \frac{4\ell^3}{125}\right]$$

$$= \frac{W\ell^3}{24EI}\left(\frac{324}{125} - \frac{108}{125} + \frac{4}{125}\right)$$

$$= \frac{W\ell^3}{24EI} \times \frac{220}{125} = .073\,\frac{W\ell^3}{EI}$$

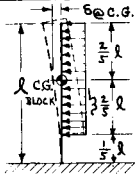

$W = \frac{4}{5}\,w\ell$

BLOCK LOAD CONCENTRATED EQUALLY AT ITS 4 ATTACH POINTS

$$\delta_{@\,C.G.} = \frac{.5W}{6EI}\left[\left(\tfrac{2}{5}\ell - \tfrac{1}{10}\ell\right)^3 - 3\left(\tfrac{9}{10}\ell\right)^2\left(\tfrac{2}{5}\ell - \tfrac{1}{10}\ell\right) + 2\left(\tfrac{9}{10}\ell\right)^3\right]$$

$$= \frac{W}{12EI}\left[\left(\tfrac{3}{10}\ell\right)^3 - 3\times\frac{81}{100}\ell^2\left(\tfrac{3}{10}\ell\right) + 2\times\frac{729}{1000}\ell^3\right]$$

$$= \frac{W\ell^3}{12EI}\times\left(\frac{27}{1000} - \frac{729}{1000} + \frac{1458}{1000}\right)$$

$$= \frac{W\ell^3}{12EI}\times\frac{756}{1000} = .063\,\frac{W\ell^3}{EI}$$

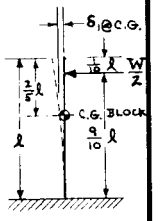

$$\delta_{2@C.G.} = \frac{.5W}{6EI}\left[-\left(\tfrac{3}{10}\ell\right)^3 + 3\left(\tfrac{3}{10}\ell\right)^2\ell - 3\left(\tfrac{2}{10}\ell\right)^2\left(\tfrac{2}{5}\ell\right)\right]$$

$$= \frac{W\ell^3}{12EI}\left(-\frac{27}{1000} + \frac{27}{100} - 3\times\frac{9}{100}\times\frac{4}{10}\right)$$

$$= \frac{W\ell^3}{12EI}\left(-\frac{27}{1000} + \frac{270}{1000} - \frac{108}{1000}\right)$$

$$= \frac{W\ell^3}{12EI}\times\frac{135}{1000} = .011\,\frac{W\ell^3}{EI}$$

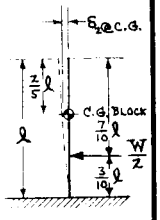

$$\Sigma\,\delta_{@\,C.G.} = \delta_1 + \delta_2 = (.063 + .011)\,\frac{W\ell^3}{EI}$$

$$= .074\,\frac{W\ell^3}{EI}$$

CANTILEVER TYPE DEFLECTIONS

W = BLOCK WEIGHT = 5.0 LB/g

$$\delta_c = \frac{1}{3}\times\frac{W}{2EI}\times 3^3 = \frac{4.5\,W}{EI}$$

E (6061) = 9.9×10^6 PSI

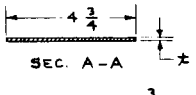

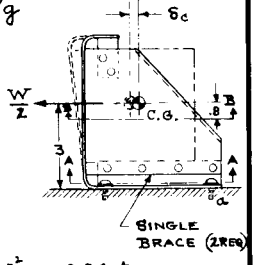

$$I_{A-A} = \frac{1}{12}t\,(4.75)^3$$

$$= 8.93\,t$$

$$I_{B-B} = \frac{1}{12}t\,(4.0)^3 + .75\times t\times 2.0^2 = 8.34\,t$$

$$\therefore\ I = 8.5\,t \quad (-\text{MEAN})$$

$$\delta_C = \frac{4.5\,W}{EI} = \frac{4.5\times 5}{9.9\times10^6\times 8.5\,t}$$

$$= \frac{.268\times10^{-6}}{t}$$

REF: FIFTH MONTHLY PROG. REPORT, FIG. 1 (A2-260-ABD1-85)

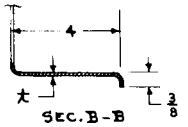

GAGE (t)	DEFLECTION (δ_c)
.025 IN.	.00001070 IN.
.032	.00000838
.040	.00000670
.050	.00000537
.063	.00000425
.071	.00000377
.080	.00000335
.090	.00000298

FLANGE DEFLECTIONS

W = BLOCK WEIGHT = 5.0 LB/g

LOAD PER BOLT @ "a" = $\frac{5\times3}{2\times4.3}$ = 1.75 LB. TENSION

REF: PP. 1 & 2

IMAGINARY RESISTANCE LINE IS ESTIMATED TO EFFECTIVELY EXTEND FOR 1 INCH FROM END.

AREA IN BENDING

BENDING MOMENT ARM (ℓ) (SCALED)

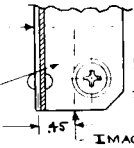

$$\delta = \frac{\text{LOAD}\times\ell^3}{3EI} \qquad I = \frac{1}{12}\times1\times t^3$$

$$= \frac{1.25\times(.45)^3\times12}{3\times9.9\times10^6\times t^3}$$

$$= \frac{.645\times10^{-7}}{t^3}$$

SINGLE BENDING IS ASSUMED – UP STAND WEB IS UNRESTRAINED

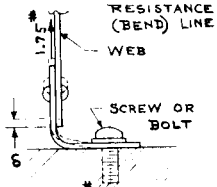

$$d_1 = (1.74^2 + 3^2)^{\frac{1}{2}}$$

$$= 3.47 \text{ IN.}$$

$$d_2 = \frac{.645\times10^{-7}}{t^3}\times\frac{3.47}{4.30}$$

$$= \frac{.52\times10^{-7}}{t^3}$$

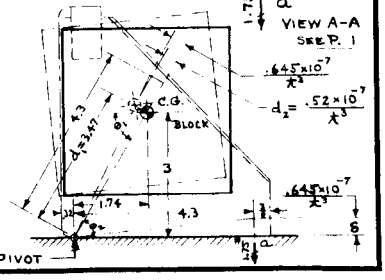

FLANGE DEFLECTIONS CONT'D.

$\theta_1 = \theta_2 = \tan^{-1} \frac{3.00}{1.74}$

$= 59.9°$

$\delta_F = d_2 \cos 30.1°$

$= \frac{.52 \times 10^{-7}}{t^3} \times \cos 30.1°$

$= \frac{.45 \times 10^{-7}}{t^3}$

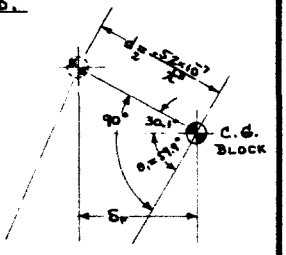

GAGE (t)	DEFLECTION (δ_F)
.025 IN.	.0028900 IN.
.032	.0013750
.040	.0007040
.050	.0003600
.063	.0001800
.071	.0001258
.080	.0000880
.090	.0000618

PANEL DEFLECTIONS

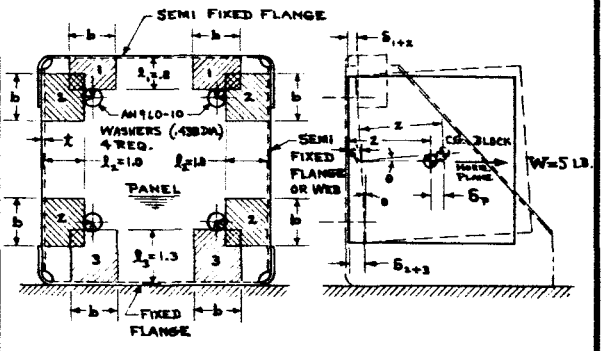

l_n = PERPENDICULAR DISTANCE FROM CENTER OF FLANGE THICKNESS (t) TO CHORD OF 45° SECTOR.

b = LENGTH OF IMAGINARY RESISTANCE (TO BENDING) LINE
= 45° ARC OF WASHER + 15 t
= $.438\pi/8 + 15 \times t$ = .172 + 15 t

BENDING RESISTANCE OF PANEL IS ESTIMATED AS FOLLOWS:
FREE FLANGE – SINGLE BENDING = M/1
SEMI FIXED FLANGE – 150% BENDING = M/1.5
FIXED FLANGE – DOUBLE BENDING = M/2

LOAD AT EACH ATTACHMENT (¼ WASHER) = 5/4 = 1.25 LB.

PANEL DEFLECTIONS CONT'D.

I FOR AREAS NO. 1 + NO. 2 OR NO. 2 + NO. 3

$= \frac{1}{12} b t^3 = \frac{2}{12}(.172 + 15t)\, t^3$

$= .0287 t^3 + 2.5000 t^4 = (.0287 + 2.5000t) t^3$

CUBE MEAN l_n FOR AREAS NO. 1 + NO. 2

$= \left(\frac{l_1^3 + l_2^3}{2}\right)^{\frac{1}{3}} = \left(\frac{.8^3 + 1.0^3}{2}\right)^{\frac{1}{3}} = .911$ IN.

MEAN M – AREAS NO. 1 + NO. 2 (SEMI FIXED FLANGES)

$= \frac{1.25 \times .911}{1.5} = .760$ IN. LB.

$\delta_{(WASHER)}$ FOR AREAS NO. 1 + NO. 2

$= \frac{M l_n^2}{3EI} = \frac{.760 \times .911^2}{3 \times 9.9 \times 10^6 (.0287 t^3 + 2.5 t^4)}$

$= \frac{.212 \times 10^{-7}}{(.0287 + 2.5t) t^3}$

CUBE MEAN l_n FOR AREAS NO. 2 + NO. 3

$= \left(\frac{l_2^3 + l_3^3}{2}\right)^{\frac{1}{3}} = \left(\frac{1.0^3 + 1.3^3}{2}\right)^{\frac{1}{3}} = 1.17$ IN.

MEAN M – AREAS NO. 2 + NO. 3 (SEMI FIXED & FIXED FLANGES)

$= \frac{1.25 \times 1.17}{\frac{1.5 + 2.0}{2}} = .835$ IN. LB.

$\delta_{(WASHER)}$ FOR AREAS NO. 2 + NO. 3

$= \frac{M l_n^2}{3EI} = \frac{.835 \times 1.17^2}{3 \times 9.9 \times 10^6 (.0287 + 2.5t) t^3}$

$= \frac{.385 \times 10^{-7}}{(.0287 + 2.5t) t^3}$

PANEL DEFLECTIONS CONT'D.

δ_P' = BLOCK C.G. DEFLECTION IN HORIZONTAL PLANE

$= \frac{(.212 + .385) \times 10^{-7}}{2(.0287 + 2.5t) t^3}$

$= \frac{.299 \times 10^{-7}}{(.0287 + 2.5t) t^3}$

REF: P. 8

$\theta = \tan^{-1}\left(\frac{.385 - .212}{3.000}\right)$

$= 3.3°$

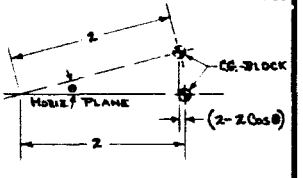

C.G. MOTION ALONG HORIZ. PLANE FROM BLOCK ROTATION

$= 2 - 2\cos\theta$

$= 2 - 2\cos 3.3°$

$= 2.000 - 1.997$

$= .003$ IN

$\delta_P = \frac{(.299 - .003) \times 10^{-7}}{(.0287 + 2.5t) t^3} = \frac{.296 \times 10^{-7}}{(.0287 + 2.5t) t^3}$

GAGE (t)	DEFLECTION (δ_P)
.025 IN.	.020800 IN.
.032	.008350
.040	.003600
.050	.001540
.063	.000634
.071	.000402
.080	.000253
.090	.000160

SUMMATION — DEFLECTIONS

GAGE (t)	δ_c	δ_F	δ_P	$\Sigma\delta$
.025 IN.	.0000107 +	.0028900 +	.0208000 =	.0237007 IN.
.032	.0000084 +	.0013750 +	.0083500 =	.0097334
.040	.0000067 +	.0007040 +	.0036000 =	.0043107
.050	.0000054 +	.0003600 +	.0015400 =	.0019054
.063	.0000043 +	.0001800 +	.0006340 =	.0008183
.071	.0000038 +	.0001258 +	.0004020 =	.0005316
.080	.0000034 +	.0000880 +	.0002530 =	.0003444
.090	.0000030 +	.0000618 +	.0001600 =	.0002248
REF:	P. 5	P. 7	P. 10	

NATURAL FREQUENCIES

f_o .025 GAGE $= \frac{1}{2\pi}\left(\frac{386}{.02370}\right)^{\frac{1}{2}} =$ 20.4 CPS

f_o .032 $= \frac{1}{2\pi}\left(\frac{386}{.00973}\right)^{\frac{1}{2}} =$ 31.7

f_o .040 $= \frac{1}{2\pi}\left(\frac{386}{.00431}\right)^{\frac{1}{2}} =$ 47.8

f_o .050 $= \frac{1}{2\pi}\left(\frac{386}{.001908}\right)^{\frac{1}{2}} =$ 71.5

f_o .063 $= \frac{1}{2\pi}\left(\frac{386}{.000818}\right)^{\frac{1}{2}} =$ 109.0

f_o .071 $= \frac{1}{2\pi}\left(\frac{386}{.000532}\right)^{\frac{1}{2}} =$ 135.0

f_o .080 $= \frac{1}{2\pi}\left(\frac{386}{.000344}\right)^{\frac{1}{2}} =$ 168.5

f_o .090 $= \frac{1}{2\pi}\left(\frac{386}{.000225}\right)^{\frac{1}{2}} =$ 208.0

MAXIMUM STATIC STRESSES S_{st}

FLANGE STRESSES @ LOCATION "a" REF: PP. 1 & 6

b = LENGTH OF IMAGINARY RESISTANCE LINE TO BENDING $= .172 + 15t$ REF: P. 8

"b" SHALL NOT EXCEED 1 INCH FOR THIS END ATTACHMENT.

$I = \frac{1}{12} b t^3 = \frac{1}{12}(.172 + 15t)\, t^3$

LOAD PER BOLT @ "a" = 1.75 LB. TENSION REF: P. 6

$M = 1.75 \times .45 = .788$ IN. LB./BOLT

MAX. STATIC STRESS $= S_{st} = \frac{M\frac{t}{2}}{I}$

$= \frac{12 \times .788\,\frac{t}{2}}{(.172 + 15t)\, t^3}$

$= \frac{4.73}{(.172 + 15t)\, t^2}$

PANEL STRESSES

MAX. M IS FOR AREAS NO. 2 + NO. 3 $= .835$ IN. LB. REF: P. 9

I FOR AREAS NO. 2 + NO. 3 $= \frac{1}{6}(.172 + 15t)\, t^3$ "b" IS NOT LIMITED.

$S_{st} = \frac{M\frac{t}{2}}{I} = \frac{6 \times .835\,\frac{t}{2}}{(.172 + 15t)\, t^3}$

$= \frac{2.51}{(.172 + 15t)\, t^2} < \frac{4.73}{(.172 + 15t)\, t^2}$

∴ PANEL STRESS IS NOT CRITICAL

MAXIMUM STATIC STRESSES CONT'D.

PSI/1g

$S_{st} = \frac{4.73}{(.172 + 15t)\, t^2}$

$(.172 + 15t) \leqq 1$ (MAX)

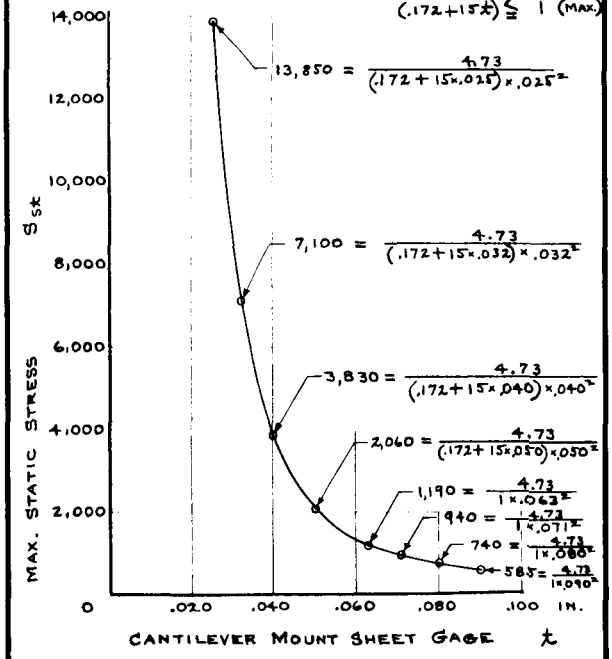

MAX. STATIC STRESS × SQUARE ROOT OF NATURAL FREQ.

GAGE t	S_{st}	f_o	$f_o^{\frac{1}{2}}$	$S_{st} \times f_o^{\frac{1}{2}}$
.025 IN.	13,850 PSI	20.4 CPS	4.52	62,600 $(CPS)^{\frac{1}{2}}$PSI
.032	7,100	31.7	5.63	39,900
.040	3,830	47.8	6.92	26,500
.050	2,060	71.5	8.46	17,420
.063	1,190	109.0	10.43	12,400
.071	940	135.0	11.62	10,900
.080	740	168.5	13.00	9,620
.090	585	208.0	14.42	8,440
REF:	P. 14	PP. 11 & 12		

σ_{RMS} = ROOT-MEAN-SQUARE STRESS $= \left(\frac{\pi}{2} Q f_o \text{ PSD}\right)^{\frac{1}{2}} \frac{S_{st}}{g}$

$\frac{S_{st}}{g} \times f_o^{\frac{1}{2}} = \frac{\sigma_{RMS}}{\left(\frac{\pi}{2} Q \text{ PSD}\right)^{\frac{1}{2}}}$

WHEN: $\sigma_{RMS} = 25{,}000$ PSI

$Q = 15$ REF: P. 2

PSD $= 0.3\ g^2/\text{CPS}$

$\frac{S_{st}}{g} \times f_o^{\frac{1}{2}} = \frac{25{,}000 \text{ PSI}}{\left(\frac{\pi}{2} \times 15 \times .3\ g^2/\text{CPS}\right)^{\frac{1}{2}}} = \frac{25{,}000}{(7.08)^{\frac{1}{2}}}$

$S_{st} \times f_o^{\frac{1}{2}} = 9400\ (\text{CPS})^{\frac{1}{2}}\ \text{PSI}$

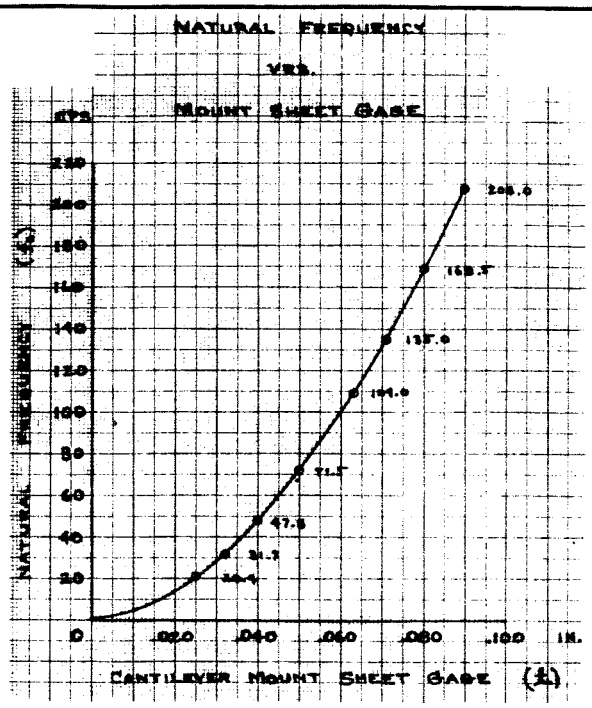

Cantilever Mount for 5-lb Block

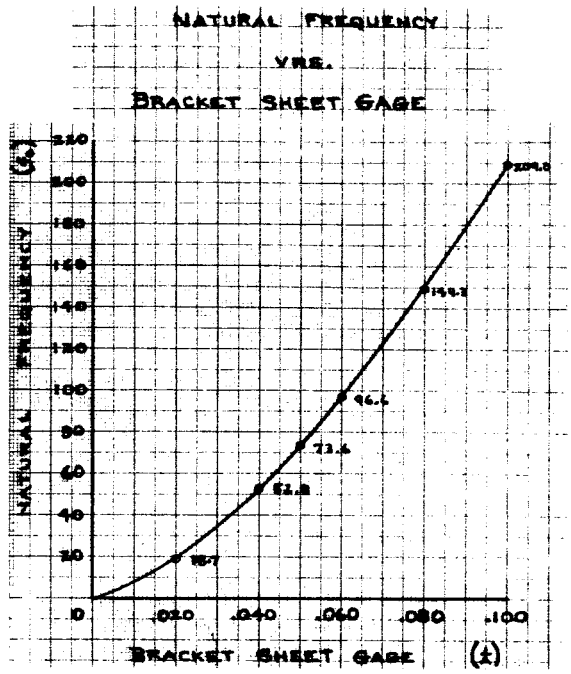

Box Mounted on Hat Section – 2nd Configuration

PREPARED BY: [illegible] DOUGLAS AIRCRAFT COMPANY, INC.
CHECKED BY: [illegible]
DATE: 3-21-62 M.S.S. DIVISION
TITLE: CANTILEVER MOUNT FOR 5 LB BLOCK
PAGE 17
MODEL
REPORT NO

REQUIRED SHEET GAGE FROM STRESS CALCULATIONS

REVISED f_o = 109 CPS FOR .063 GAGE REF: P. 11
REVISED Q = 15
PSD = .3 g^2/CPS

RMS ACCELERATION = $\left(\frac{\pi}{2} Q f_o PSD\right)^{\frac{1}{2}}$ REF: P. 1
$= \left(\frac{\pi}{2} \times 15 \times 109 \times .3\ g^2\right)^{\frac{1}{2}} = (771)^{\frac{1}{2}}\ g$
$= 27.8\ g$

W = BLOCK WEIGHT × RMS ACCELERATION
= 5.0 × 27.8 = 139 LB.

LOAD PER BOLT @ "a" = $\frac{3 \times 139}{4.3 \times 2}$ = 48.5 LB. TENSION

M ALONG IMAGINARY BEND RESISTANCE LINE @ "a"
= 48.5 × .45 = 21.8 IN. LB.

REQ. SHEET GAGE = $t = \left(\frac{6M}{b F_{b(RMS)}}\right)^{\frac{1}{2}}$

WHERE: b = 1 IN. @ t = .071
$F_{b(RMS)}$ = 25,000 PSI
REF: P. 2

$t = \left(\frac{6 \times 21.8}{1 \times 25{,}000}\right)^{\frac{1}{2}} = (.00523)^{\frac{1}{2}}$
= .0724 IN.

FROM PRECEDING GRAPH, REQUIRED t = .081 IN.
DIFFERENCE = $\left(1 - \frac{t_{STRESS}}{t_{GRAPH}}\right) \times 100 = \left(1 - \frac{.072}{.081}\right) 100$ = 11 %

IN SIXTH MONTHLY PROGRESS REPORT ON PAGE 2,
REQUIRED t VIA STRESS CALCULATIONS = .071 IN.

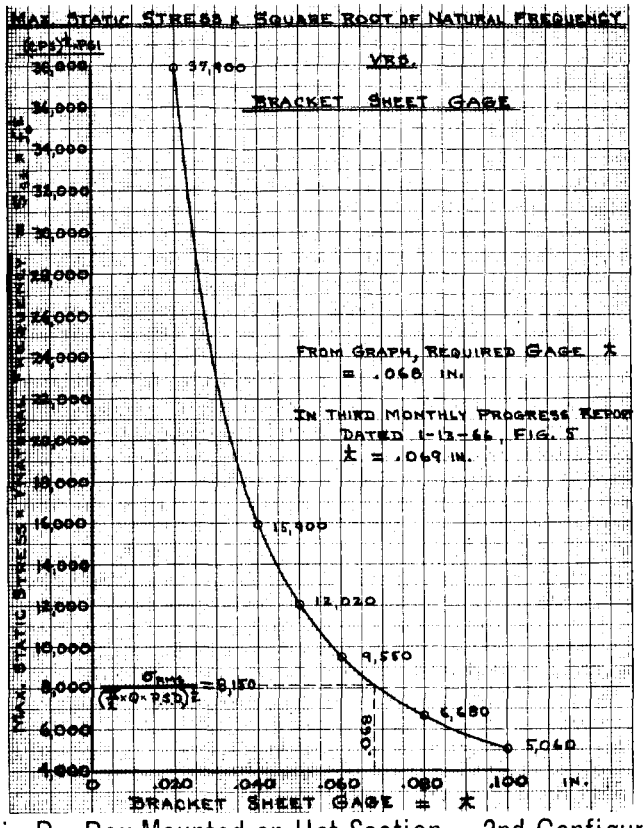

Appendix D. Box Mounted on Hat Section – 2nd Configuration

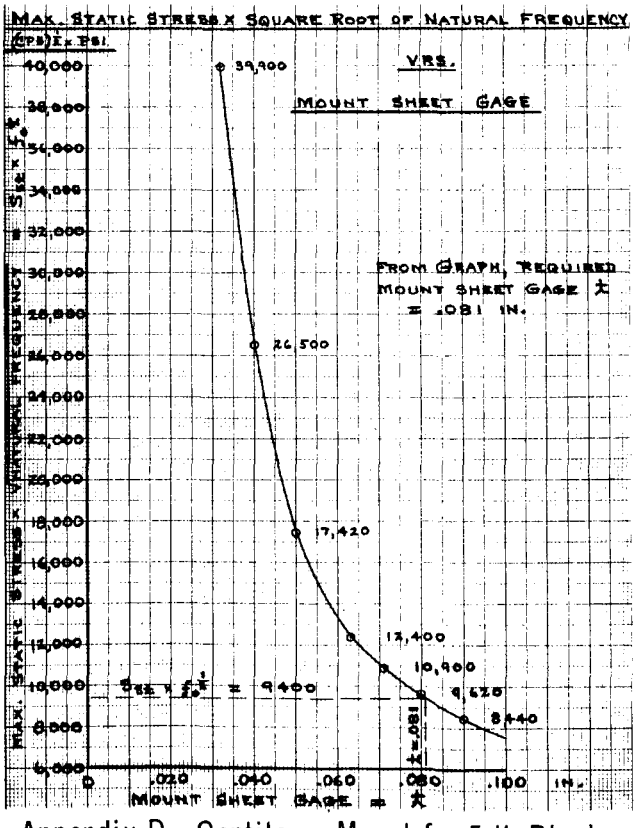

Appendix D. Cantilever Mount for 5-lb Block

Appendix E
NOMOGRAMS

Nomograms for the hat section bracket, and cantilever bracket were constructed in the form of Alignment Charts rather than the more complicated Cartesian Charts because of the simplicity afforded in their use.

Nomograms are advantageous in solving multiplication equations with power functions, especially where repeated use is made of the equations in design problems. By observation, relationships of variable limits to final solutions can quickly be made. Nomograms were developed according to the method outlined in the second edition of "Nomography" by A. S. Levens.

E. 1 HAT SECTION NOMOGRAM

Bracket sheet gage = t

$$= 203.81(W)^{0.6} \times \left(\frac{a}{F_b}\right)^{0.8} \times \frac{1}{(C)^{0.6}} \times \frac{1}{(\ell)^{0.6}} \times (PSD)^{0.4}$$

where

W	=	simulated load weight
a	=	mounting surface (table) to load center of gravity
C	=	bracket width
ℓ	=	table mounting surface to load mounting surface
$F_{b_{(rms)}}$	=	allowable stress
PSD	=	random environment

$$\text{RMS acceleration} = \left(\frac{\pi}{2} \times Q \times f_o \times PSD\right)^{1/2}$$

where

Q	=	amplification factor
f_o	=	natural frequency

Bending moment at each (4) bend of hat section $= M = \frac{Wa}{4}\left(\frac{\pi}{2} \times Q \times f_o \text{ PSD}\right)^{1/2}$

$F_b = \frac{Mt}{2I}$

I = moment of inertia $= \frac{Ct^3}{12}$

where

C = hat section width (bend length)

$$F_b = \frac{M \times 12 \times 12^6}{2 \times C \times t^{32}}$$

$$t = \left(\frac{6M}{F_b \times C}\right)^{1/2}$$

$$= \left(\frac{6Wa}{4F_b \times C}\right)^{1/2} \left(\frac{\pi}{2} \times Q \times f_o \times \text{PSD}\right)^{1/4}$$

$$= (1.5)^{1/2} \left(\frac{\pi}{2}\right)^{1/4} \left(\frac{Wa}{F_b \times C}\right)^{1/2} (Q \times f_o \times \text{PSD})^{1/4}$$

$$= 1.37 \left(\frac{Wa}{F_b \times C}\right)^{1/2} (Q \times f_o \times \text{PSD})^{1/4}$$

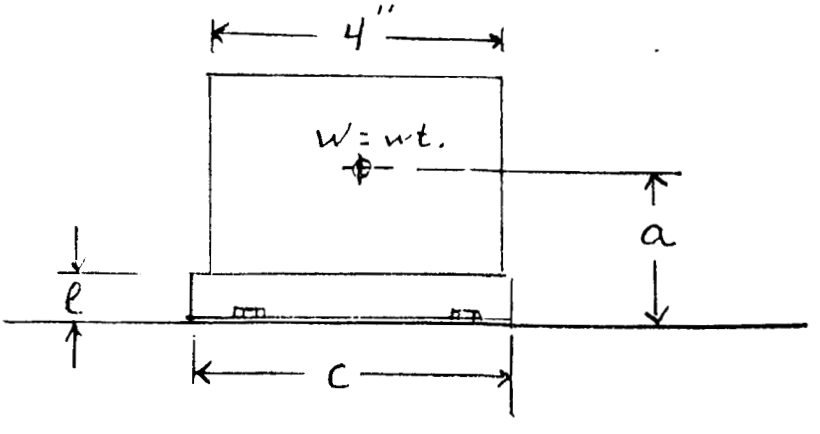

Natural frequency $= f_o = \frac{1}{2\pi}\left(\frac{386}{\delta}\right)^{1/2}$

δ = static deflection (joint displacement) $= \frac{M\ell^2}{6EI}$

(Ref: Peery$_I$, p. 545)

where

$$I = \frac{1}{12} Ct^3$$

$$M = \frac{W\ell'}{4} = \frac{k_1 W\ell}{4}$$

$$\ell' = k_1 \ell$$

$$\delta = \left(\frac{k_1 W\ell}{4}\right)\frac{\ell^2}{6EI} = \frac{k_1 W\ell^3 \times 12}{24 \times ECt^3}$$

$$f_o = \frac{1}{2\pi}\left(\frac{386 \times 2 \times ECt^3}{k_1 W\ell^3}\right)^{1/2}$$

$$k_1 = \frac{386 \times 2 \times ECt^3}{W\ell^3 (2\pi f_o)^2}$$

In actual tests:

f_o = 170 cps
C = 4-5/8 in.
t = 0.063 in.
W = 5 lb. at 1 g
ℓ = 1 in.

$$k_1 = \frac{386 \times 2 \times 4.63 \times 0.063^3 E}{5 \times 1^3 \times 4 \times \pi^2 \times 170^2} = 1.56 \times 10^{-7} E$$

$$f_o = k_2\left(\frac{Ct^3}{W\ell^3}\right)^{1/2}$$

where

$$k_2 = \frac{1}{2\pi}\left(\frac{772E}{1.56 \times 10^{-7}E}\right)^{1/2} = 11,200$$

$$f_o = k_2\left(\frac{Ct^3}{W\ell^3}\right)^{1/2} = 11,200\left(\frac{Ct^3}{W\ell^3}\right)^{1/2}$$

$$t = 1.37(Q)^{1/4} \times \left(\frac{Wa}{F_bC}\right)^{1/2} \times (PSD \times f_o)^{1/4}$$

$$= 1.37(Q)^{1/4} \times \left(\frac{Wa}{F_bC}\right)^{1/2} \times (PSD)^{1/4} \times \left[11,200\left(\frac{Ct^3}{W\ell^3}\right)^{1/2}\right]^{1/4}$$

$$= 1.37(Q)^{1/4} \times (11,200)^{1/4} \times \left(\frac{Wa}{F_bC}\right)^{1/2} \times (PSD)^{1/4} \times \left(\frac{Ct^3}{W\ell^3}\right)^{1/8}$$

$$= 1.37\,(11,200\,Q)^{1/4} \times \left(\frac{Wa}{F_bC}\right)^{1/2} \times (PSD)^{1/4} \times \left(\frac{Ct^3}{W\ell^3}\right)^{1/8}$$

when

$$Q = 15$$

$$k_3 = 1.37\,(11,200\,Q)^{1/4} = 1.37\,(11,200 \times 15)^{1/4} = 27.75$$

$$t = k_3\left(\frac{Wa}{F_bC}\right)^{1/2} \times (PSD)^{1/4} \times \left(\frac{Ct^3}{W\ell^3}\right)^{1/8}$$

$$= k_3\left(\frac{W^{1/2}}{W^{1/8}}\right) \times \left(\frac{a}{F_bC}\right)^{1/2} \times (PSD)^{1/4} \times \left(\frac{Ct^3}{\ell^3}\right)^{1/8}$$

$$\frac{t}{t^{3/8}} = k_3W^{3/8}\left(\frac{a}{F_bC}\right)^{1/2} \times (PSD)^{1/4} \times \left(\frac{C}{\ell^3}\right)^{1/8}$$

$$t^{5/8} = k_3 W^{3/8} \left(\frac{a}{F_b}\right)^{1/2} \times (PSD)^{1/4} \times \left(\frac{1}{\ell^3}\right)^{1/8} \times \left(\frac{C^{1/8}}{C^{1/2}}\right)$$

$$t = k_3^{8/5} W^{3/5} \left(\frac{a}{F_b}\right)^{4/5} \times (PSD)^{2/5} \times \left(\frac{1}{\ell^{3/5}}\right) \times \left(\frac{1}{C^{3/5}}\right)$$

$$= k_3^{1.6} W^{0.6} \left(\frac{a}{F_b}\right)^{0.8} \times (PSD)^{0.4} \times \left(\frac{1}{\ell^{0.6}}\right) \times \left(\frac{1}{C^{0.6}}\right)$$

$$K = k_3^{1.6} = (27.75)^{1.6} = 203.81$$

$$t = K(W)^{0.6} \left(\frac{a}{F_b}\right)^{0.8} \times (PSD)^{0.4} \times \left(\frac{1}{\ell^{0.6}}\right) \times \left(\frac{1}{C^{0.6}}\right)$$

$$= 203.81\ (W)^{0.6} \times \left(\frac{a}{F_b}\right)^{0.8} \times \left(\frac{1}{C^{0.6}}\right) \times \left(\frac{1}{\ell^{0.6}}\right) \times\ (PSD)^{0.4}$$

The nomogram for the hat section is constructed to the above equation.

E. 2 SHELF BRACKET NOMOGRAM

Mount sheet gage = t

$$= 0.6305 \left(\frac{Wac}{\ell F_{b_{(rms)}}}\right)^{1/3} \times (PSD \times Q \times f_o)^{1/6}$$

where

W	=	simulated load weight
a	=	mounting surface to load center of gravity
c	=	bend resistance line to $\mathbb{C}_L$ web
ℓ	=	critical bolt to pivot
$F_{b_{(rms)}}$	=	allowable stress
PSD	=	random environment
Q	=	amplification factor
f_o	=	natural frequency

RMS acceleration $= \left(\frac{\pi}{2} \times Q \times f_o \times PSD\right)^{1/2}$

Bolt load (per bolt) $= \frac{Wa}{2\ell}\left(\frac{\pi}{2} \times Q \times f_o \times PSD\right)^{1/2}$

Bending along bend resist line $= M = \frac{Wac}{2\ell}\left(\frac{\pi}{2} \times Q \times f_o \times PSD\right)^{1/2}$

$$t = \left(\frac{6M}{b\ F_{b_{(rms)}}}\right)^{1/2}$$

where

$b = 15t$

$$t = \left[\frac{3}{b\ F_{b_{(rms)}}} \times \frac{Wac}{2\ell}\left(\frac{\pi}{2} \times Q \times f_o \times PSD\right)^{1/2}\right]^{1/2}$$

$$= (3)^{1/2} \times \left(\frac{\pi}{2}\right)^{1/4} \times \left(\frac{Wac}{15t\ell\ F_{b_{(rms)}}}\right)^{1/2} \times (Q \times f_o \times PSD)^{1/4}$$

$$t \times t^{1/2} = t^{3/2} = \left(\frac{3}{15}\right)^{1/2} \times \left(\frac{\pi}{2}\right)^{1/4} \times \left(\frac{Wac}{\ell\ F_{b_{(rms)}}}\right)^{1/2} \times (Q \times f_o \times PSD)^{1/4}$$

$$t = \left(\frac{3}{15}\right)^{\frac{1}{2}\times\frac{2}{3}} \times \left(\frac{\pi}{2}\right)^{\frac{1}{4}\times\frac{2}{3}} \left(\frac{Wac}{\ell\ F_{b_{(rms)}}}\right)^{\frac{1}{2}\times\frac{2}{3}} \times (Q \times f_o \times PSD)^{\frac{1}{4}\times\frac{2}{3}}$$

$$= (0.2)^{1/3} \times (1.5708)^{1/6} \times \left(\frac{Wac}{\ell\ F_{b_{(rms)}}}\right)^{1/3} \times (Q \times f_o \times PSD)^{1/6}$$

$$K = (0.2)^{1/3} \times (1.5708)^{1/6} = 0.6305$$

$$t = K\left(\frac{Wac}{\ell \, F_{b_{(rms)}}}\right)^{1/3} \times (Q \times f_o \times PSD)^{1/6}$$

$$= 0.6305\left(\frac{Wac}{\ell \, F_{b_{(rms)}}}\right)^{1/3} \times (PSD \times Q \times f_o)^{1/6}$$

The nomogram for the cantilever (shelf) bracket is constructed to the above equation and similarly to that of the hat section bracket.

REFERENCES

1. D. E. Hines, D. E. Stewart. Evaluation of a Design Factor Approach to Space Vehicle Design for Random Vibration Environments. 35th Sym on Shock, Vibration, and Ass. Env. (Also Douglas Paper No. 3538) 1965.

2. J. W. Miles. On Structural Fatigue Under Random Loading. Journal of Applied Mechanics, November 1954.

3. R. E. Peterson. WADC Technical Report 59-507, Aeronautical Systems Division, Dayton, Ohio, August 1959.

4. Metallic Materials and Elements for Flight Vehicle Structures. MIL-HDBK-5, June 1965.